THE ASSESSMENT OF SEISMIC PERFORMANCE OF MULTI-SPAN
HIGHWAY BRIDGES IN TURKEY INCLUDING COLUMN DETERIORATION

A THESIS SUBMITTED TO
THE GRADUATE SCHOOL OF NATURAL AND APPLIED SCIENCES
OF
MIDDLE EAST TECHNICAL UNIVERSITY

BY

CANAN ELİF OCAK

IN PARTIAL FULFILLMENT OF THE REQUIREMENTS
FOR
THE DEGREE OF MASTER OF SCIENCE
IN
CIVIL ENGINEERING

SEPTEMBER 2016

Approval of the thesis:

**THE ASSESSMENT OF SEISMIC PERFORMANCE OF MULTI-SPAN
HIGHWAY BRIDGES IN TURKEY INCLUDING COLUMN
DETERIORATION**

submitted by **CANAN ELİF OCAK** in partial fulfillment of the requirements for the
degree of Master **of Science in Civil Engineering Department, Middle East
Technical University** by,

Prof. Dr. Gülbin Dural Ünver
Dean, Graduate School of **Natural and Applied Sciences**   _____

Prof. Dr. İsmail Özgür Yaman
Head of Department, **Civil Engineering**   _____

Assoc. Prof. Dr. Alp Caner
Supervisor, **Civil Engineering Dept., METU**   _____

Examining Committee Members:

Prof. Dr. Murat Altuğ Erberik
Civil Engineering Dept., METU   _____

Assoc. Prof. Dr. Alp Caner
Civil Engineering Dept., METU   _____

Prof. Dr. Kurtuluş Soyluk
Civil Engineering Dept., Gazi University   _____

Assoc. Prof. Dr. Afşin Sarıtaş
Civil Engineering Dept., METU   _____

Assoc. Prof. Dr. Eray Baran
Civil Engineering Dept., METU   _____

                                              Date: 08.09.2016

I hereby declare that all information in this document has been obtained and presented in accordance with academic rules and ethical conduct. I also declare that, as required by these rules and conduct, I have fully cited and referenced all material and results that are original to this work.

Name, Last Name : CANAN ELİF OCAK

Signature   :

ABSTRACT

**THE ASSESSMENT OF SEISMIC PERFORMANCE OF MULTI-SPAN
HIGHWAY BRIDGES IN TURKEY INCLUDING COLUMN
DETERIORATION**

Ocak, Canan Elif

M.S., Department of Civil Engineering

Supervisor: Assoc. Prof. Dr. Alp Caner

Considering the latest three major earthquakes occurred in Turkey, the performance of the bridges could be evaluated as successful. Bridges are one of the most important members of transportation network and it is important for them to survive during earthquakes. Contrary to the general belief, minimum damage during earthquakes mean very high safety factors included to the design rather than a success. Up to now, the bridges designed in Turkey are based on AASHTO (American Association of State Highway and Transportation Officials) and a modified version of LFD Bridge Design Specification. General Directorate of Highways (KGM) and Middle East Technical University (METU) conducted a project, (Türkiye Köprü Mühendisliğinde Tasarım ve Yapıma İlişkin Teknolojilerin Geliştirilmesi Kılavuzu) based on Load and Resistance Factor Design (LRFD) to update current practice in Turkey. However this recently published specification has not been used widely in design practice. For this reason, in this study the bridges are designed based on AASHTO LFD. By selecting different number of spans, column heights and lengths of column long side, the models are generated. The bridge columns are designed with gross and effective sections. The effect of 50 years of deterioration is taken into consideration and the initial and final conditions of bridges

are compared. Based on this study, it is concluded that, overdesigned bridges are obtained due to selection of gross section columns. In addition, a deterioration model and average strength loss due to deterioration are proposed.

Keywords: seismic design, bridge column, highway bridge, deterioration, corrosion

ÖZ

BETONARME ORTA AYAKLARA SAHİP ÇOK AÇIKLIKLI KÖPRÜLERİN DEPREM DAVRANIŞININ TÜRKİYE'DEKİ MEVCUT TASARIM YÖNTEMLERİNE GÖRE KOLON YIPRANMASINI KAPSAYACAK ŞEKİLDE DEĞERLENDİRİLMESİ

Ocak, Canan Elif
Yüksek Lisans, İnşaat Mühendisliği Bölümü
Tez Yöneticisi: Doç. Dr. Alp Caner

September 2016, 118 sayfa

Türkiye'de meydana gelen son üç büyük deprem göz önüne alındığında, köprülerin deprem performansının çok iyi olduğu ortadadır. Köprüler ulaşım ağının en önemli elemanlarından biridir ve maruz kaldıkları depremler sonrasında ayakta kalmaları çok önemlidir. Depremler esnasında oluşan hasarların çok az oluşu bir başarı gibi görünse de bu durum bir taraftan da tasarımda gereğinden fazla emniyet faktörlerinin gömülü olduğuna işaret etmektedir. Bugüne kadar Türkiye'de inşa edilen köprüler AASHTO (American Association of State Highway and Transportation Officials) LFD Köprü Tasarım Şartnamesi'nin değiştirilmiş bir versiyonuna göre tasarlanmaktaydı. Karayolları Genel Müdürlüğü ve ODTÜ işbirliği ile hazırlanan Türkiye Köprü Mühendisliğinde Tasarım ve Yapıma İlişkin Teknolojilerin Geliştirilmesi Kılavuzu oluşturulsa da henüz yaygın olarak kullanıma geçilmemiştir. Bu yüzden bu araştırma kapsamında köprüler AASHTO LFD' ye göre tasarlanmıştır. Bu çalışmada, farklı köprü açıklık sayısı, kolon yüksekliği ve kolon uzun kenar boyutu seçilerek köprü modelleri oluşturulmuştur. Köprü kolonları dolu ve etkin kesite göre tasarlanmıştır. Kolonların korozyona bağlı 50 yıllık bozulma durumu modellenmiştir. Köprü ilk durumu ve 50 yıllık bozulma sonrası durumu

karşılaştırılmıştır. Araştırmalar sonucunda Türkiye'deki köprülerin tasarımında dolu kolon kesitleri kullanıldığı için, aşırı güvenli sonuçlar elde edildiğine kanaat getirilmiştir. Ek olarak bir bozulma modeli önerilip, bozulmaya bağlı ortalama dayanım kaybı saptanmıştır.

Anahtar kelimeler: deprem tasarımı, kolon, karayolu köprüsü, bozulma, korozyon

To My Beloved Family

ACKNOWLEDGEMENTS

TABLE OF CONTENTS

LIST OF TABLES

LIST OF FIGURES

FIGURES

xviii

LIST OF SYMBOLS AND ABBREVIATIONS

A: the acceleration coefficient

A_{bp}: bearing cross sectional area

Acc: the area of composite section

A_{tr}: area of transformed girder

C (x, t): chloride content at the location x in a given time t

CI: chloride concentration

CI_{Th}: threshold value

Cs: elastic seismic coefficient

$D_{(0)}$: the initial diameter of steel bars

$D_{(t)}$: reduced diameter of corroded steel bars

Da: apparent diffusion coefficient

d_{bl}: column longitudinal reinforcement diameter

d_c: concrete cover depth

DL: dead load

D_m: averaged diffusion coefficient

DX: response value in longitudinal direction

DY: response value in transverse direction

E_c: modulus of elasticity of concrete

E_{dec}: modulus of elasticity of deck

E_{girder}: modulus of elasticity of girder

E_s: modulus of elasticity of steel

f $_{Tseasonal}$: temperature effect

f: the yield strength of corroded steel bars

f_c: compressive strength of concrete

f_{CI}: chloride concentration parameter

f_{dc}: concrete cover depth parameter

f_{mc}: moisture content parameter

$f_{O2:}$ oxygen concentration parameter

f_{res}: concrete resistivity parameter

f_T: temperature parameter

$f_{Tmean:}$ annual mean temperature factor

$f_{w/c}$: water – cement ratio parameter

$f_{y,new}$: yield strength of corroded reinforcing bars

f_y: the initial yield strength of noncorroded steel bars

f_{ye}: yield strength of the longitudinal reinforcement

G_b: shear modulus of bearing

H: column height

h_{bp}: height of elastomeric parts

H^L_x: longitudinal component of shear force in x direction

H^L_y: longitudinal component of shear force in y direction

H^T_x: transverse component of shear force in x direction

H^T_y: transverse component of shear force in y direction

H_x: shear force in x direction

H_y: shear force in y direction

I: impact fraction

I_{EFF}: inertia of the effective column section

I_{GROSS}: inertia of the column gross section

I_{tr}: the moment of inertia of transformed girder

I_x^*: moment of inertia about x axis

I_{xc}: moment of inertia about x axis

I_y^*: moment of inertia about y axis

I_{yc}: moment of inertia about y axis

i_{cor}: corrosion rate

k: effective length factor of column

k_1: data fitting factor

k_2: data fitting factor

k_c: constant

k_{ht}: translational stiffness coefficient for one bearing

k_{vt}: vertical stiffness coefficient for one bearing

L: column height

L: length in meters of the portion of the span that is loaded to produce the maximum
 stress in the member

L_{bp}: bearing length

LF: braking load

LL: live load

L_p: plastic hinge length

l_u: column height

m: constant represents mix proportions of concrete

mc: moisture content

M^L_x: longitudinal component of moment about x axis

M^L_y: longitudinal component of moment about y axis

M^T_x: transversel component of moment about x axis

M^T_y: transversel component of moment about y axis

M_u: column maximum demand moment

M_u: moment of the ultimate point

Mw: the magnitude of the earthqauke

M_x: moment about x axis

M_y: moment about y axis

M_y: moment of the first yield point

n: the number of beams

n_{layer}: number of elastomeric parts

PL: pedestrian load

Q_{corr}: the amount of corrosion of reinforcement area loss

R: load reduction factors

r: radius of gyration

R: response modifications factor

RST: temperature load

s: number of spans

S: site coefficient

SF: shape factor

SPC: seismic performance category

T: period

t: time

T_{high}: average high temperature

T_{low}: average low temperature

T_{mean}: annual mean temperature

t_R: the time when diffusion coefficient is assumed to be constant

t_{ref}: the reference time

v_{bp}: shear stress

vbp: shear stress

w / c: water - cement ratio

W: wind load on superstructure

W_{bp}: bearing width

w_c: unit weight of concrete

WL: wind load on substructure

W_{pier}: Weight of superstructure

x: distance from any point inside the concrete to the surface

x_1: pier height

x_2: column long edge

ϕ_{new}: diameter of corroded reinforcing bars

Δ: displacement

Δ_{bp}: unit displacement

Δc: displacement capacity

Δd: displacement demand

Δ_e: elastic component of displacement

Δ_p: plastic component displacement

Δ_u: ultimate displacement

Δ_y: nominal yield displacement

ε_c: compressive strain

ϕ: diameter of noncorroded reinforcing bars

ϕ'_y: curvature of the first yield point

ϕ_c: condition factor

ϕM_n: column nominal moment capacity

ϕ_p: plastic curvature

ϕ_u: curvature of the ultimate point

ϕ_y: nominal yield curvature

γ_{bp}: rotation for unit displacement

σ_{bp}: compressive strain

α: constant

CHAPTER 1

INTRODUCTION

1. 1   Background

Since early times, transportation has been one of humanity's most basic needs. At the same time, the frequency of a country's transport network, the length and quality of it is also one of the indicators of the development of that country. There is no doubt that, bridges are one of the most important elements of transportation systems. Due to the mountainous nature of our country, which makes it difficult to transport, it becomes necessary to construct transportation elements like bridges and tunnels. Before the proclamation of the Republic of Turkey there exist 94 bridges. Bridges are continued to be constructed and reach to a number of 7713 with a total length of 408 km by 2015 (Republic of Turkey, General Directorate of Highways, Bridge Inventory Data).

As of the other countries which that are in active fault zones, earthquake is one of the most decisive parameter for the bridges designed in Turkey. In Turkey, in bridge design the modified version of American Association of State Highway and Transportation Officials Standard Specifications for Highway Bridges (AASHTO LFD) is used. General Directorate of Highways (KGM) and Middle East Technical University (METU) conducted a project, (Türkiye Köprü Mühendisliğinde Tasarım ve Yapıma İlişkin Teknolojilerin Geliştirilmesi Kılavuzu) based on Load and Resistance Factor Design (LRFD) to update current practice in Turkey. However this recently published specification has not been used widely in design practice. In this study, bridge models were designed according to AASHTO LFD.

In Turkey, in the 1950s, bridges with continuous cast-in-place reinforced concrete beams with a rocker type of bearing or concrete decks without beams were

constructed. In same years besides reinforced concrete bridges, bridges with steel I-girder were built. In 1980s, simple spanned bridges with cast-in-place reinforced concrete beams were constructed. In last two decades, construction of simply supported pre-stressed I girders with composite slab has accelerated and this type of bridges became the most popular ones (Caner et al., 2008). In this study, bridge models having simply supported pre-stressed I girders with composite slab are preferred.
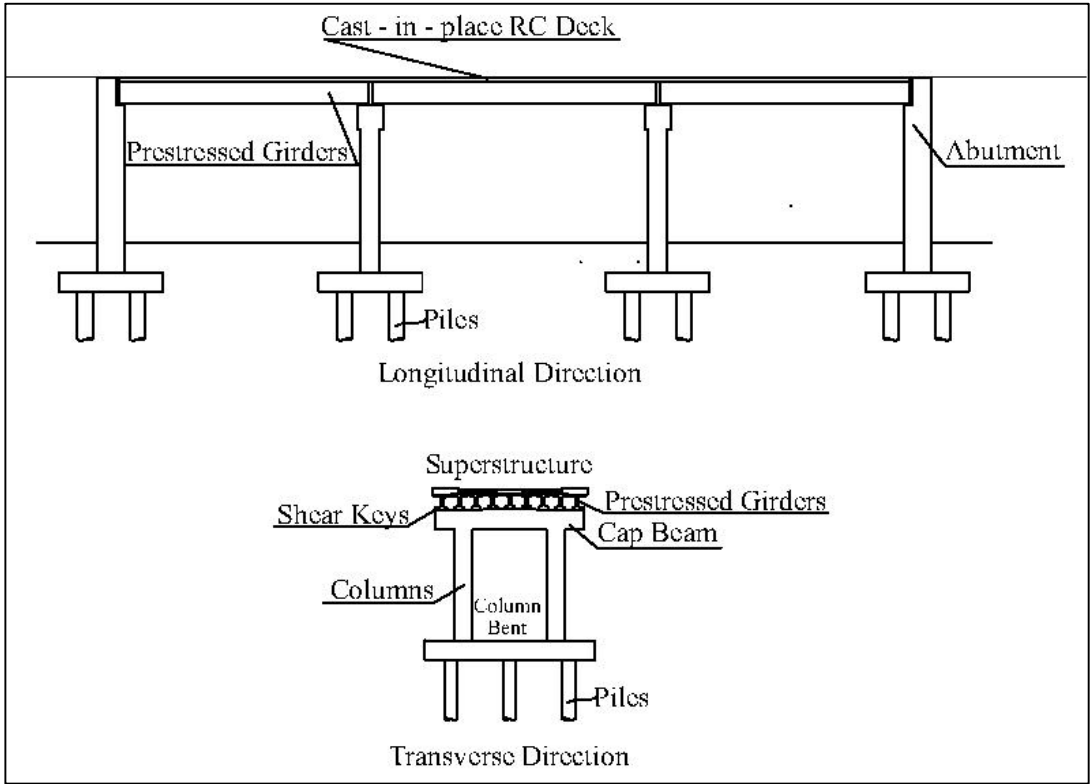
Figure 1.1: General presentation of the ordinary highway bridges

1. 2   Aim and Scope of the Study

Regular buildings experienced huge damages after recent destructive earthquakes in Turkey. On the other hand, bridge system performed well even they were located near the fault. The reasons of performance difference between regular building and bridges are not known. Besides, the success of bridges implies hidden factor of safety in the bridges. The magnitude of factor of safety is also unknown.

On the other hand, it is obvious that bridges are subjected to deterioration during their service life. The effect of deterioration on bridge performance is another problem that should be focused.

The aim of this study can be listed as:

- To evaluate seismic performance of bridges in Turkey in terms of Force Based Design and Displacement Based Design.
- To compare the results of analysis with cracked column section and uncracked column section.
- To investigate the effects of deterioration of bridge columns on bridge performance.

In Chapter 2, brief review of literature on bridge failures, seismic performance of Turkish bridges and deterioration were provided. Studied deterioration models due to corrosion in the past were explained.

In Chapter 3, the geometrical properties of generated bridges were expressed. The modeling of bridges and column design were explained. Proposed deterioration model were explained..

In Chapter 4, fundamental periods of bridge models, column nominal moment capacity over column maximum demand ratios, displacement capacity over displacement demand ratios were provided.

.

In Chapter 5, obtained results of analyses were discussed. The reasons of results were explained. A relation between column nominal moment capacity over column maximum demand ratio and displacement capacity over displacement demand ratio were revealed. The results of using cracked sections rather than uncracked section were discussed. Finally, the effect of corrosion on column performance was explained. Obtained conclusions were summarized.

CHAPTER 2

LITERATURE REVIEW

2. 1 Bridge Failures

Bridge failures were categorized as either total or partial collapse by New York State Department of Transportation (NYDOT, 2004). Total collapse was described as "structures which all primary members of a span or several spans have undergone severe deformation such that no travel lanes are passable". Partial collapse was defined as "structures on which all or some of the primary structural members of a span or multiple spans have undergone severe deformation such that the lives of those travelling on or under the structure would be in danger" (NYDOT, 2004). As an illustration, both of the conditions were provided in Figure 2.1 and Figure 2.2.

Figure 2.1 Total Collapse of a Bridge in Minnesota (The Denver Post, 2007)

A study conducted by Wesley Cook (2015) showed that between the years of 1987 and 2011, 240 total and 190 partial collapses were occurred in the United States. The reasons for both of the collapse type were listed as hydraulics, overloading, vehicle collisions, deterioration, natural disasters such as fire, storm, hurricane, earthquake; geotechnical reasons, design errors, fatigue, wrong bearings and etc.

Figure 2.2 Partial Collapse of a Bridge in Texas (ABC News, 2016)

The majority of the bridges collapsed due to the hydraulic reasons including flood, scour, debris, ice and drift. Within the above mentioned reasons, collapses due to deterioration and earthquakes, which were the subject of this study, were occurred with a percentage of 5,00 and 2,08 for total collapses and 13,16% and 0% for partial collapses, respectively (Figure 2.3 and Figure 2.4).
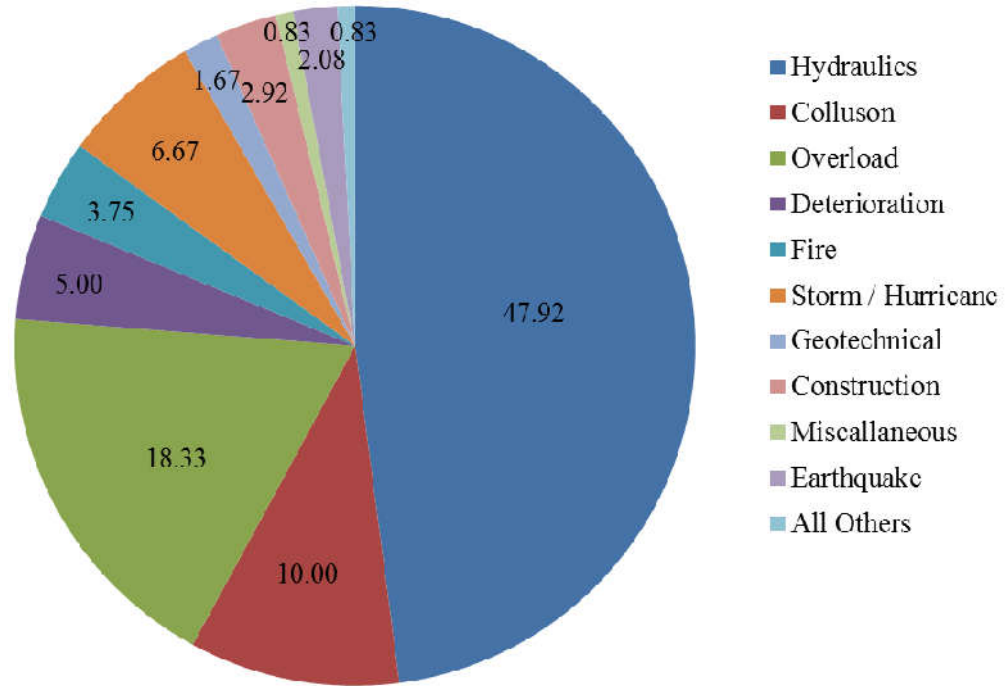
Figure 2.3: Reasons of Bridge Total Failures in the United States in 1987 – 2011
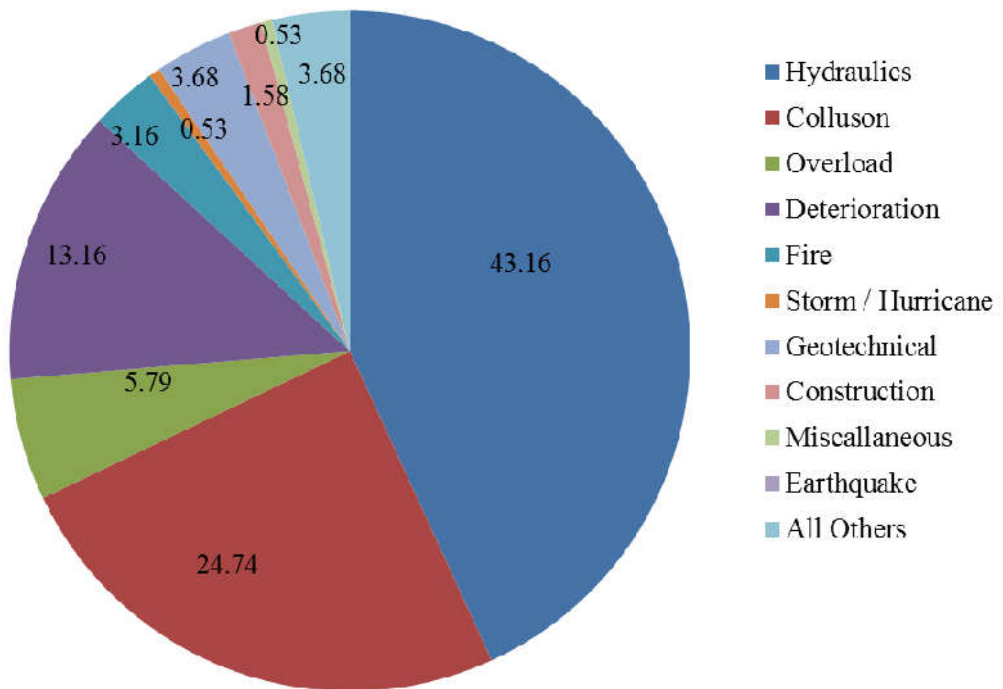
Figure 2.4: Reasons of Bridge Partial Failures in the United States in 1987 – 2011

7

2. 2   Seismic Performance of Existing Bridges in Turkey

Turkey was located in Alpin – Himalayan Orogeny which is one of the important seismic belts in the world. There exist numerous active faults due to complicated geomorphologic nature and geodynamics location of Turkey. According to Active Fault Maps of Turkey (General Directorate of Mineral Research & Exploration, 2012), North Anatolian Fault, Eastern Anatolian Fault and West Anatolian Fault have potential to generate massive earthquakes.

Earthquakes having a magnitude of four or more occurred between 1900 and 2013 were provided in Figure 2.5.

Within the hazardous earthquakes occurred, the performances of the bridges during three recent ones were examined. These were; 23 September 2013 Van (Mw = 7,2), 17 August 1999 Kocaeli (Mw = 7,4) and 12 November 1999 Düzce (Mw = 7,2) earthquakes.
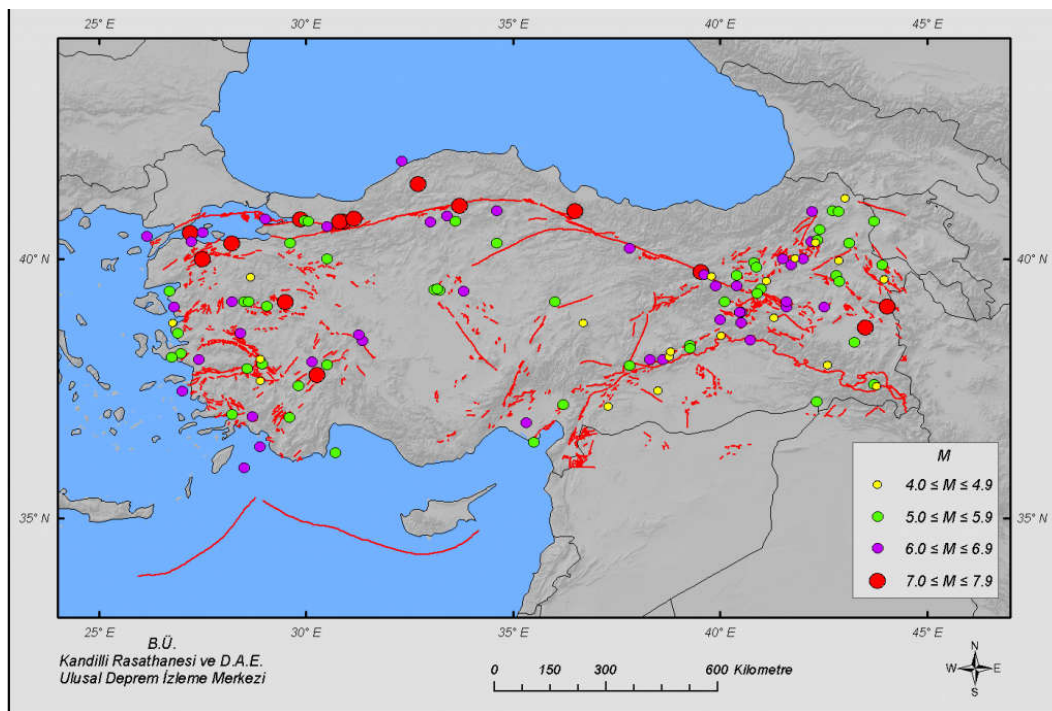
Figure 2.5: Earthquakes with a Magnitude Higher Than 4,0. (KOERI, 2015)

2.2. 1 23 September 2013 Van Earthquake

On 23 September 2013, in the eastern Anatolian region of Turkey an earthquake having a moment magnitude of 7,2 occurred. This earthquake affected the city of Van and its district Erciş. 604 people died and more than 2000 people injured because of this disaster. In the scope of a study conducted by Middle East Technical University Earthquake Engineering Research Center (2011) the condition of structures after earthquake were investigated. Accordingly, 49% of investigated buildings were categorized as failed, heavily damaged or moderately damaged. Building conditions in terms of damage in Van and Erciş were provided in Figure 2.6 and related photos were shown in Figure 2.7.
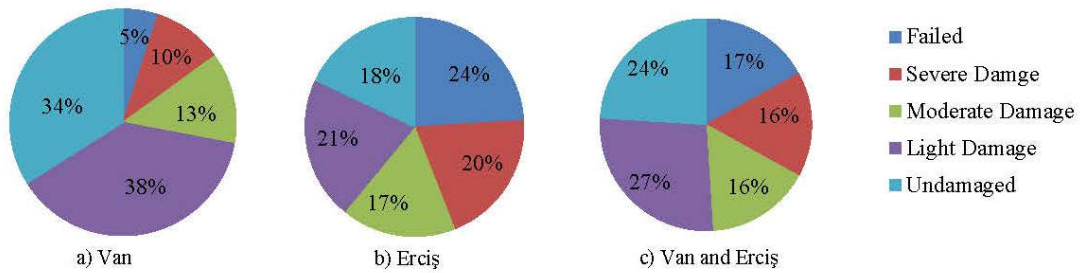
Figure 2.6: Damage Percentages

9

Figure 2.7 : Wrecked Buildings (23 Ekim 2011 Mw 7.2 Van Depremi Sismik ve Yapisal Hasara İlişkin Saha Gözlemleri, 2011)

Seismic performances of regular buildings could be evaluated as unsuccessful, considering moderate or higher damage levels. On the other hand situation was totally different for bridges. Majority of these bridges were simply supported I - girders with continuous slabs. For all of the bridges, the traffic flow was not interrupted after the earthquake. 14 bridges which were located near the fault experienced light damage after the earthquake. The most common type of damages were listed as shear key failures, spalling and cracking of cover concrete, permanent displacements in elastomeric bearings and flexural cracks in columns.

Observed damages of bridges were considered in the category of minimum damage level, according to the classification provided by Applied Technology Council (ATC32 - 1, 1996) (23 Ekim 2011 Mw= 7,2 Van Depremi Sismik ve Yapısal Hasara

İlişkin Saha Gözlemleri, 2011). According to this report, design earthquake forces were much higher than forces which were subjected due to earthquake.

Figure 2.8: Damaged Shear Keys (23 Ekim 2011 Mw 7,2 Van Depremi
Sismik ve Yapisal Hasara İlişkin Saha Gözlemleri, 2011)

Figure 2.9: Flexural Cracks in Columns (23 Ekim 2011 Mw 7,2 Van Depremi
Sismik ve Yapisal Hasara İlişkin Saha Gözlemleri, 2011)

Figure 2.10: Photo of a Bridge after Van Earthquake that was damaged due to a flood few years before (23 Ekim 2011 Mw 7,2 Van Depremi Sismik ve Yapisal Hasara İlişkin Saha Gözlemleri, 2011)

2.2. 2 17 Augustus 1999 Kocaeli and 12 November Düzce Earthquakes

On 17 August 1999, an earthquake with a magnitude of 7,4 hit the north-west of Turkey. The epicentre of the earthquake was Koceli, located on the western extension of the North Anatolian fault system. It was considered to be largest event to have devastated a modern, industrialized area since the 1923 Tokyo Earthquake (Erdik, 2001). On November 12, another segment at the eastern end of the fault ruptured and generated another earthquake with a magnitude of 7,2. Because of these two devastating earthquakes, more than 16,400 building totally collapsed or experienced severe damage. Approximately 120,000 families were obliged to leave their homes.

But according to experts, the scale of the fault rupture and magnitude of the ground motion considered, highway system performed well. In Koceali Earthquake, bridge collapses were observed only at the locations of fault crossing in the region of

southeast Adapazarı. Arifiye overpass totally collapsed because of fault rupture at a distance of less than 3 km (Figure 2.13).

Figure 2.11: A General View of Kocaeli after Earthquake (Erdik, 2001)

Figure 2.12: A General View of Düzce after Earthquake (Erdik, 2001)

Figure 2.13: Arifiye Overpass (Erdik, 2001)

Duzce Earthquake caused damage to Bolu crossing. Misalignment of #1 Viaduct and collapse of Bolu Tunnel were occurred. #1 Viaduct was remained in elastic limits in Kocaeli Earthquake, however in Duzce Earthquake, fault passed between the number of 47 and 45 piers with an angle of 20º - 30º. 2 – 2,5 meter length of fault offset was formed (Yılmaz and Türer, 2002).
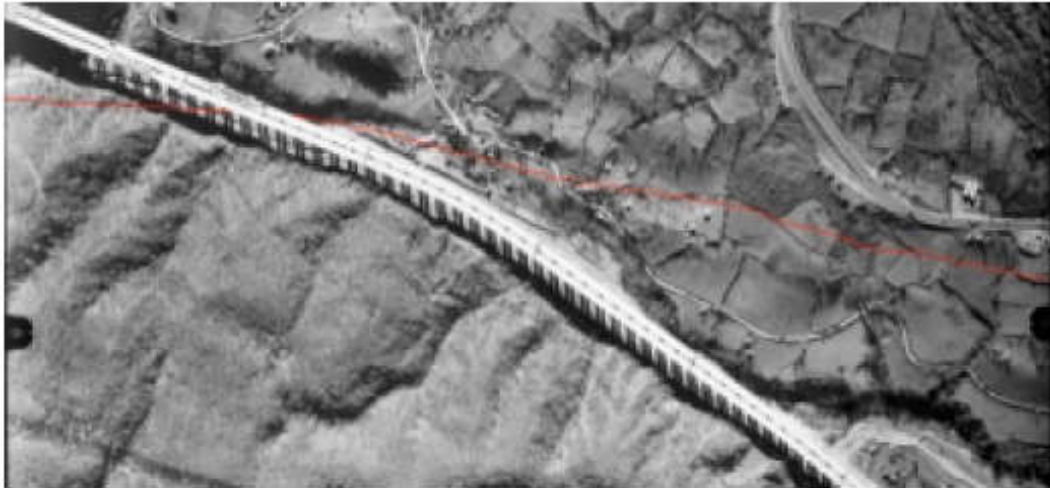
Figure 2.14: View of the Bolu 1 Viaduct. Red line represents the fault rupture. (Erdik, 2001)

Apart from these, in other bridges shear key failures, spalling and cracking of cover concrete, permanent displacements of girders in seating were determined as expected.

Considering the performance of structures during the above mentioned three major earthquakes, it was concluded that regular buildings were heavily damaged. On the other hand, the bridge performance could be evaluated as successful except the ones that were located on or near the faults.

2. 3   Ageing Model

Reinforced concrete bridges are generally subjected to different environmental conditions during their lifetimes. For structures placed in a moderately or highly aggressive environment, deterioration would be inevitable. Such deterioration will diminish the service life of bridges in addition to direct and indirect loses. Maintenance cost is considered as direct cost, whereas closure of bridges, increase in the average travel time are related to indirect costs.

In North America, because of aging, aggressive environment and increased load and traffic volume, an important percentage of highway bridges are graded as structurally deficient or functionally deficient. According to American Society for Civil Engineers' Report card for America's infrastructure, approximately 26% of bridges in the United States are either structurally deficient or functionally obsolete; accumulating total needed investment of $930 billion (ASCE 2010). On the other hand, a study conducted by "Council of Virginia's Future" in 2014, showed that percentage of functionally obsolete or structurally deficient bridges were dropped to 23,9. Although   decline was observed, the ratio was still high.
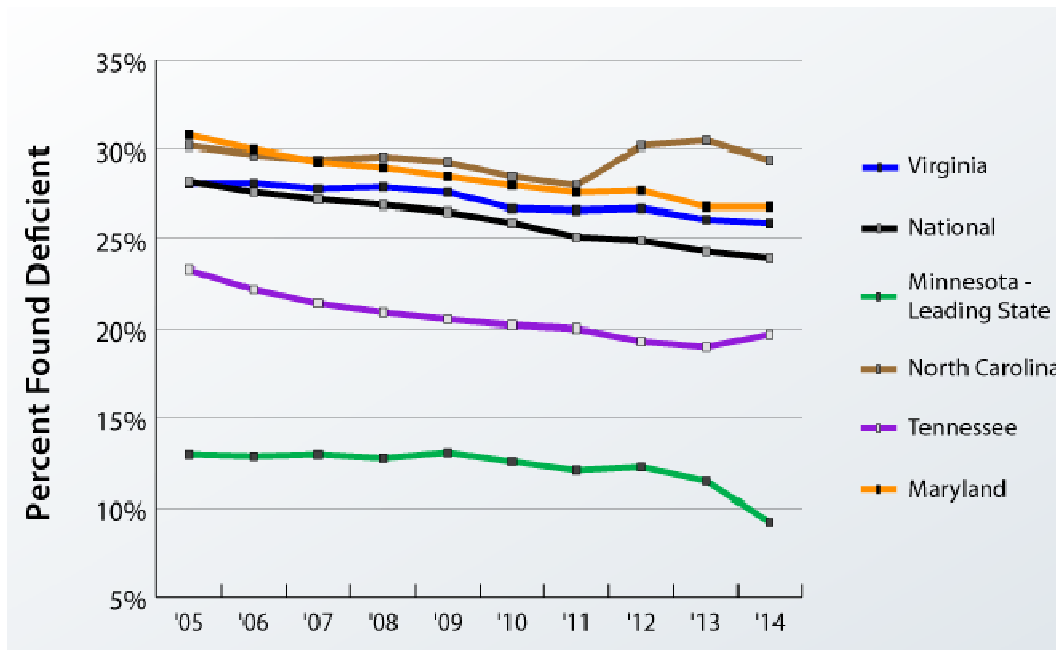
Figure 2.15: Deficient Bridges by State (Infrastructure Condition, 2014)

The corrosion deterioration in reinforced concrete structures has gained outstanding attention from researchers. A considerable amount of studies have been conducted worldwide. The objective of studies were generally to find a relationship between the corrosion process and service life of the structures. Different researchers offered different deterioration models including empirical, numerical and analytical models (Alonso et al. 1988, Andrade et al 1993, Stewart and Rosowsky 1998, Ahmad and Bhattacharjee 2000, Martinez and Andrade 2009, Otieno et al. 2011).

The variety of methods used in their studies are as a result of the fact that, the effect of reinforcement corrosion in the long term conditions and effect on structure performance were not provided in the specifications.

Deterioration includes cracking, spalling and corrosion of reinforcement. Among them corrosion of reinforcement is the main concern since it leads to loss of steel area and reduction in yielding strength of reinforcement. Even corrosion may induce the total collapse of bridges.

16

Figure 2.16: Example of Corroded Reinforcement (Özdemir and Topkara, 2015)

Carbonation and chlorides lead to corrosion. Carbonation is formed due to carbon dioxide interaction to the concrete surface. Chemically, carbon dioxide is in acidic form whereas concrete is alkaline. This alkalinity provides a passive protection from environmental acidity for reinforcing steel. This phase is called initiation phase. In initiation phase, corrosion does not occur but chloride ions enter gradually in RC members. Nevertheless as time passes alkalinity of concrete starts to become neutralized due to carbon dioxide in the atmosphere. The protective iron oxide layers break down and corrosion starts. This process is called as propagation phase. Chlorides mechanism is similar to carbonation. First chloride content at the surface of the reinforcing steel exceeds a critical value, in the presence of oxygen and water protective layer is destroyed and chloride ions reach the reinforcement steel layer.

The mechanism of chloride transportation is a complex phenomenon. It can be formed in different forms such as diffusion, capillary suction and permeation. It also depends on concrete characteristics such as pore size distribution, water cement ratio; pore saturation degree, environmental conditions, free chloride content etc. Among them diffusion is assumed to be the dominant mode of chloride intrusion into concrete by researchers (Shafei et al. 2013).

2.3. 1 Modeling of Corrosion

For inspection and maintenance activities time of initiation and propagation processes should be estimated accurately. Corrosion initiation time is described when the chloride concentration at reinforcing steel reaches the critical chloride concentration. Different chloride content values were suggested by different researchers. Shafei et al. (2013) proposed the total chloride content as 1% of cement weight which corresponds to 3,5 kg / m^3. Guo et al. (2010) recommended the chloride content 1,45 kg / m^3 with the coefficient of variation of 0,2. Chien- Kuo Chiu (2014) assumed that corrosion starts when the chloride content reaches 1,0 – 1,2 kg / m^3.

Many models such as STADIUM, Life-365, ConcreteWorks and DuraCrete have been generated to predict the initiation time. In STADIUM ingress of chloride into concrete was simulated with finite-element analysis. Other models used Fick's second law as follows:

$$C(x, t) = Cs[1 \quad erf \frac{x}{2\sqrt{Da\ t}}]$$ (2.1)

where

Cs = chloride concentration on the concrete surface

Da = apparent diffusion coefficient (length^2 / time)

t = time

x = distance from any point inside the concrete to the surface (length)

Shafei et al. (2013) found the initiation time as 9,33 years, 10,40 years and 12,66 years for linear, Freundlich and Langmuir isotherms respectively using finite difference algorithm. On the other hand 6 years of initiation time were proposed by different researchers (Liu and Weyers 1998, Vu et al. 2005; Williamson 2007). Phurkhao and Kassir (2005) determined the time to start corrosion as 5 years by ramp – type surface concentration.

Besides mathematical solutions, field observations were also used to predict corrosion initiation time. For example Kwon et al. (2009) determined the initiation time as 8 – 11 years.

Propagation starts when surface chloride content reaches critical chloride content and it will continue till the end of service life of reinforced concrete structures. Most important factor that affects the time of propagation and corrosion damage is the corrosion rate, i_{cor}. Corrosion rate depends on several factors including physical properties of concrete and environmental conditions. Water – cement ratio, moisture content within the concrete pores, concrete cover depth and ohmic resistance of concrete cover are the physical properties that determine the corrosion rate. In addition to this, surface chloride content, annual mean temperature, seasonal temperature fluctuations, oxygen and moisture concentration of surface, humidity are among the environmental properties.

Developed propagation models generally depend on corrosion rate. But in most of the studies corrosion rate was assumed as constant during service life (Alonso et al. 1988; Andrade et al. 1993; Stewart and Rosowsky 1998; Ahmad and Bhattacharjee 2000; Martinez and Andrade 2009). Other researchers developed corrosion rate models as a function of time (Yalçın and Ergun 1996; DuraCrete 2000; Vu and Stewart 2000; Li 2004). Obtained propagation models could be summarized as follows.

The model by Stewart and Rosowsky (1998) assumed corrosion rate constant as 1,5 $\mu A / cm^2$. In Alonso et al. (1988) corrosion rate was function of concrete resistivity and constant in time. Martinez and Andrade (2009) developed a model depend on cathodic and anodic Tafel slopes and polarization resistance in $k\Omega \ cm^2$. Ahmad and Bhattacharjee (2000) suggested using cement content, water – cement ratio and calcium chloride ratio to determine corrosion rate. In DuraCrete (2000) corrosion rate decreased with time exponentially. In this study, corrosion rate depend on regression parameter, chloride content, galvanic effects, formation of oxides, aging, resistivity of concrete. Yalçın and Ergun (1996) assumed that corrosion rate was function of time from corrosion initiation and $i_{corr,0}$ which equals to 0,53. Vu and Stewart (2000) developed a model similar to Yalçın and Ergun (1996) in terms of

relation of time and corrosion rate and depending parameters. In their approach, corrosion rate exponentially decreases as time and also depends on concrete cover and water – cement ratio. But this model gives infinite corrosion rate at time zero. Li (2004), found a logarithmic relationship between time and corrosion rate but this formula lacks contribution of the environmental factors. Guo et al. (2014) developed a formula by considering drawbacks of existing models. They believed that corrosion rate function could be expressed as:

$$i_{corr} = i_{corr.0} \quad f_{0_2} \quad f_{mc} \quad f_{CI} \quad f_{w/c} \quad f_{dc} \quad f_{mc} \quad f_T \qquad (2.2)$$

Where f_{O2}, f_{mc}, f_{res}, f_{CI}, $f_{w/c}$, f_{dc}, f_T parameters that related to oxygen concentration, moisture content, concrete resistivity, water – cement ratio, concrete cover depth, temperature and chloride concentration namely.

Electrochemical reactions need oxygen and moisture to be formed. According to Kobayashi and Shuttoh (1991) the oxygen coefficient increases with increasing water – cement ratio, temperature and decreasing moisture content whereas it decreases with increasing salt content. But moisture content in concrete pores determines oxygen concentration at the steel surface. Since diffusion coefficient of oxygen in air is higher than the diffusion coefficient in water, when moisture content of concrete pores is high, oxygen diffusion rate is low.

According to Bertolini et al. (2004) exposure conditions determine the moisture content. Conducted experiments showed that when the moisture content in the concrete pores is between 65% and 85 %, corrosion rate remains same. When the moisture content decreases from 65% to 50%, it decreases exponentially. Under the 50% of moisture content, corrosion rate is very low (Balafas and Bargoyne, 2010). Moisture content effect can be predicted as:

$$f_{mc} = e^{-600 \ (mc-0,75)^6} \qquad (2.3)$$

where mc is the moisture content. Above formula depends on experimental data prepared by Balafas and Bargoyne (2010).

Liu and Weyers (1998) found a relation between corrosion rate and chloride concentration. According to experiments, corrosion rate increases as chloride concentration increases and the chloride factor can be formulated as:

$$f_{CI} = \frac{(CI + CI_{Th})}{2 \ CI_{Th}} \tag{2.4}$$

where CI is the chloride concentration in steel surface (kg / m^3) and CI$_{Th}$ is the threshold value of steel reinforcement necessary for corrosion initiation.

In the literature, it was determined that corrosion rate is highly depend on concrete cover and water – cement ratio. Water – cement ratio controls resistivity of uncontaminated concrete. The time of transportation of water, oxygen and chloride from concrete surface to steel reinforcement is directly related to concrete cover depth and water – cement ratio. Corrosion rate increases as water – cement ratio increases and decreases with increasing cover depth. Increase in cover depth makes difficult to transportation of elements. Vu and Stewart (2000) proposed a formula that combined concrete cover depth and water – cement ratio as follows;

$$f_{CI} = k_c \ \frac{(1 - w/c)^{-1,64}}{d_c} \tag{2.5}$$

where k_c is constant, d_c is the concrete cover depth in mm and w / c is the water – cement ratio. This formula represents concrete characteristics.

Besides concrete characteristics, temperature is the one of the important factor that affects corrosion rate. The corrosion rate increases as temperature increases but increase in temperature leads to decrease in the solubility of oxygen. The annual mean temperature factor will be estimated using Arrhenius equation as follows:

$$f_{T_{mean}} = e^{228 \ 3(1/28 \ 415 - 1 /T_{mean})^{\wedge}6} \tag{2.6}$$

where T$_{mean}$ is the annual mean temperature in Kelvin.

Corrosion rate is not only dependent on annual temperature values but also influenced by seasonal temperature fluctuations. Liu and Weyers (1998) found that in midsummer, corrosion rates are highest and in midwinter they are lowest. So a sine function was used to express changes in corrosion rates due to seasonal fluctuations. They developed a formula to estimate seasonal variations as follows:

$$f_{T_{seasonal}} = \frac{k_1 \ \sin(t)}{t} + k_2 \tag{2.7}$$

where k_1 and k_2 factors obtained by data fitting and t is the time in years.

If the average high and low temperature values were added the seasonal fluctuations, temperature effect in corrosion rate could be described as follows:

$$f_{Tseasonal} = \{ (T_{high} - T_{low}) * \sin [2 * \pi (t - a_s)] \} / (8,6 * (t - a_s) + 7,6 \tag{2.8}$$

where T_{high} is the average high temperature and T_{low} is the average low temperature in Kelvin; as is the corrosion initiation season factor, which are 0,07, 0,7, 0,43 and 0,25 for spring, summer, fall and winter respectively. Function was moved and stretched in order to fit the data and constants of 8,6 and 7,6 were obtained (Guo et al. 2014)

Guo et al. (2014) used recent studies and revised the corrosion rate formula as a function of chloride and moisture content, concrete characteristics and temperature. If all the terms were combined the formula of corrosion rate could be expressed as follows:

$$i_{cor}(t) = \frac{(1 - w/c)^{-1.64}}{d_c} \frac{(Cl + Cl_{Th})}{2Cl_{Th}} \left\{ \frac{(T_{high} - T_{low}) \sin[2\pi(t - a_s)]}{8.6(t - a_s)} + 7.6 \right\}$$

$$e^{-228 \ 3(1/28 \ 415 - 1/T_{mean}) - 6000(mc - 0.75)^6} \tag{2.9}$$
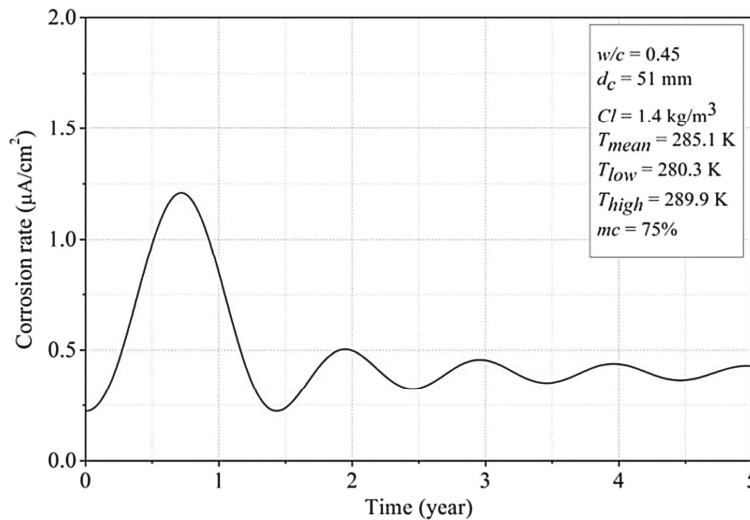
Figure 2.17: Proposed Corrosion Rate Model by Guo et al. (2014)

22

Estimation of corrosion rate using the proposed formula (2.9) was shown in Figure 2.17. Corrosion rate increased from approximately 0,25 to 1,25 at the beginning of time and decreased. Then it oscillated around a constant value. The reason of oscillations was the seasonal temperatures. Guo et al. (2014) investigated the reliability of the proposed corrosion rate model and they compared with other models which were conducted earlier. Obtained results showed that in early ages the percent error of their model was about zero and it increased with time to a constant value of 5% (Figure 2.18).
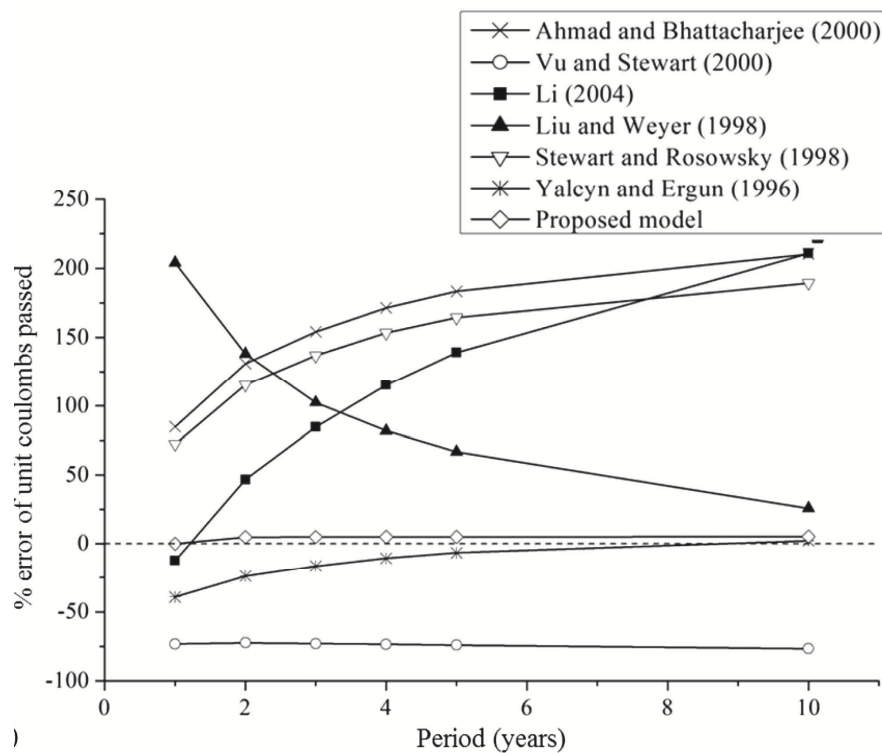
Figure 2.18: Comparison of Proposed Model of Guo et al. (2014) with Other Studies

In their study, Guo et al. (2014) managed to develop a corrosion rate formula which is a function of time. But they assumed that chloride content will be constant during propagation of corrosion. However, it was expected that induced chloride content increases with time. One dimensional chloride diffusion models based on Fick's

23

second law of one - dimensional steady state (2.1) were generated in order to determine induced chloride content.

$$C(x,t) = C_S \left[1 \quad \text{erf}(\frac{x}{2\sqrt{D_m \ t}})\right]$$ (2.10)

Where $C(x,t)$ is chloride content at the location x in a given time t. C_s is the surface chloride content. D_m is the averaged diffusion coefficient and it can be defined as :

$$D_m = \frac{1}{t} \int_0^t D_{ref} \ (\frac{t_{ref}}{\tau})^m \ d\tau = \frac{D_{ref}}{1-m} \ (\frac{t_{ref}}{\tau})^m \qquad (\text{t} < \text{t}_R)$$ (2.11)

$$D_m = D_{ref} \left[1 + \frac{t_R}{t} \left(\frac{m}{1-m}\right)\right] (\frac{t_{ref}}{\tau})^m \qquad (\text{t} \geq \text{t}_R)$$ (2.12)

where t_R is the time when diffusion coefficient is assumed to be constant and suggested as 30 years by Thomas and Bentz (2002). t_{ref} is the reference time for diffusion coefficient and recommended as 28 days by Kwon et al. (2009). m is a constant represents mix proportions of concrete and suggested as -0,3 by Biondini et al. (2012).

The term surface chloride C_s is used to define the amount of chloride on the surface of the concrete structure. It shows differences depending on the location of the structure and different parts in the structure. For surface chloride content (C_s) different studies offered different values. Val and Pavel (2008) gave C_s having mean value of 15 kg / m^3 with the coefficient of variation of 0,2. Kwon et al. (2009) proposed surface chloride content mean values depending on crack width. According to this study which utilized from field investigations, C_s was recommended as 14,15 kg / m^3, 12,95 kg / m^3, 12,40 kg / m^3 and 13,00 kg / m^3 for sound concrete, having a crack width of 0,1 mm, 0,2 mm and 0,3 mm respectively. Shafei and Alipour (2013) suggested C_s as 5 kg / m^3. Zhu et al. (2015) used 2,95 kg / m^3 for surface chloride content. On the other hand Özdemir et al. (2015) classified the environmental conditions as mild, moderate and high depending on level of concentration of aggressive chemical substance. Mild environments were excluded whereas river bridges and highway bridges exposed to salting because of harsh winters were defined as moderate. Marine type structures and structures located near to salted water sources were called high aggressiveness. Accordingly, surface chloride content

values were suggested as 2 kg / m^3, 4,5 kg / m^3 and 12 kg / m^3 for structures having mild, moderate and high aggressiveness respectively.

Averaged diffusion coefficient D_m, is another parameter which needs literature research. Val and Pavel (2008) suggested a mean value of 63,1 mm^2 / year with the coefficient of variation of 0,2 for D_m. Kwon et al. (2009) proposed D_m values as 46,04 mm^2 / year for sound concrete, 95,24 mm^2 / year for 0,1 mm crack width 13,66 mm^2 / year for 0,2 mm crack width and 246,61 mm^2 / year for 0,3 mm crack width. Shafei and Alipour (2013) suggested D_m as 214,44 mm^2 / year. Zhu et al. (2015) used 63,07 mm^2 / year for surface averaged diffusion coefficient. On the other hand Özdemir et al. (2015), suggested D_m values as 30 mm^2 / year, 80 mm^2 / year and 600 mm^2 / year for structures having mild, moderate and high aggressiveness respectively.

2.3. 2 Decrease in Steel Reinforcement Area

Corrosion leads to decrease in reinforcement area. Different researchers proposed similar formulas to predict area loss of reinforcement due to corrosion. Formulas are generally proposed as a function of corrosion rate, noncorroded diameter of reinforcement and exposed time to corrosion. Main formula to find reduced diameter of corroded steel bars is as follows:

$$D_{(t)} = D_{(0)} \propto 0,0116 \quad i_{corr} \quad t \tag{2.13}$$

Where $D_{(t)}$ is the reduced diameter of reinforcement in mm, $D_{(0)}$ is the initial diameter of steel bars, 0.0232 is the corrosion rate conversion factor from μA / cm^2 to mm / year, i_{corr} is the corrosion rate in μA / cm^2 and t is the time elapsed since the initiation of corrosion in years. α is the constant and differs from study to study. Gonzalez (1995) claimed that α varied from 4 to 8 depending on study on specimens subjected to repeated periods of wetting and drying in chloride environment. On the other hand Tuutti (1982) found a range from 4 to 10 for α constant.

2.3. 3 Decrease in Yield Strength of Steel Reinforcement

In addition to decrease in steel reinforcement area, corrosion causes decline in yielding strength of steel bars. Du et al. (2005) suggested an empirical equation in order to calculate residual strength of corroded reinforcement as follows:

$$f = (1 \quad 0,005 \, Q_{corr}) f_y \tag{2.14}$$

Where f is the yield strength of corroded steel bars, f_y is the initial yield strength of noncorroded steel bars and Q_{corr} is the amount of reinforcement area loss due to corrosion (%).

Above formula was used by different researchers such as Saad et al. (2014), Shafei et al. (2014), Tapan and Aboutaha (2008).

CHAPTER 3

ANALYSIS PROCEDURE

An analysis procedure is formed as shown in Figure 3.1 in order to explain design steps.
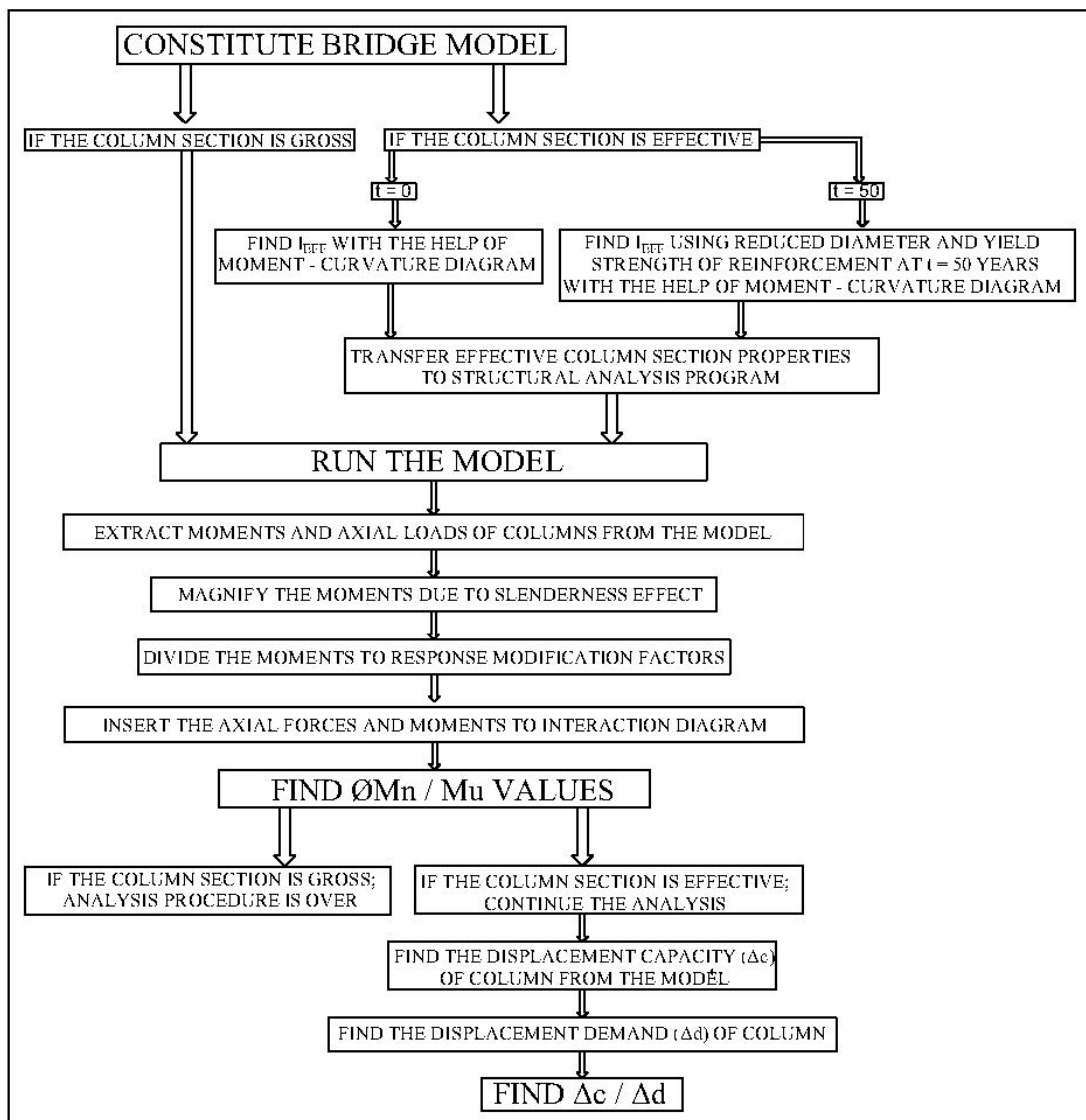
Figure 3.1: Analysis Flow Chart

3.1 Bridge Definition

The bridge models used in analytical studies were selected based on the most common types found in Turkish bridge engineering practice. The seismic evaluation of bridges not only included common geometric properties but also included the aged condition.

At each set, the span length, the superstructure cross-section, the bearings and the number of spans were the same while the pier heights and the pier cross-sections were different. The investigated geometric parameters, x_1 and x_2, were presented in Figure 3.2. x_1 represented the pier height of 3, 6, 9 and 12 meters. x_2 could take values of 1,25, 1,5, 2 and 3 meters. The selection of x_1 and x_2 represented the majority of real cases that could be found in Turkish bridge stock. The other features of the bridges were explained in the following paragraphs.
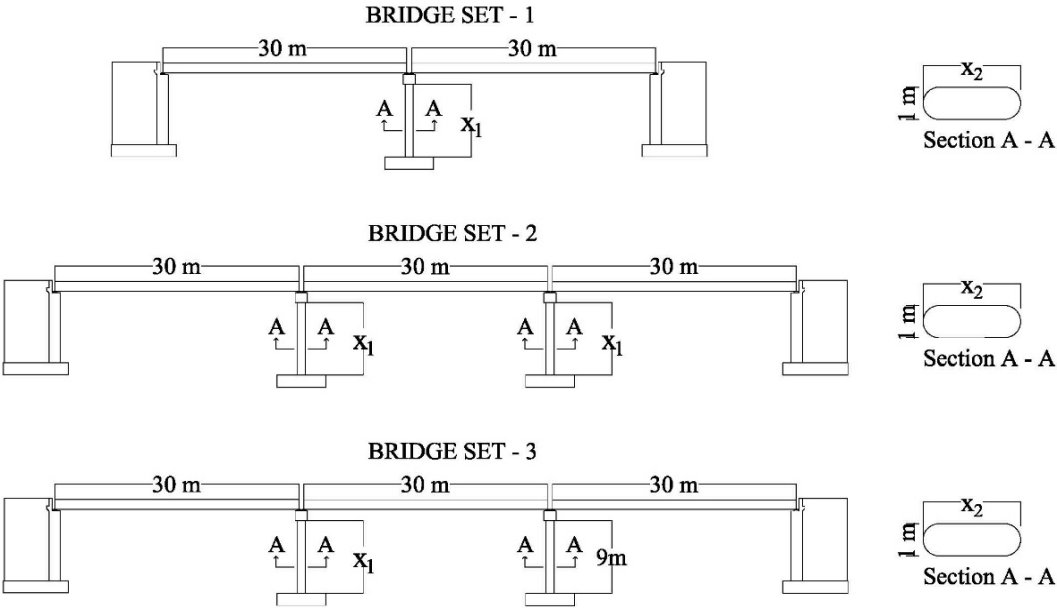
Figure 3.2: Investigated Geometric Parameters

The bridges under investigation had the same 13,0m wide slab on multiple girders composed of ten simply supported pre-stressed I girders spaced with 1,3m. The

width of the highway lanes was selected as 10,0m for three traffic lanes. Typical view of bridge cross section and layout of beams were shown in Figure 3.3.
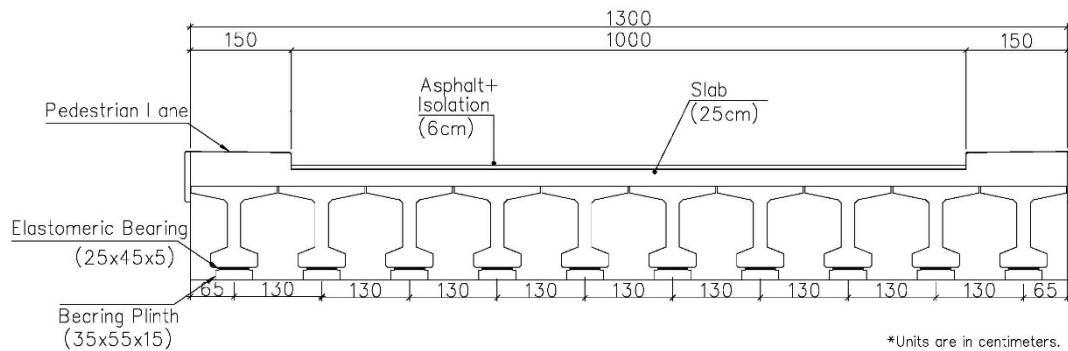
Figure 3.3 : Bridge Cross Section in Transverse Direction

Bridge models had a constant span length of 30m and each span had a 1,2m girder depth. For bridges consisted of simply supported pre–stressed I girders, the most convenient span length is between 15 m and 40 m. Considering these limits, 30m span length is chosen.

The same rectangular cross section was used for a 13 m long cap beam, a common section for hydraulic bridges as shown in Figure 3.4. Beam and column layouts in cap beam were also presented in Figure 3.5.
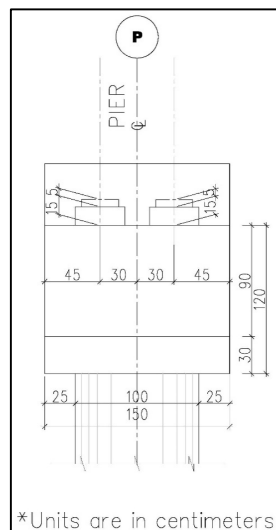
Figure 3.4: Cap Beam Cross Section

29
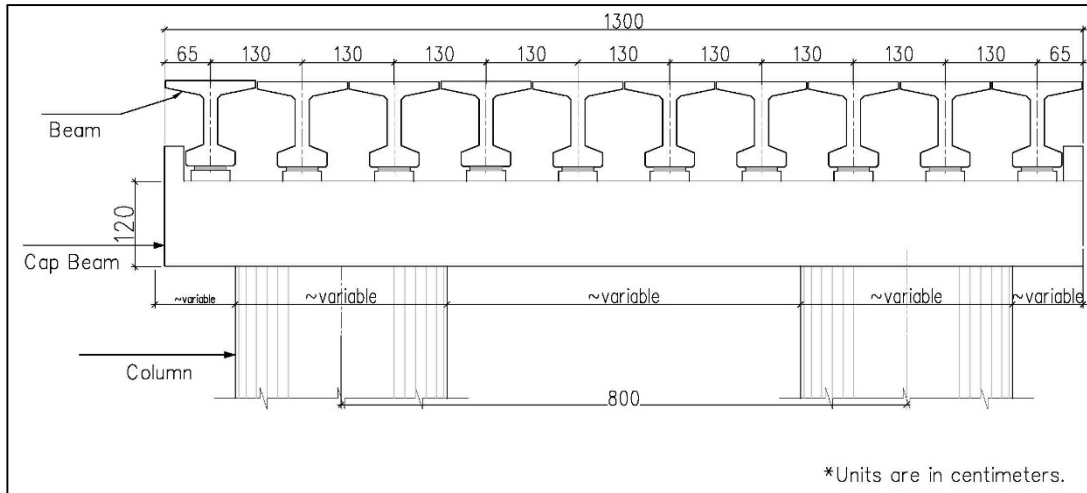
Figure 3.5: Cap Beam Layout

Column spacing measured from centerline to one other centerline was 8,0m. The clear cantilever lengths of cap beams were variable since the column width was not constant. The bridge was assumed to have no skew in plan and no horizontal curve alignment.

The seismic performance analyses of bridges include aging and deterioration effects in models per different ages. Bridges have been investigated at new condition, t = 0, and at aged condition, t = 50 years. The analyses also looked into cracked and uncracked condition of piers determined from moment-curvature relationship to effective stiffness evaluation. Aged condition models consider reduction in steel reinforcement area and steel yield strength from start to 50 years.

In the scope of this study, 144 different computer models were generated based on the analysis parameters matrix. Models can be divided three parts respectively; Set-1, Set-2, Set-3.

Table 3.1: Analysis Matrix

Bridge Set	x_1 (m)	x_2 (m)	Condition	Pier Cross Section
1	3, 6, 9, 12	1,25, 1,5, 2, 3	New, Aged	Cracked, Uncracked
2	3, 6, 9, 12	1,25, 1,5, 2, 3	New, Aged	Cracked, Uncracked
3	3, 6, 9, 12	1,25, 1,5, 2, 3	New, Aged	Cracked, Uncracked

3.2 Model Description

All bridges were modeled in structural analysis software, SAP2000 using the same modeling technique. Bridge models comprised of two main groups namely, superstructure, and substructure. In the following parts, these two main groups will be explained in detail. As the elements of bridge models, beam girder, cap beam, elastomeric bearings, and columns were shown in Figure 3.6. Among these elements, girders, cap beams, and elastomeric bearings were the parts of superstructure, whereas, the columns constituted the substructure.
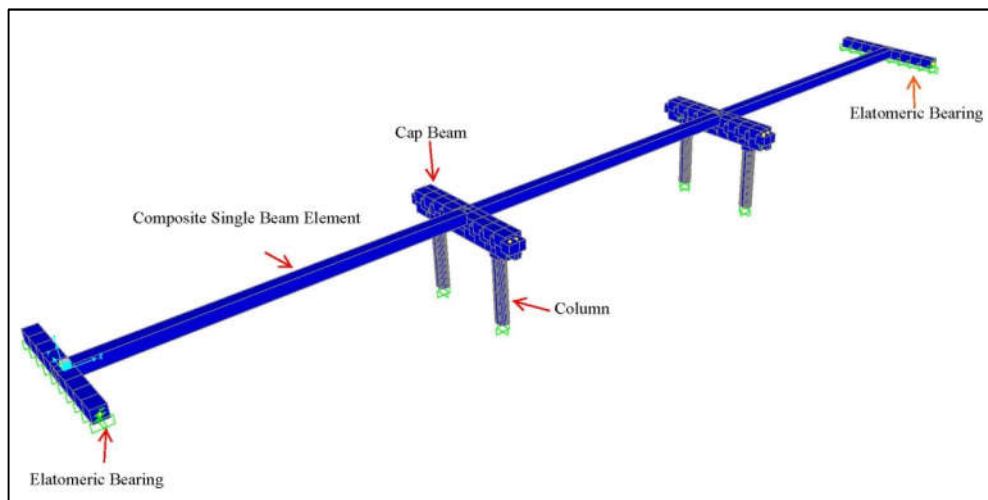
Figure 3.6: Elements of Model

3. 2. 1 Superstructure Modeling

Bridge superstructure consisted of beams, cap beam, and elastomeric bearings. The real focus of the study was to investigate column response after earthquake and additively to embed the corrosion effect on the columns. Therefore, superstructure was modeled in a very simple form. It had been known that the slab-on-multiple girder models with equivalent beam elements almost give similar results with detailed FEM models for pier seismic evaluation as also documented by Domanic (2008).

Domanic (2008) made a sensitivity analysis to determine the effect of different modeling techniques on bridge dynamic response. Four different models were generated. First model was a detailed model with staged construction analysis. Second model was again a detailed model without staged construction analysis. In third model, whole superstructure was represented with single beam, called simple model and cap beam stiffness was included. Finally, fourth model was simple model with rigid cap beam stiffness. Obtained pier moments were compared. Results showed that least error was occurred in fourth model, which was approximately 15% in average. Periods of fundamental modes were very close to each other. This study showed that whole superstructure could be modeled with single beam not to cause a significant error. Therefore, slab on multiple girders were represented with composite single beam elements

To have an equivalent beam element, stiffness and mass properties of the whole superstructure were superposed to a single element using frame section. The deck and the girder had different compressive strengths and elastic modulus of concrete. Each girder was made composite to the deck and the tributary deck width on a girder was usually equal to girder spacing. The deck concrete properties needed to be transformed into girder concrete properties to determine a single I_{tr} and A_{tr} for one single composite girder. The deck width or in this case, the girder spacing needed to be multiplied with modular ratio of E_{deck} / E_{girder}, to execute this transformation. For the entire slab on multiple girder structure, the equivalent I_x^*, I_y^* and A was

32

computed by multiplying the single composite girder properties with number of girders (n).

	A (m²)	I_{xc}(m⁴)	I_{yc}(m⁴)
Girder	0.540	0.103	0.031
Composite Section	0.805	0.183	0.056
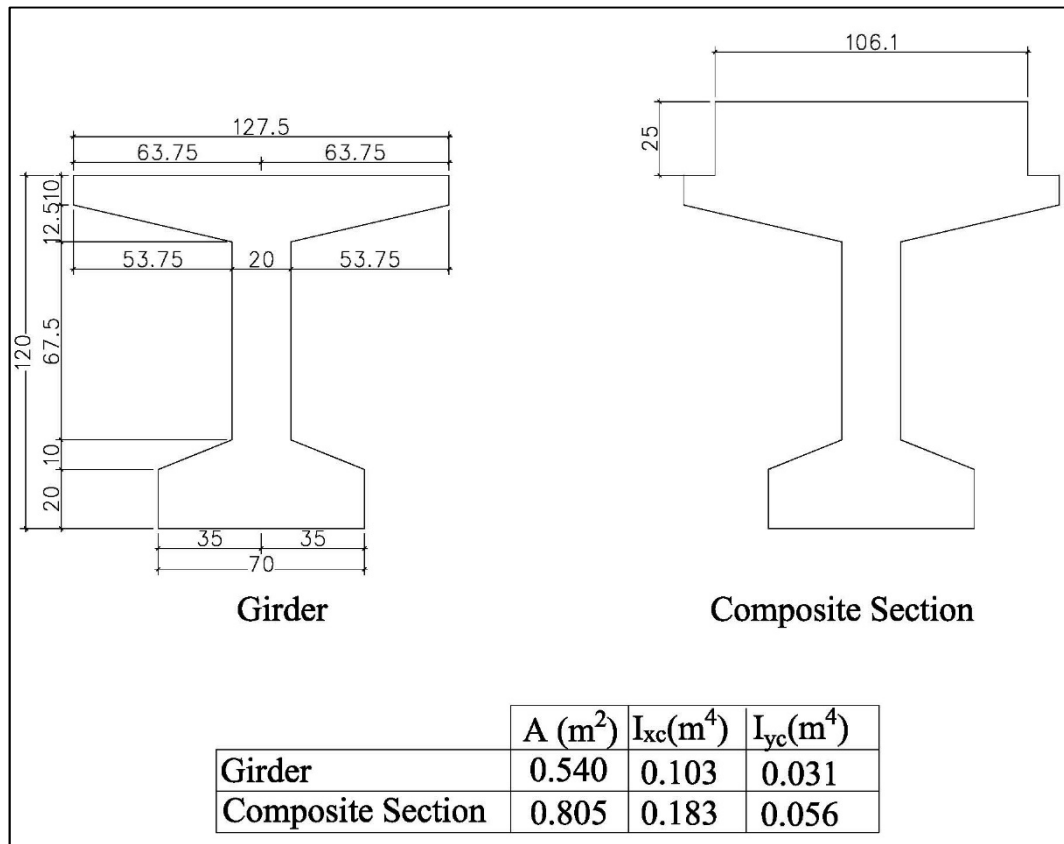
Figure 3.7: Girder and Composite Section Properties

$A^* = n \times A_{cc}$ $A^* = 8.05$ m²
$I_x^* = n \times I_{xc}$ $I_x^* = 1.83$ m⁴
$I_y^* = n \times I_{yc} + A_{cc}(d1^2 + d2^2 + d3^2 + d4^2 + d5^2) *2$ $I_y^* = 112.79$ m⁴
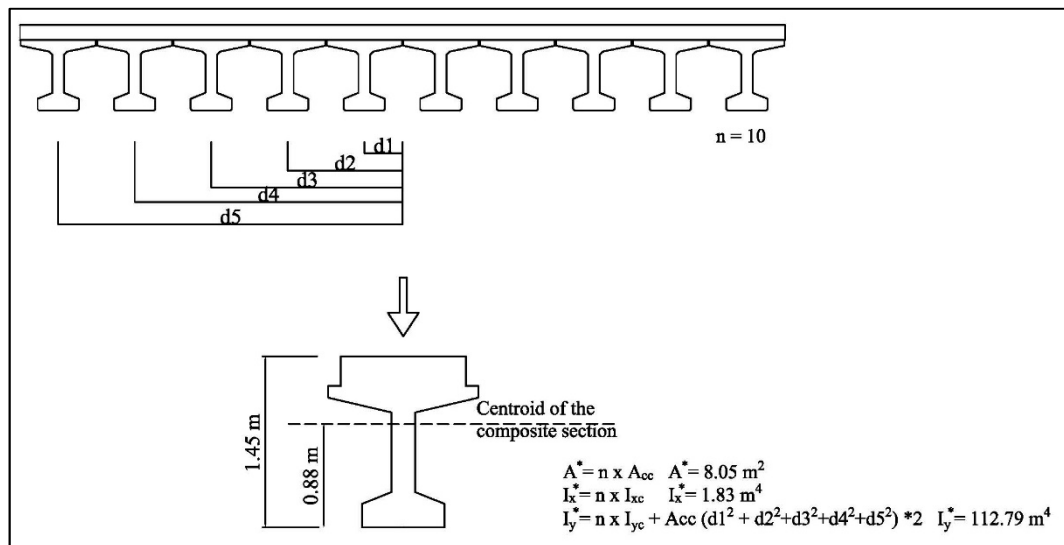
Figure 3.8: Equivalent Section Properties

33

Highway structure was modeled in longitudinal direction in the elevation at the neutral axis of the equivalent composite section of slab on multiple girder structure. It was divided into several segments along its length. Moment releases were assigned to both ends of each span to simulate simply supported span response. For supports, no horizontal or transverse restraints were defined for this equivalent element.

Cap beam was modeled as a rectangle frame section of 13 m length. It was modeled in the elevation of the sum of centroid of the composite section and height of the elastomeric rubber. No restraint was defined in the cap beam.

Throughout the cap beam, "rigid" frames were used to represent the locations of beams. Rigid frames were placed with a spacing of 1,3 m, which is equal to beam spacing in transverse direction. They were modeled from top of the slab to the centroid of composite slab in vertical direction. Rigid frames were defined as weightless elements, which were shown in Figure 3.9.
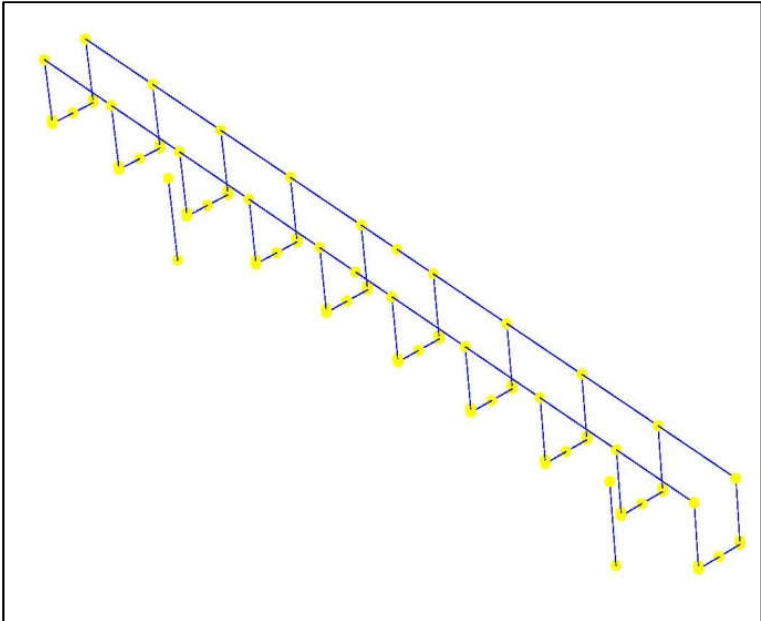
Figure 3.9: Rigid Elements

Elastomeric bearings were designed to resist loads and to transduce the movement. They were connected to superstructure by link elements. Number of link elements

was determined considering the number of beams. In abutments, number of elastomeric bearings equals to number of beams but in piers double the number of beams was selected. By this way, all bearings were modeled individually. Bearing dimensions were 250 x 500 x 50 mm as indicated before (Figure 3.10).
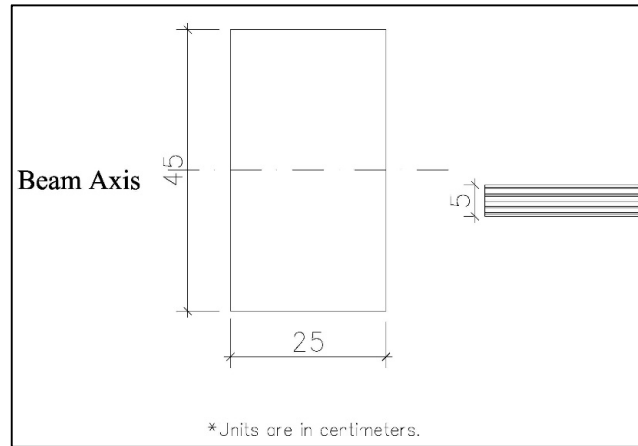
Figure 3.10: Elastomeric Bearing Dimensions

Elastomeric bearing physical properties were transferred to the SAP2000 by finding rotational and translational stiffness values. These values were calculated according to AASHTO Division 1A, Section 14 (2007). Accordingly, translational stiffness coefficients were calculated in bridge longitudinal and transverse direction, on the other hand vertical stiffness coefficients were determined in vertical direction. Rotational stiffness's were ignored.
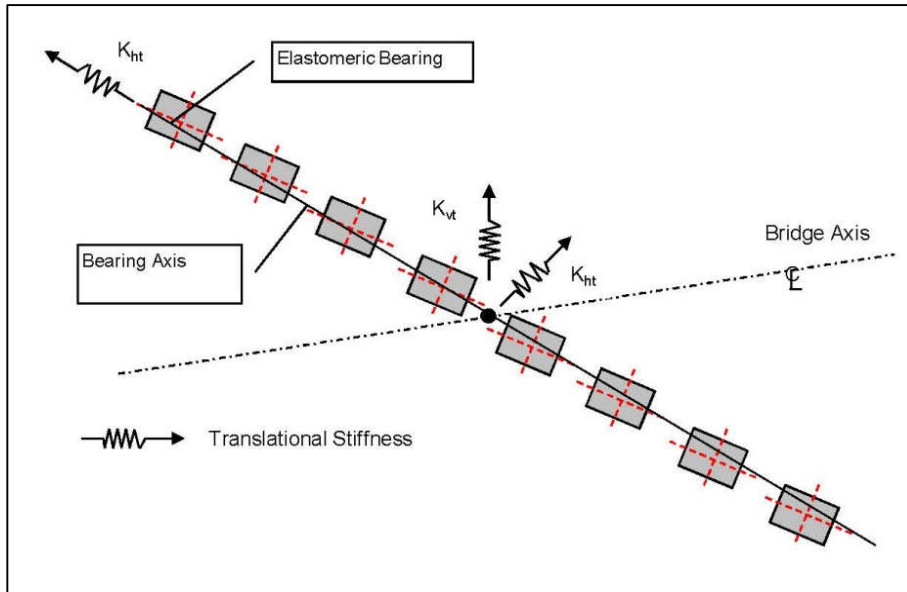
Figure 3.11: Elastomeric Bearing Representation

Calculation steps for translational stiffness coefficients were given below.

$G_b = 10 \text{ kg} / \text{cm}^2$: Shear Modulus Of Bearing   (AASHTO Table 14.6.5.2-1)

$L_{bp} = 45 \text{ cm}$: Bearing Length

$W_{bp} = 25 \text{ cm}$: Bearing Width

$A_{bp} = 1125 \text{ cm}^2$: Bearing Cross Sectional Area

$h_{bp} = 4 \text{ cm}$: Height Of Elastomeric Parts

$n_{layer} = 4$: Number Of Elastomeric Parts

$\Delta_{bp} = 1 \text{ m}$: Unit Displacement

$\gamma_{bp} = \Delta_{bp} / h_{bp} = 25$: Rotation For Unit Displacement   (3.1)

γ_{bp} : Rotation For Unit Displacement

$v_{bp} = \gamma_{bp} \cdot G_b = 24.52 \text{ MPa}$ (3.2)

v_{bp} = Shear Stress

$V_{bp} = v_{bp} \cdot A_{bp} = 2.76 \text{ kN}$ (3.3)

$k_{ht} = V_{bp} / \Delta_{bp} = 2700 \text{ kN} /\text{m}$ (3.4)

k_{ht} = Translational Stiffness Coefficient For One Bearing

Calculation of vertical stiffness coefficients were given below.

$$\sigma_{bp} = W_{pier} / (L_{bp} . W_{bp} .n_{bp}) \tag{3.5}$$

W_{pier} = 748 kN : Weight of superstructure

σ_{bp} = 6523,82 kPa

$$SF = (L_{bp} . W_{bp}) / (2. h_{layer}. (L_{bp} + W_{bp}) = 8,0 \tag{3.6}$$

ε_c= 0,04

In the case of shape factor (SF) was eight and σ_{bp} was 6523,82 kPa, ε_c was found as 4% according to AASHTO Figure 14.6.5.3.3-1 for 60 durameter reinforced bearings (Figure 3.12).

$$E = \sigma_{bp} / \varepsilon_c = 163,06 \text{ MPa} \tag{3.7}$$

$$k_{vt} = A_{bp} . E / h_{bp} = 449014 \text{ kN /m} \tag{3.8}$$

k_{vt} = Vertical Stiffness Coefficient For One Bearing

a) Elastomeric properties at different hardness (AASHTO Table 14.5.3.1)

b) Load Deflection Behavior of Elastomeric Bearings (AASHTO Table14.6.5.3.3-1)
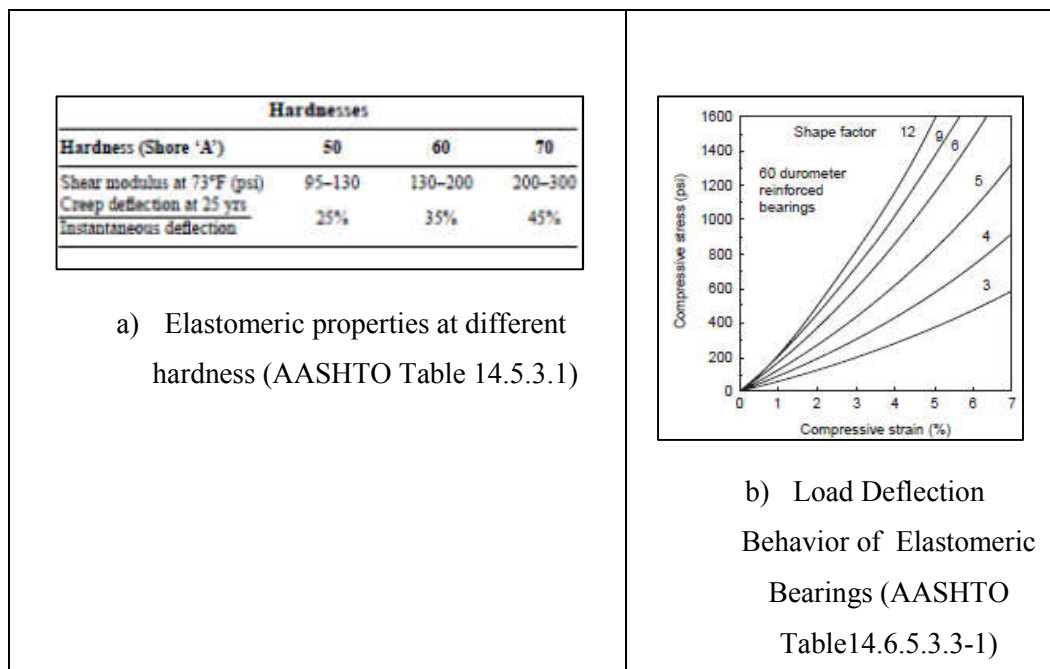
Figure 3.12: Elastomeric Bearing Properties

Elastomeric bearings have no horizontal restraints at the top end. At the bottom end, they were restrained in all directions in terms of translation and rotation.
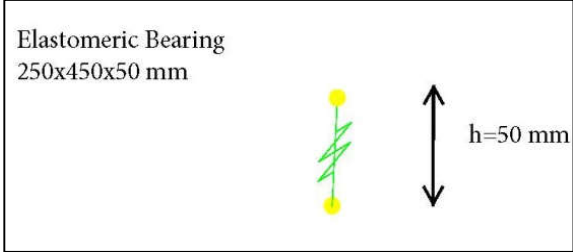
Figure 3.13 : Model view of elastomeric bearings

3. 2. 2 Substructure Modeling

Four different chamfered column sections in case of geometry were used to model substructure (Figure 3.14). In addition to the difference in section geometry, different column heights were also defined in the model, namely 3, 6, 9 and 12m. Two identical columns constituted each pier. Column elements were modeled as frame sections in structural analysis software and were placed 8m apart from each other. Column ends were restrained in all directions in terms of translation and rotation. For modeling, column heights were divided into smaller elements each having a height of 3m, in order to increase the accuracy of the model.
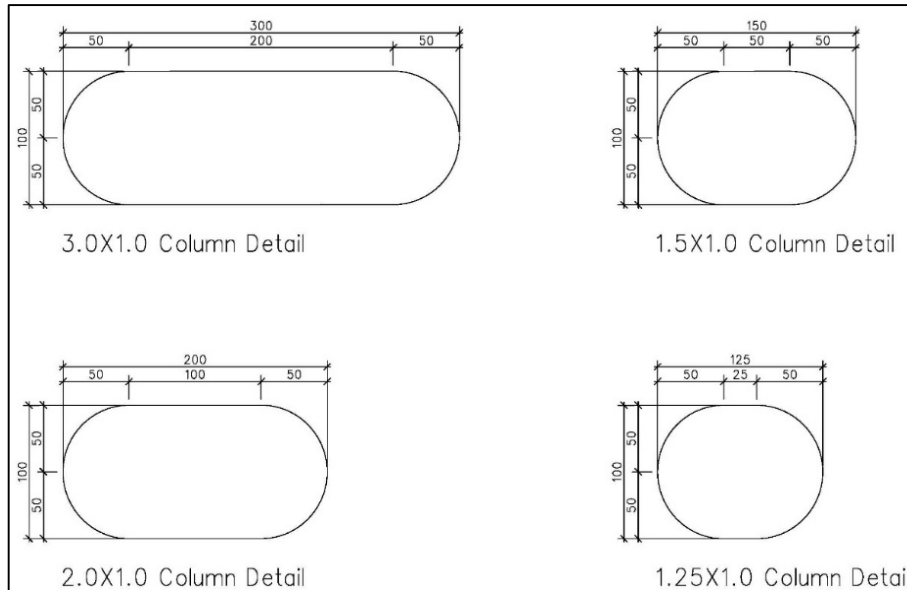
Figure 3.14: Column Sections
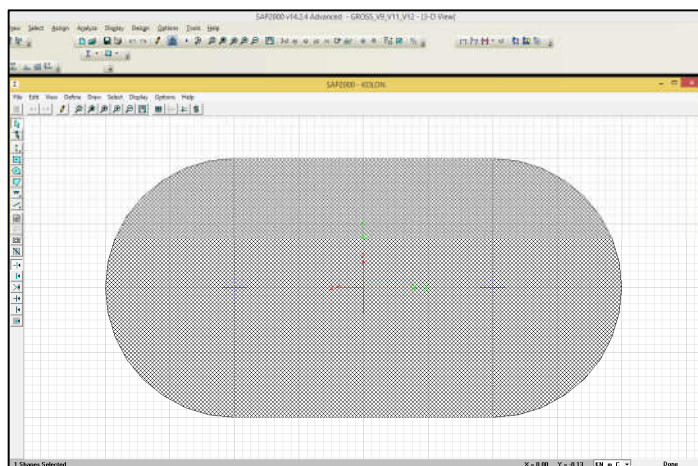
Figure 3.15 : Section Designer in SAP2000

3. 2. 3   Bridge Loads

In addition to the self – weight of the members used in the model, the weights of the components of the slab such as asphalt, walkway, precast facia element, hand rail were also applied as "Dead Load (DL)".

Other than the Dead Loads applied to the structure, the remaining loading was applied as stated in AASHTO Section 3.

As "Live Load (LL)" H30-S24 type of loading and related lane loading was applied to superstructure as shown in Figure 3.16. For traffic loads, load reduction factors stated in Section 3.12.1 of AASHTO were used in view of improbability of coincident maximum loading. Due to 10 m platform width, three lanes were loaded and load reduction factor was taken as 0,9 as shown in Table 3.2 Lane loads were amplified by impact factor due to fraction of live load stress with below formula.

$$I = 50 / (L + 37) \text{ (AASHTO 3.8.2.1)} \tag{3.9}$$

where;

I = impact fraction (maximum 30 percent);

L = length in meters of the portion of the span that is loaded to produce the maximum stress in the member.
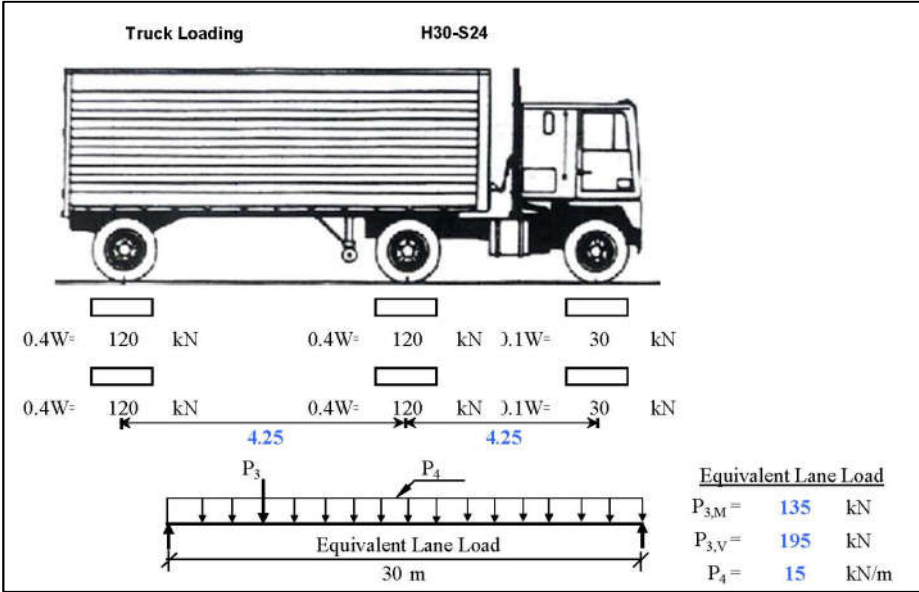
Figure 3.16: H30S24 Loading

40

Table 3.2: Load Reduction Factors, R (%)

Loading	Percentage of Design Load (%)
One or two lanes loaded	100
Three lanes loaded	90
Four lanes or more	75

Pedestrian load (PL) was acted as 3,0 kN / m^2 to the whole width of the walkway.

Braking loads (LF) were taken as 5 % of live loads without impact factor acted and they were applied 180 cm above the slab. Braking load was determined according to below formula.

$$LF = 0,05 \times ((15 \times L + 135 \times s) \times n \times R) \tag{3.10}$$

where;

15 kN / m and 135 kN are lane load values defined in H30S24 type of loading.

L = Total length of bridge in meters

s = Number of spans

R = Load reduction factor (%)

Wind loads (W&WL) were applied uniformly to the exposed area of structure including the floor system as stated in AASHTO Section 3.15. Wind load on superstructure (W) was taken as 2,4 kN / m^2 in transverse direction and 0,6 kN / m^2 in longitudinal direction. In addition, 1,95 kN / m^2 was applied as wind loading (WL) to substructure in both directions. Wind effect on live load was also taken into consideration. Wind loads of 1,5 kN/m and 0,6 kN/m were acted in transverse and longitudinal direction, respectively.

Forces developed due to temperature differences were also included in the model. Loads due to 19 ºC and 31 ºC temperature differences were applied to model that reflected positive and negative conditions, respectively.

Response spectrum analyses were performed for earthquake loads. Response spectrum is widely used concept in earthquake engineering to represent ground motion characteristics and their effects on structures. In terms of natural frequency and damping ratio, response spectrum expresses the maximum response of a single degree of freedom system. For a specified damping ratio and at different periods, response spectra curves give maximum responses for acceleration, displacement and velocity of single degree of freedom systems. With response spectra curves, peak responses of multi degree of freedom systems could also be determined.

Elastic seismic response coefficient (Cs) versus time function was generated according to AASHTO 3.6 Division 1A. As it was previously mentioned, all models were subjected to same environmental conditions. For this reason, it was assumed that all models were located in first seismic zone to reflect extreme design earthquake intensity and so acceleration coefficient (A) was taken as 0.4g according to Turkish Specifications for Structures to be Built in Disaster Areas, 1997 (Figure 3.17). Related return period was selected as 475 years.

AASHTO Bridge Classification divided bridges into four groups according to "An Importance Classification (IC)". Selected acceleration coefficient corresponded "D" importance class was provided in Table 3.3.

Table 3.3: Seismic Performance Category (SPC)

Acceleration	Importance Classification (IC)	
	I	II
A ≤ 0,09	A	A
0,09 < A ≤ 0,19	B	B
0,19 < A ≤ 0,29	C	C
0,29 < A	D	D
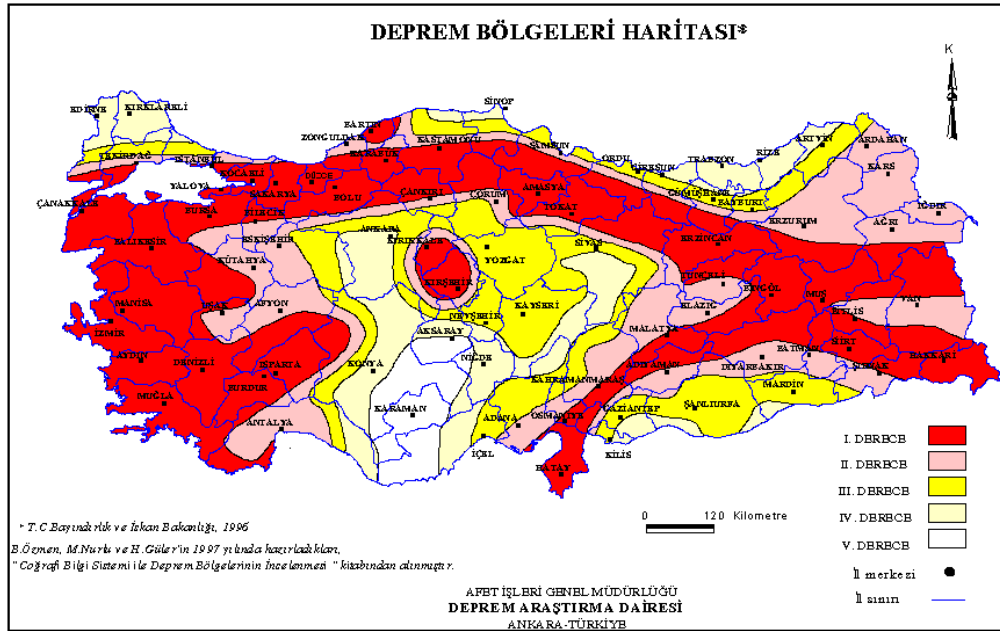
Figure 3.17: Turkey Seismic Zone Map (1996)

According to AASHTO Bridge Specifications, site condition effects were taken into consideration by the "Site Coefficient (S) ". AASHTO classified soils into four groups provided here.

Table 3.4: Soil Classification

Soil Profile 1	Rock of any characteristic, or stiff soil where soil depth is less than 60 m
Soil Profile 2	Stiff clay of deep cohesionless conditions where soil depth exceeds 60m
Soil Profile 3	Soft to medium stiff clays and sands where soil depth is 9 m or more
Soil Profile 4	Soft clays or silts where layer depth greater than 12 m

43

Soil Profile Type was selected as Soil Profile 1 in order to ignore soil-structure interaction.

Site coefficient was chosen as 1,0 according to Table 3.5. (AASHTO Table 3.5.1).

Table 3.5: Site Coefficients

S	Soil Profile Type			
	I	II	III	IV
	1,0	1,2	1,5	2,0

With detailed parameters above elastic seismic coefficient was calculated by the formula:

$$Cs = 1,2 \text{ x } A \text{ x } S / T^{(2/3)} \tag{3.11}$$

where;

A = Acceleration coefficient (A)

S = Soil profile coefficient (S)

T = Period (sec)

The value of Cs was limited by 2,5A. The determined response spectrum was sketched in Figure 3.18.
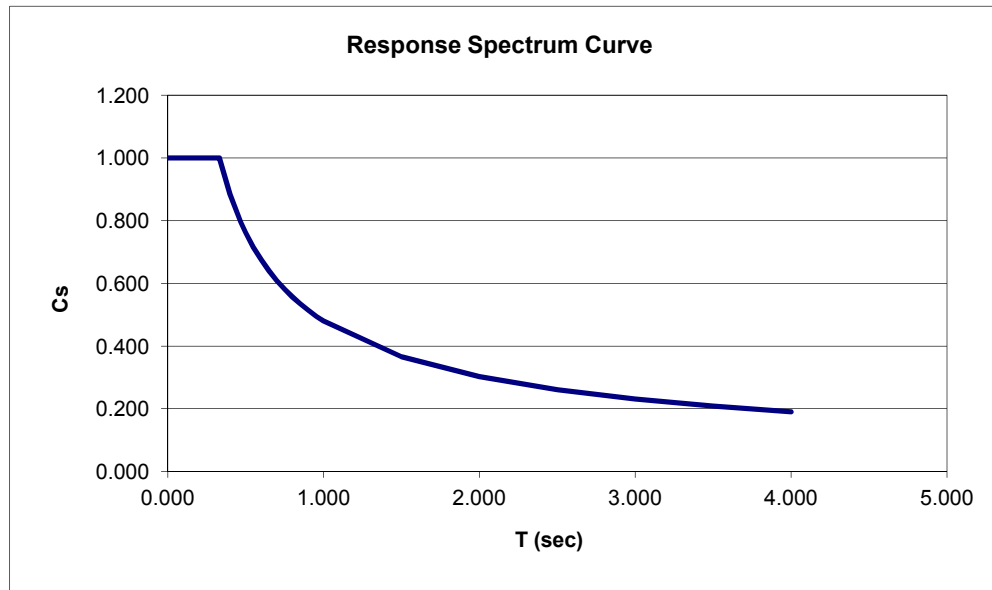
Figure 3.18 : Response Spectrum Curve

In the scope of this study, all models were analyzed for 60 modes of vibration.

3. 2. 4 Loading Combinations

Loading combinations were applied according to AASHTO Section 3.22 Table 3.22.1A. Total 9 numbers of combinations were considered during modeling.

Load Combination 1: 1,3 DL + 2,17 PL + 2,17 LL

Load Combination 2: 1,3 DL + 2,86 PL + 2,86 LL

Load Combination 3: 1,3 DL + 1,3 W

Load Combination 4: 1,3 DL + 1,3 PL + 1,3 LF + 0,39 W+ 1,3 WL + 1,3 LL

Load Combination 5: 1,3 DL + 1,3 PL + 1,3 LL + 1,3 RST

Load Combination 6: 1,25 DL + 1,25 W + 1,25 RST

Load Combination 7: 1,25 DL + 1,25 PL + 1,25 LF + 0,375 W + 1,25 WL + 1,25 LL +1,25 RST

Load Combination 8: 1,0 DL + DX   (Earthquake Combination)

Load Combination 9: 1,0 DL + DY   (Earthquake Combination)

45

where;

DX : Response value in longitudinal direction

DY : Response value in transverse direction

Perpendicular directions were not combined in load combinations. They were taken into account during column design.

Vertical response was ignored and it was not included in load combinations.

3.3   Material Properties

Modulus of elasticity was calculated according to AASHTO (8.7.1)

$$E_c = 0.0428 w_c^{1.5} \sqrt{f_c} \quad \text{(in MPa)} \tag{3.12}$$

Where;

w_c : Unit weight of concrete (in kg/m^3)

f_c : Compressive strength of concrete (in MPa)

Steel yield strength and modulus of elasticity were taken as $f_y = 420$ MPa and $E_s = 200000$ MPa, respectively.

Material properties used in the design were listed in Table 3.6.

Table 3.6: Material Properties

Structural Element	f_c' (MPa)	E_c (MPa)	Poissson Ratio	Thermal Expansion (1/°C*10^{-5})	Unit Weight kN/m^3)
Girder	45	35889	0.2	1.08	25
Cap Beam	30	29303	0.2	1.08	25
Column	30	29303	0.2	1.08	25
Rigid	45	35889	0.2	0.99	0

3.4   Pier Design

The columns were designed considering the gross and effective sections in weak direction in order to identify the effects of cracked and uncracked sections on column strength. For the analyses conducted considering uncracked sections, no changes were made in column properties. However for cracked section analyses, effective inertias were found with the help of moment curvature diagrams. Effective inertia over gross inertia was determined and acted on structural analysis program by section modifiers.

The behaviour of confined concrete and reinforcement could be idealised using the stress-strain models which was used for moment curvature diagrams. An Excel Spreadsheet used for creating the moment-curvature diagram. This spreadsheet created moment-curvature relationships of chamfered cross-sections that were subjected to axial loading. It could idealize the actual moment – curvature curve to a bilinear curve. At each neutral axis change, load difference was found by force balance and corresponding moment value was plotted. The procedure of moment – curvature analysis was as follows.

- Material properties in were defined.
- Clear cover was taken as 5 cm.
- Column section geometry was defined.
- Number and diameter of steel reinforcement were entered. Reinforcement ratio was taken as about 1 % for all column sections.
- Stress- strain models were generated according to Specifications for Buildings to be Built in Seismic Zones (2007). Obtained graphs were presented in Figure 3.19 and Figure 3.20.
- First value of the concrete strain was calculated considering applied axial load.
- Depth of neutral axis was calculated.
- Magnitude and location of force occurred in concrete were determined and related moment value was found and moment – curvature diagram was plotted.

47

- This procedure was repeated at each neutral axis change.
- Volumetric ratio of transverse reinforcement was taken as 0,006.
- Effective confinement coefficient was taken as 0,75.
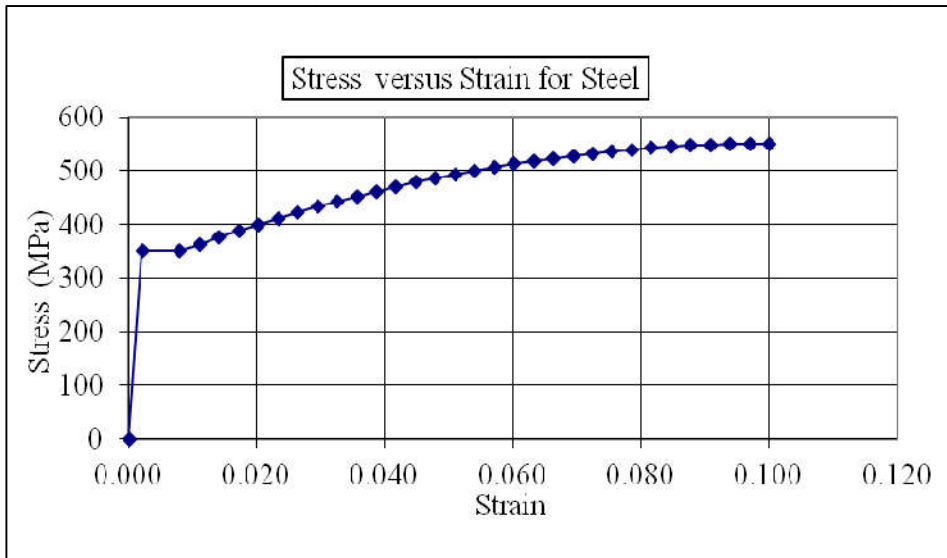
Figure 3.19: Stress- Strain Graph for Steel Reinforcement
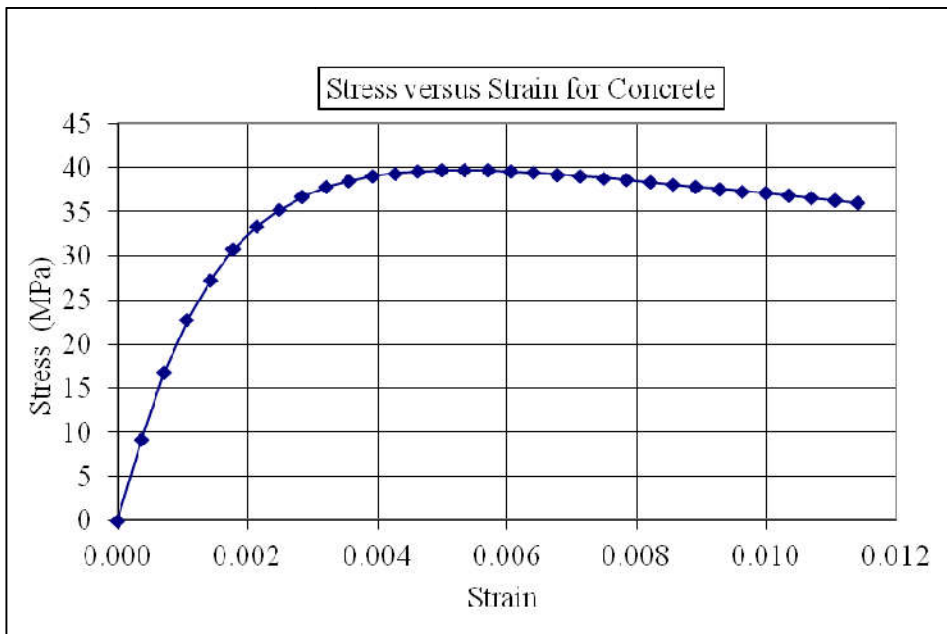
Figure 3.20 : Stress- Strain Graph for Concrete

Effective inertias were computed using the moment – curvature diagrams obtained.

The two main points to be examined in theses diagrams were the first yield point (ϕ'_y, M_y) which is the point when either the extreme tension reinforcement reaches yield strength or when the extreme concrete fiber reaches a strain of 0,0002 under compression and the ultimate point (ϕ_u, M_u) which represented the maximum capacity of the section in terms of moment and displacement.

First yield point gave the effective inertia by the formula below.

$$I_{EFF} = M_y / (E \times \phi'_y) \tag{3.13}$$
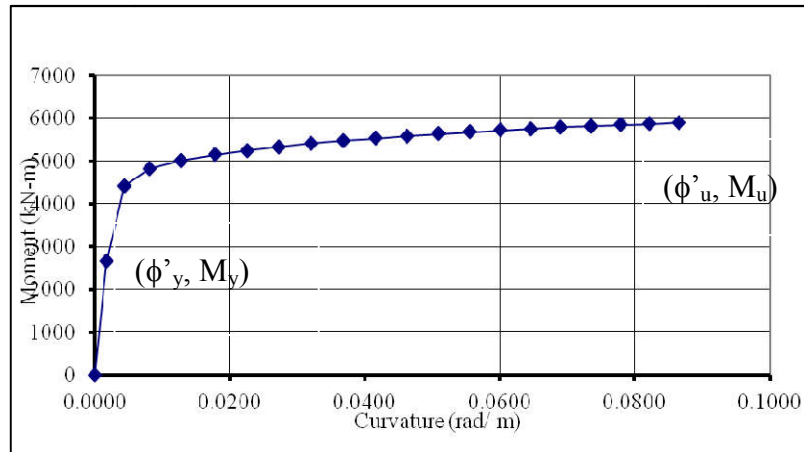
Figure 3.21 : Moment Curvature Diagram at t = 0
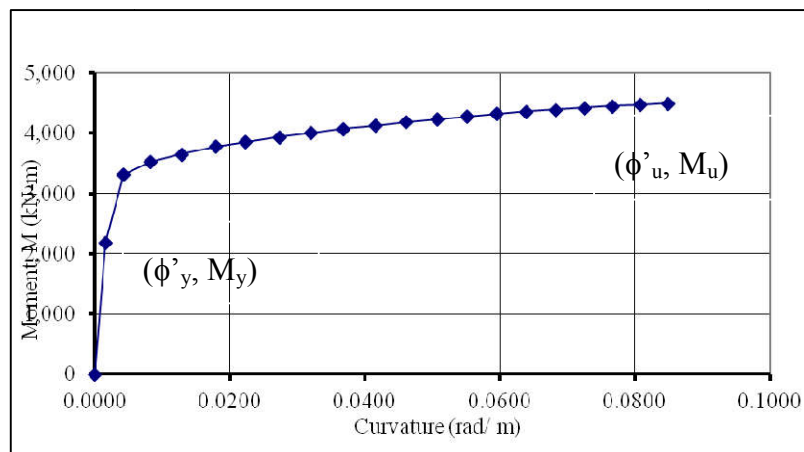
Figure 3.22: Moment Curvature Diagram at t = 50

49

Table 3.7: Inertias of Set-1 Columns

Column Section	I_{gross} (m^4) t = 0	I_{EFF} (m^4) t = 0	I_{EFF} (m^4) t = 50	Column Section	I_{gross} (m^4) t = 0	I_{EFF} (m^4) t = 0	I_{EFF} (m^4) t = 50
Column Height, H = 3m				**Column Height, H = 9m**			
3 x 1	0,2151	0,0727	0,0596	3 x 1	0,2151	0,0763	0,0632
2 x 1	0,1318	0,0532	0,0464	2 x 1	0,1318	0,0535	0,0501
1,5 x 1	0,0901	0,0328	0,0284	1,5 x 1	0,0901	0,0329	0,0286
1,25 x 1	0,0693	0,0283	0,0252	1,25 x 1	0,0693	0,0284	0,0264
Column Height, H = 6m				**Column Height, H = 12m**			
3 x 1	0,2151	0,0763	0,0630	3 x 1	0,2151	0,0763	00634
2 x 1	0,1318	0,0533	0,0498	2 x 1	0,1318	0,0569	0,0504
1,5 x 1	0,0901	0,0328	0,0285	1,5 x 1	0,0901	0,0341	0,0297
1,25 x 1	0,0693	0,0283	0,0263	1,25 x 1	0,0693	0,0296	0,0269

Table 3.8: Inertias of Set-2 Columns

Column Height, H = 3m				Column Height, H = 9m			
Column	I_{gross} (m^4)	I_{EFF} (m^4)		Column	I_{gross} (m^4)	I_{EFF} (m^4)	
Section	t = 0	t = 0	t = 50	Section	t = 0	t = 0	t = 50
3 x 1	0,2151	0,0727	0,0596	3 x 1	0,2151	0,0763	0,0632
2 x 1	0,1318	0,0534	0,0501	2 x 1	0,1318	0,0534	0,0501
1,5 x 1	0,0901	0,0328	0,0284	1,5 x 1	0,0901	0,0329	0,0285
1,25 x 1	0,0693	0,0283	0,0253	1,25 x	0,0693	0,0284	0,0264
Column Height, H = 6m				Column Height, H = 12m			
Column	I_{gross} (m^4)	I_{EFF} (m^4)		Column	I_{gross} (m^4)	I_{EFF} (m^4)	
Section	t = 0	t = 0	t = 50	Section	t = 0	t = 0	t = 50
3 x 1	0,2151	0,0727	0,0629	3 x 1	0,2151	0,0763	0,0632
2 x 1	0,1318	0,0534	0,0501	2 x 1	0,1318	0,0534	0,0501
1,5 x 1	0,0901	0,0328	0,0284	1,5 x 1	0,0901	0,0329	0,0285
1,25 x 1	0,0693	0,0283	0,0253	1,25 x	0,0693	0,0284	0,0264

Table 3.9: Inertias of Set-3 Columns

Column Height, H = 3m				Column Height, H = 9m			
Column	I_{gross} (m^4)	I_{EFF} (m^4)		Column	I_{gross} (m^4)	I_{EFF} (m^4)	
Section	t = 0	t = 0	t = 50	Section	t = 0	t = 0	t = 50
3 x 1	0,2151	0,0727	0,0596	3 x 1	0,2151	0,0763	0,0632
2 x 1	0,1318	0,0531	0,0464	2 x 1	0,1318	0,0534	0,0498
1,5 x 1	0,0901	0,0328	0,0283	1,5 x 1	0,0901	0,0329	0,0285
1,25 x 1	0,0693	0,0283	0,0252	1,25 x	0,0693	0,0284	0,0264
Column Height, H = 6m				Column Height, H = 9 m			
Column	I_{gross} (m^4)	I_{EFF} (m^4)		Column	I_{gross} (m^4)	I_{EFF} (m^4)	
Section	t = 0	t = 0	t = 50	Section	t = 0	t = 0	t = 50
3 x 1	0,2151	0.0727	0,0629	3 x 1	0,2151	0,0763	0,0632
2 x 1	0,1318	0,0533	0,0498	2 x 1	0,1318	0,0533	0,0501
1,5 x 1	0,0901	0,0328	0,0284	1,5 x 1	0,0901	0,0329	0,0285
1,25 x 1	0,0693	0,0283	0,0253	1,25 x	0,0693	0,0284	0,0264

Table 3.10: Inertias of Set-3 Columns

Column Height, H = 9 m				Column Height, H = 9 m			
Column	I_{gross} (m⁴)	I_{EFF} (m⁴)		Column	I_{gross} (m⁴)	I_{EFF} (m⁴)	
Section	t = 0	t = 0	t = 50	Section	t = 0	t = 0	t = 50
3 x 1	0,2151	0,0763	0,0632	3 x 1	0,2151	0,0763	0,0632
2 x 1	0,1318	0,0534	0,0501	2 x 1	0,1318	0,0534	0,0501
1,5 x 1	0,0901	0,0329	0.0285	1,5 x 1	0,0901	0,0329	0,0285
1,25 x 1	0,0693	0,0284	0.0264	1,25 x	0,0693	0,0284	0,0264

Column Height, H = 12 m				Column Height, H = 9 m			
Column	I_{gross} (m⁴)	I_{EFF} (m⁴)		Column	I_{gross} (m⁴)	I_{EFF} (m⁴)	
Section	t = 0	t = 0	t = 50	Section	t = 0	t = 0	t = 50
3 x 1	0,2151	0,0763	0,0632	3 x 1	0,2151	0,0763	0,0632
2 x 1	0,1318	0,0569	0,0504	2 x 1	0,1318	0,0533	0,0501
1,5 x 1	0,0901	0,0340	0,0297	1,5 x 1	0,0901	0,0329	0,0285
1,25 x 1	0,0693	0,0295	0,0265	1,25 x	0,0693	0,0284	0,0264

Column axial loads and moments were extracted from structural analysis program. Compression member design should be based on forces and moments determined from analysis of structure. This type of analysis should consider the influence of axial loads and variable moment of inertia on member stiffness and fix end moments. In addition to that, it should include effect of deflections on the forces and moments. Therefore, obtained moments were amplified by moment magnification due to slenderness effect according to AASHTO 8.16.5. In Figure 3.23, calculation of moment magnification factor in longitudinal direction of 6 m length column having 2,0 x 1,0m section dimensions was presented. Same procedure was applied in transverse direction, too. Parameters used in calculation could be seen with their definitions. Radius of gyration, r was square root of column cross- section area over column moment of inertia. Effective length factor of column was taken as two. However, moment coefficient could be calculated for members braced again sidesway and without transverse loads between supports with a formula but for all other cases it should be taken as one. k l_u / r value was limited to 100, since when it exceeded 100, detailed analysis was required. The effect of slenderness could be neglected when k l_u / r smaller than 22. In this study, moment magnification was not applied when k l_u / r was under 22. When k l_u / r was greater than 22, moments were multiplied with obtained moment magnification factors.

SLENDERNESS EFFECT

Calculations are based on AASHTO 8.16.5.

Column Cross-section =	Ag =	**1.78** m^2
Column Moment of Inertia =	Ix-x =	**0.13** m^4
Radius of Gyration =	r =	0.27 m
Column Moment of Inertia =	Iy-y =	**0.49** m^4
Radius of Gyration =	r =	0.53 m
Column Height =	lu =	**6.00** m
Effective Length Factor =	k =	**2.00**
Moment Coefficient =	Cm =	**1.00**

Strength Reduction Factor = $\phi = 0.9 - \dfrac{0.4\,P_u}{0.2\,f_c'\,A_g} = 0.741$

Vertical Load =	Pu =	**4251.06** kN
Maximum Dead Load Moment =	M$_{DL}$ =	**0** kNm
Modulus of Concrete =	Ec =	2.93E+07 kN/m^2
Concrete Compressive Strength =	f$_c'$ =	**30** MPa

AASHTO 8.16.5.2.5

Longitudinal Direction

$\dfrac{k * lu}{r}$ = 44.1 > **22** Slenderness Effect Will Be Consi

Critical Load = $P_c = \dfrac{\pi^2\,E\,I}{(kl_u)^2}$ AASHTO 8.16.5.2.7

$E\,I = \dfrac{\dfrac{E_c I_g}{2.5}}{1+\beta_d} = 1.54E+06$ $\qquad \beta_d = \dfrac{M_{DL}}{M_T} = 0$

$P_c =$ 105883 kN

Moment Magnification Coefficient

$\delta = \dfrac{C_m}{1 - \dfrac{Pu}{\phi\,Pc}} =$ **1.057**

Moment of the compressive member will be multiplied by using moment magnification coefficient.

Figure 3.23 : Slenderness Effect Spreadsheet

As mentioned earlier orthogonal forces were not combined in load combinations. It was done in this step. Orthogonal seismic forces were combined as the earthquake motion direction was uncertain and could occur in two perpendicular directions simultaneously. As a result of, seismic forces of a principal axis was calculated by

55

including 100% of the absolute value of force and moments of longitudinal direction to 30% of the absolute value of force and moments of transverse direction and vice versa. Combination of forces could be summarized with formulas below. In the formulas, M denotes moment and H denotes shear force.

$$M_x = M_x^L + 0,3\ M_x^T \qquad\qquad (3.13)$$

$$M_y = M_y^L + 0,3\ M_y^T \qquad\qquad (3.14)$$

$$M_x = 0,3\ M_x^L + M_x^T \qquad\qquad (3.15)$$

$$M_y = 0,3\ M_y^L + M_y^T \qquad\qquad (3.16)$$

$$H_x = H_x^L + 0,3\ H_x^T \qquad\qquad (3.17)$$

$$H_y = H_y^L + 0,3\ H_y^T \qquad\qquad (3.18)$$

$$H_x = 0,3\ H_x^L + H_x^T \qquad\qquad (3.19)$$

$$H_y = 0,3\ H_y^L + H_y^T \qquad\qquad (3.20)$$

Obtained forces and moments were divided Response Modifications Factors which were chosen from AASHTO Standard Specifications for Highway Bridges Seventh Edition, 2002, Table 3.7 (Division 1A). According to table in bent direction R should be taken as 5. On the other hand, if clear height over column section dimension ratio was greater than 2,5, pier could be designed as column, which gave R = 3. In this study, minimum column dimension was equal to one, so for all models clear height over minimum column dimension was greater than 2,5 (For column weak axis R = 3, for column strong axis; R = 5).

Model modified moments and axial loads were transferred to moment-axial load diagram after dividing only the moment term by R factor and combining seismic forces. Same reinforcement areas in moment - curvature diagrams were used. Clear cover was taken as 5 cm. Compression block depth coefficient, compression block width coefficient; concrete maximum strain and capacity reduction factor were taken from AASHTO Standard Specifications for Highway Bridges, Seventh Edition, 2002. For the same column height following procedure was applied. For each column height, column cross-section was started from 3,0 x 1,0, and continued 2,0 x 1,0, 1,5 x 1,0, 1,25 x 1,0 respectively. For each cross-section relevant $\phi M_n / M_u$

value was found from moment-interaction diagram by interpolation. This ratio showed that how much the section was overdesigned. It should be underlined that column design was made in bridge longitudinal direction which was weaker than transverse direction. It was assumed that column weak direction would give smaller $\phi M_n / M_u$ ratios.

Turkish practice uses "Force Based Design Method" and in column design, it is required that all axial load-moment pairs should be inside the moment-axial load diagram. An alternative method could be "Displacement Based Design". In this method, design evaluation methods are focused on displacements rather than forces. To understand dynamic response of columns, deformation performance should also be investigated. For this purposes, push over analysis were performed using a simple hand computation method described in Seismic Retrofitting Manual for Highway Structures: Part-1 Bridges (2013). It was believed that this method will yield to some conservative results compared to results of sophisticated softwares such as SAP 2000, LARSA and KSU_RC.

A displacement capacity evaluation of a bridge, or push – over analysis should be able to track nonlinear relationship between load and deformations for the columns and beams as the lateral load is monotonically increased from an elastic condition to failure (Seismic Retrofitting Manual for Highway Structures: Part-1 Bridges, Section 7.8). It means structural member capacities should be approximated from first yield to failure even in intermediate limit states. For this reason, deformations and rotations should be included in design procedure.

Stated manual suggests six different methods to evaluate the seismic performance of bridges, Method A, Method B, Method C, Method D1, Method D2 and Method E, respectively. Method A and Method B are for the bridges where seismic demand analysis is not required. In these two methods, capacities are checked for minimum load requirements. On the other hand, Method C calculates capacity / demand ratio for bridge components under seismic hazard. However, disadvantage of this method is that it focuses on individual component behavior rather than the response of a bridge as a whole structure. Therefore, it may overestimate overall vulnerability of a bridge. Besides all of these, Method D1 calculates the seismic demands by uniform

load method. A simplified bilinear strength curve is needed to determine capacity assessment. For each limit state, a capacity spectrum was utilized to find capacity / demand ratio for the bridge. However, this method could not be applied when the relatively different column displacements are observed. In this study, in Set 3, in different column heights different displacement values are determined. So, Method D1 was not applied. Method A and Method B were also eliminated because the fact that all the models were generated for first seismic zone. For Method E, nonlinear time history analysis is required. Method D2 was the most suitable method for this study. It determines seismic demands with elastic methods such as multi – mode response spectrum method or an elastic time history method. Evaluation of capacity depends on displacement capacity of individual piers and it was found by push – over analysis. This method is more advanced than other methods. It is also known as push - over method or the nonlinear static procedure (NSP).

Method D2 consists of two steps. Firstly, displacement capacity is found by push – over analysis. Secondly, displacement demands are determined by response spectrum analysis. Second step was done in structural analysis program and the first step would be explained in following lines.

The maximum displacement capacity could be determined by hand calculation for columns having simple geometry. Plastic hinge mechanism should be considered. It should be underlined that this method is based on individual pier capacity. Though, it is possible that for piers of different stiffness and strength force distribution may be unequally from pier to pier when the displacement values goes up and yielding begins. On the other hand, in demand calculations, this method considers the behavior of whole bridge.

Ultimate displacement, Δ_u, of a cantilever column under a lateral load was calculated by formula, according to Seismic Retrofitting Manual for Highway Structures: Part-1 Bridges, 7.8.1.1.

$$\Delta_u = \Delta_e + \Delta_p \tag{3.21}$$

Where Δ_e is the elastic component and Δ_p is the plastic component of displacement.

When the member reached the plastic strength, $\Delta_e = \Delta_y$, and nominal yield displacement was calculated by:

$$\Delta_y = \phi_y * L^2 / 3 \qquad\qquad (3.22)$$

where L is the fix end to free tip, was taken as column height and ϕ_y is the nominal yield curvature. ϕ_y was the same curvature, which was used calculating effective inertia.

For the plastic component, Δ_p was found by:

$$\Delta_p = \phi_p * L_p * (L-0,5\ L_p) \qquad\qquad (3.23)$$

where L_p is the plastic hinge length is given by:

$$L_p = 0,08 *L+0,022*f_{ye}*d_{bl} >= 0,044*f_{ye}*d_{bl} \qquad\qquad (3.24)$$

where f_{ye} is the yield strength of the longitudinal reinforcement and d_{bl} is the column longitudinal reinforcement diameter.

ϕ_p is the plastic curvature, which is equal to ϕ_u Figure 3.21.

Displacement demand was found from bridge models under seismic forces in bridge longitudinal axis (column weak axis). Obtained demand values were divided to ultimate displacement, Δ_u. For all models, same procedure was repeated. Displacement capacity over demand ratio $\Delta c / \Delta d$ versus $\phi M_n / M_u$ graphs was prepared. After the studies, a linear relation between $\Delta c / \Delta d$ and $\phi M_n / M_u$ was noticed. Relevant equations will be tabulated.

3.5   Proposed Deterioration Model

This study covered the assessment of seismic performance of existing river bridges including deterioration effects in Turkey. It was assumed that investigated bridge models were exposed to moderate environmental conditions. So, aging parameters reflected the moderate aggressiveness conditions in terms of chemical substance.

Corrosion did not start till the surface chloride content reaches the critical chloride concentration. This value was taken as 1,2 kg / m^3 which was one of the proposed

values in recent studies. Required time in order to start corrosion was taken as 5 years. In literature this value varies from 5 to 12,66 years.

Deterioration formula proposed by Guo et. al (2014) was used to determine corrosion rate with some modifications. The formula assumed constant chloride content that should change as ingress of chloride ions increases. So, chloride content in steel surface (CI) in (3.25) was made function of time with the above formula (3.26).

$$i_{cor}(t) = \frac{(1-w/c)^{-1.64}}{d_c} \frac{(CI + CI_{Th})}{2CI_{Th}} \left\{ \frac{(T_{high} - T_{low})\sin[2\pi(t-a_s)]}{8.6(t-a_s)} + 7.6 \right\}$$

$$e^{-228\ 3(1/28\ 415 - 1/T_{mean}) - 6000(mc - 0.75)^6} \tag{3.25}$$

where CI was defined as follows:

$$C(x,t) = C_S \left[1 \quad erf\left(\frac{x}{2\sqrt{D_m\ t}}\right) \right] \tag{3.26}$$

x was the cover depth and taken as 50 mm which was used for columns in engineering practice.

where D_m was expressed as follows:

$$D_m = \frac{1}{t} \int_0^t D_{ref} \left(\frac{t_{ref}}{\tau}\right)^m d\tau = \frac{D_{ref}}{1-m} \left(\frac{t_{ref}}{\tau}\right)^m \qquad (t < t_R) \tag{3.27}$$

$$D_m = D_{ref} \left[1 + \frac{t_R}{t} \left(\frac{m}{1-m}\right) \right] \left(\frac{t_{ref}}{\tau}\right)^m \qquad (t \geq t_R) \tag{3.28}$$

Surface chloride content was taken as 4,5 kg / m³ and reference diffusion value was taken as 80 mm² / year since the bridges were river bridges (Table 3.11) . For t_R , t_{ref} and m; 30 years, 28 days and -0.3 were used respectively to be consistent with recent studies.

Table 3.11: Surface Chloride Content Cs (kg / m³), and Reference Diffusion Values D_{ref} (mm² / year) for Different Environmental Conditions (Özdemir and Topkaya, 2015)

Aggressiveness	C_s (kg / m³)	D_{ref} (mm² / year)
Mild	2	30
Moderate	**4,5**	**80**
High	12	600

Water – cement ratio was taken as 0,5 and moisture content was assumed as 0.75. Seasonal constants were taken from Guo et al (2014). Maximum and minimum temperatures were taken as 39º and -11,2º respectively. These are the temperature values of Çanakkale and taken from Turkish State Meteorological Service. Çanakkale was selected as the location since there was a study conducted by Caner et al. (2008) which investigated the condition of highway bridges on a part of Route D200 connecting Bursa to Çanakkale.

The parameters used in order to calculate corrosion rate were provided in Table 3.12.

Table 3.12: Parameters Used in Corrosion Rate Calculation

Parameter	Value
Initiation time (years)	5
t_{ref} (days)	28
t_r (years)	30
D_{ref} (mm^2 / year)	80
CI_{Th} (kg / m^3)	1,2
C_s (kg / m^3)	4,5
w / c	0,5
d_c (mm)	50
mc	0,75
as; winter, spring, summer, fall	0,25; 0,07; 0,7; 0,43
T_{high} (K)	312
T_{low} (K)	261.8
T_{mean} (K)	286.9

The results of the analyses to determine corrosion rate with time were presented in Figure 3.24. Obtained corrosion rates for each ten years were tabulated in Table 3.13. The graph was similar to Guo's proposed corrosion rate model (2004). At early ages, it increased about 2,5 µA / cm^2 and it decreased sharply. Then it oscillated around 1 µA / cm^2.
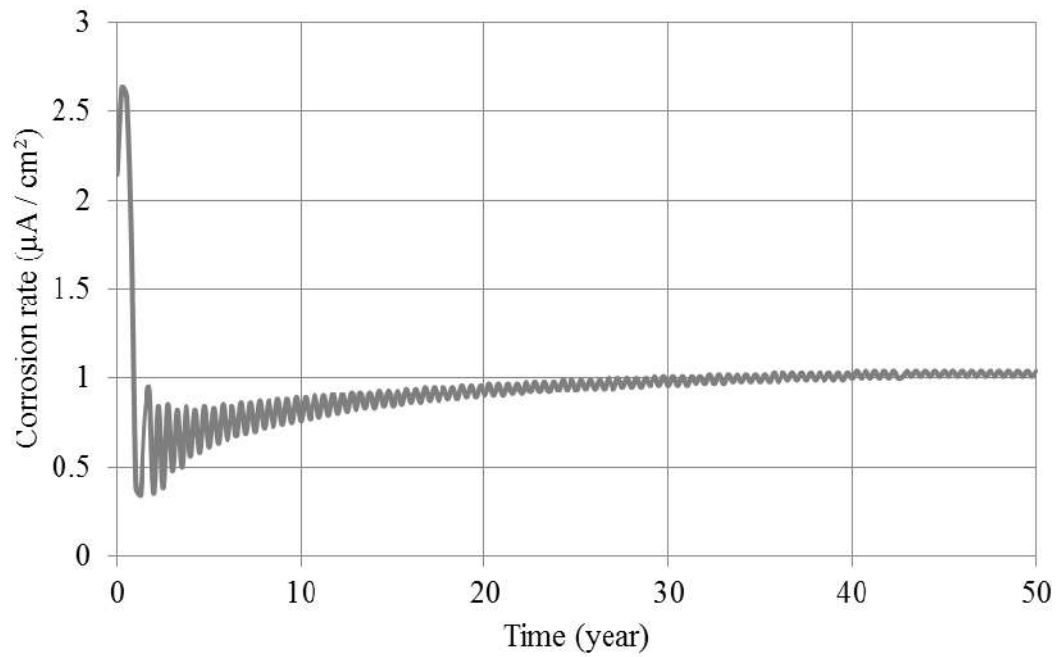
Figure 3.24: Corrosion Rate versus Time

Table 3.13: Corrosion Rate in Time

t (years)	i$_{corr}$ (µA / cm^2)
10	0,73
20	0,89
30	0,96
40	1,00
50	1,03

Reinforcement area loss due to corrosion was found with the formula expressed as follows:

$$D_{(t)} = D_{(0)} \propto 0,0116 \quad i_{corr} \quad t \tag{3.29}$$

where α was taken as 8 in the range of proposed values within the literature.

Reduced yield strength of reinforcement was calculated with the formula defined as follows:

$$f = (1 \quad 0,005 \, Q_{corr})f_y \tag{3.30}$$

Obtained diameter and yield strength values of reinforcement bars were provided in Table 3.14.

Table 3.14: Reduced Diameter and Yielding Strength Values of Corroded Reinforcement

t (years)	ϕ (mm)	ϕ_{new} (mm)	f_y (MPa)	$f_{y,new}$ (MPa)
10	26	25,32	420	409,20
20	26	24,36	420	394,38
30	26	23,34	420	379,28
40	26	22,31	420	364,63
50	26	21,26	420	350,44

Table 3.15: Percentage of Area and Strength Loss of Corroded Reinforcement

t (years)	Area loss (%)	Strength loss (%)
10	5,14	2,57
20	1,20	6,10
30	19,39	9,70
40	26,37	13,18
50	33,13	16,56

Available studies which aimed to determine deterioration of structures due to corrosion could be divided into three. First method (Method A) depends on only visual inspection (Caner et al. 2008). But this method is based on subjective decisions which can change from person to person even if same person makes different evaluations in different times. Second method (Method B) is more comprehensive than first method. It depends on concrete characteristic and environmental conditions but it ignores changes in corrosion rate with time (Özdemir et al.2015, Stewart and Rosowsky (1998), Alonso et al. (1988), Martinez and Andrade (2009)). Method C is the most complex one; it was developed by Guo et al. (2014). It shows similarity between available data. However, in this method chloride content assumed as constant during propagation phase which is expected to increase as the ingress of chloride increases. The model used in this study is based on the one proposed Guo et al. (2014) with some modifications in terms of selection of the chloride content value. Similarities and differences between methods were summarized in Table 3.16.

Table 3.16: Comparison of Existing Deterioration Models

Description	Method			
	A	B	C	Proposed
Geometry	✓	✓	✓	✓
Concrete Cover	☒	✓	✓	✓
Chloride Content	☒	✓	✓	✓
Chloride Content Change	☒	☒	☒	✓
Diffusion Coefficient	☒	✓	✓	✓
w / c	☒	☒	✓	✓
Temperature	☒	☒	✓	✓
Seasonal Constant	☒	☒	✓	✓
Crack width	✓	✓	☒	☒
Corrosion rate	✓	☒	✓	✓
Visual Inspection	✓	☒	☒	☒
Reinforcement Area Loss	☒	☒	✓	✓
Reinforcement Strength	☒	☒	✓	✓
Structural Analysis	☒	☒	✓	✓

CHAPTER 4

ANALYSES RESULTS

4. 1   Modal Analyses Results

Seismic responses of selected bridges were determined by use of response spectrum analysis. In response spectrum analysis, sixty modes were taken into account to obtain a total mass participation larger than 90%. Longitudinal and transverse modes could be detected explicitly by having large mass participation ratios at the corresponding frequency of a particular mode. The first mode was usually observed in longitudinal direction of all bridge models where the following modes were typically the transverse movement of the piers.

Modal shapes of first two modes were provided in Figure 4.1 and Figure 4.2 for a model which has 6m height of column having 3,0 x 1,0 cross section dimensions from Set–1. This model was analyzed for uncracked column section at the beginning of bridge life time.
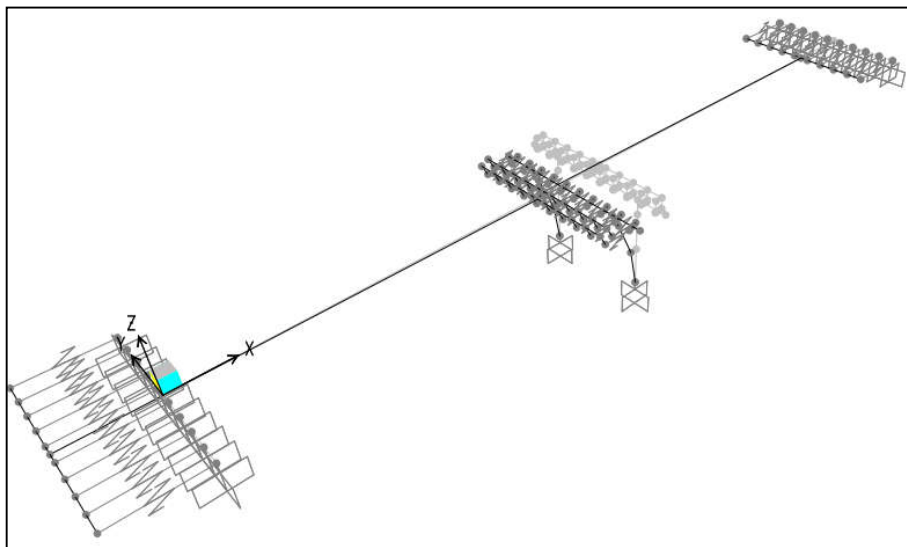
Figure 4.1: Typical 1st Mode in Longitudinal Direction
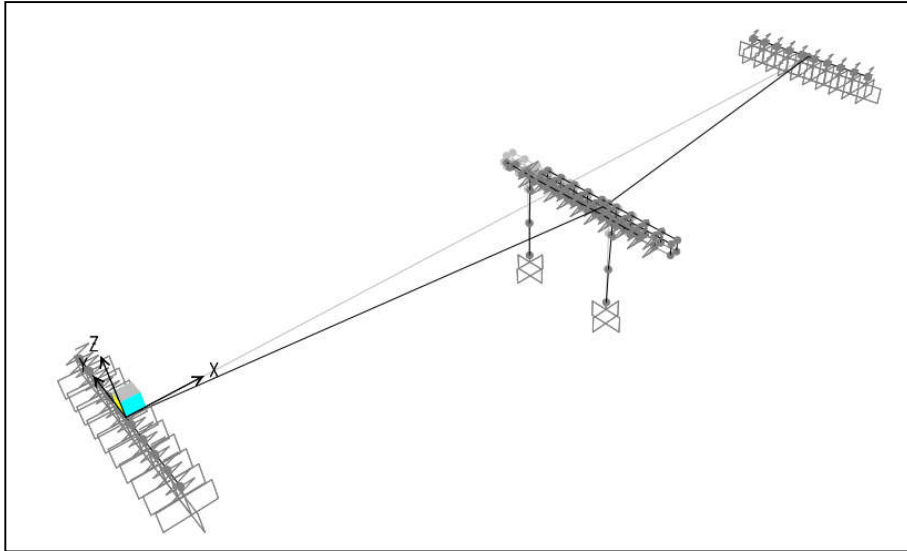
Figure 4.2: Typical 2nd Mode in Transverse Direction

Investigation of earthquake action on all bridges revealed that bridge columns had less reserve capacity in the longitudinal direction than the transverse direction. The main reason was the column weak direction was perpendicular to longitudinal direction of the bridge. Therefore, only the governing case, longitudinal direction case, had been studied in this research. First mode fundamental periods representing the longitudinal direction for all models were tabulated in Table 4.1, Table 4.2 and Table 4.3.

Table 4.1: Fundamental Periods of Set - 1 Bridges

Column Section	T (sec)				Column Section	T (sec)		
	I_{GROSS}	I_{EFF}	I_{EFF}			I_{GROSS}	I_{EFF}	I_{EFF}
	(t = 0)	(t = 0)	(t = 50)			(t = 0)	(t = 0)	(t = 50)
3 x 1	0,749	0,794	0,805		3 x 1	0,816	0,894	0,91
2 x 1	0,765	0,813	0,822		2 x 1	0,852	0,921	0,926
1,5 x 1	0,780	0,847	0,858		1,5 x 1	0,880	0,952	0,96
1,25 x 1	0,800	0,858	0,867		1,25 x	0,9	0,96	0,964

H = 3 m   H = 6 m

Column Section	T (sec)				Column Section	T (sec)		
	I_{GROSS}	I_{EFF}	I_{EFF}			I_{GROSS}	I_{EFF}	I_{EFF}
	(t = 0)	(t = 0)	(t = 50)			(t = 0)	(t = 0)	(t = 50)
3 x 1	0,889	0,962	0,973		3 x 1	0,950	0,999	1,010
2 x 1	0,903	0,979	0,982		2 x 1	0,972	1,009	1,015
1,5 x 1	0,950	1,023	1,063		1,5 x 1	1,020	1,318	1,366
1,25 x 1	0,970	1,174	1,203		1,25 x 1	1,180	1,589	1,640

H = 9 m   H = 12 m

Table 4.2: Fundamental Periods of Set - 2 Bridges

Column Section	T (sec)			Column Section	T (sec)		
	I_{GROSS}	I_{EFF}	I_{EFF}		I_{GROSS}	I_{EFF}	I_{EFF}
	(t = 0)	(t = 0)	(t = 50)		(t = 0)	(t = 0)	(t = 50)
3 x 1	0,762	0,826	0,844	3 x 1	0,860	0,995	1,105
2 x 1	0,785	0,855	0,869	2 x 1	0,916	1,036	1,044
1,5 x 1	0,810	0,909	0,927	1,5 x 1	0,970	1,097	1,113
1,25 x 1	0,830	0,927	0,942	1,25 x 1	1,000	1,135	1,126

H = 3 m   H = 6 m

Column Section	T (sec)			Column Section	T (sec)		
	I_{GROSS}	I_{EFF}	I_{EFF}		I_{GROSS}	I_{EFF}	I_{EFF}
	(t = 0)	(t = 0)	(t = 50)		(t = 0)	(t = 0)	(t = 50)
3 x 1	0,979	1,115	1,136	3 x 1	1,080	1,189	1,203
2 x 1	1,045	1,150	1,157	2 x 1	1,135	1,206	1,213
1,5 x 1	1,090	1,190	1,199	1,5 x 1	1,170	1,314	1,365
1,25 x 1	1,120	1,199	1,203	1,25 x 1	1,190	1,588	1,639

H = 9 m   H = 12 m

Table 4.3: Fundamental Periods of Set - 3 Bridges

Column Section	T (sec)		
	I_{GROSS}	I_{EFF}	I_{EFF}
	(t = 0)	(t = 0)	(t = 50)
3 x 1	0,852	0,941	0,961
2 x 1	0,889	0,973	0,985
1,5 x 1	0,922	1,023	1,062
1,25 x 1	0,951	1,173	1,202

H = 3 - 9 m

Column Section	T (sec)		
	I_{GROSS}	I_{EFF}	I_{EFF}
	(t = 0)	(t = 0)	(t = 50)
3 x 1	0,914	1,055	1,077
2 x 1	0,975	1,089	1,097
1,5 x 1	1,023	1,141	1,154
1,25 x 1	1,057	1,172	1,202

H = 6 - 9 m

Column Section	T (sec)		
	I_{GROSS}	I_{EFF}	I_{EFF}
	(t = 0)	(t = 0)	(t = 50)
3 x 1	0,979	1,115	1,136
2 x 1	1,045	1,150	1,157
1,5 x 1	1,090	1,190	1,199
1,25 x 1	1,12	1,199	1,203

H = 9 - 9 m

Column Section	T (sec)		
	I_{GROSS}	I_{EFF}	I_{EFF}
	(t = 0)	(t = 0)	(t = 50)
3 x 1	1,026	1,150	1,170
2 x 1	1,087	1,177	1,184
1,5 x 1	1,129	1,316	1,372
1,25 x 1	1,180	1,588	1,640

H = 12 - 9 m

As column height increased for the same column cross section, the period of the bridge increased in all sets as expected as the bridge gets flexible. For the given same column height, the model period values increased as column longitudinal dimension decreased as the stiffness of the pier decreases. For same column height and same column cross section, longer periods were observed in cracked section rather than uncracked analysis. Using effective inertia brought longer periods. Due to similar reasons, bridges which subjected fifty years of deterioration had longer periods than bridges at the beginning of service life time.

Intervals of longitudinal periods could be seen in Table 4.1, Table 4.2 and Table 4.3. Hereunder, in Set- 1 for uncracked section analysis periods varied from 0,75 to 1,18 seconds. For cracked section analysis at the time t = 0 year, periods changed from 0,79 to 1,59 seconds. On the other hand in the case of fifty years of deterioration, obtained periods were between 0,81 and 1,64 seconds.

For the bridges having three spans and same column heights in different piers periods were between 0,76 and 0,83 seconds for gross sections, 0,83 and 1,59 seconds for cracked sections at time t = 0 year and 0,84 and 1,64 seconds for cracked sections at time t = 50 years.

Finally periods varied from 0,85 to 1,18 seconds for gross sections; 0,94 to 1,59 seconds for cracked sections at time t = 0 year and 0,96 to 1,64 seconds for cracked sections at time t = 50 years in Set – 3 bridges.

It can be concluded that having tall piers, having small size cross-sections or having cracked section properties resulted in lower stiffness in piers than the ones with having short piers, having large size cross-sections or having uncracked section properties. The lower stiffness of piers resulted in more flexible response of bridge with longer periods of vibration. The structural deterioration of the pier also resulted in more flexible modes compared to a bridge at new condition. Using cracked properties in piers results about 10% - 20 % increase in period compared to the results obtained from uncracked properties. The deterioration models have about 1% - 5% increase in fundamental periods of the structure.

4. 2   Column Nominal Moment Capacity Over Maximum Demand Ratios

Ratios of column nominal moment capacity, ϕM_n, to column maximum demand moment, M_u, were provided in Table 4.4, Table 4.5, Table 4.6, Table 4.7 for Set – 1, Set – 2 and Set- 3 bridge models respectively. The nominal moment capacities of columns of piers were computed based on the AASHTO-LFD (2002) specification and reduced by a factor of ϕ. The demand was computed from the response spectrum analysis of the bridge per AASHTO-LFD (2002).

- It was observed that for all bridge models with uncracked section pier properties, ϕM_n / M_u decreased as column section gets smaller in size. As expected the column nominal moment capacity decreases as column section size gets smaller. The same trend was valid for cracked section at t = 0. But in cracked section at t = 50, in some bridge models, ϕM_n / M_u values increased as column section changed from 2 x 1 to 1,5 x 1. The underlying reason for this outcome was thought as difference in reinforcement ratio. In 2 x 1 sections reinforcement area over column area was 1,01 whereas in 1,5 x 1 column sections it was 1,08. The main reason of slight difference in reinforcement ratios was to maintain the minimum reinforcement ratio for all cross-sections.

- In Set – 1 bridges, for cracked section analyses, ϕM_n / M_u values increased when column height increased from 3 m to 6 m and from 9 m to 12 m. On the other hand, when column height changed from 6 m to 9 m, there was no specific relation between column height and column moment capacity over demand ratio.

- Investigation of results of all 48 bridge models has revealed that results of 11 models about 22,92 % of bridge population in Set-1 exceeded the column moment capacity. When the models had cracked column sections, the same ratio was computed to be 6,25 % and for models with 50 years of deterioration, the same ratio was determined to be 18,75%.

Table 4.4: ϕM_n / M_u values of Set - 1 Bridges

Column Section	ϕM_n / M_u			Column Section	ϕM_n / M_u		
	I_{GROSS}	I_{EFF}	I_{EFF}		I_{GROSS}	I_{EFF}	I_{EFF}
	(t = 0)	(t = 0)	(t = 50)		(t = 0)	(t = 0)	(t = 50)
3 x 1	1,69	2,02	1,51	3 x 1	1,36	2,15	1,70
2 x 1	1,12	1,38	1,12	2 x 1	1,00	1,63	1,33
1,5 x 1	**0,83**	1,14	**0,99**	1,5 x 1	**0,81**	1,54	1,41
1,25 x 1	**0,68**	**0,93**	**0,84**	1,25 x 1	**0,70**	1,29	1,17

H = 3 m   H = 6 m

Column Section	ϕM_n / M_u			Column Section	ϕM_n / M_u		
	I_{GROSS}	I_{EFF}	I_{EFF}		I_{GROSS}	I_{EFF}	I_{EFF}
	(t = 0)	(t = 0)	(t = 50)		(t = 0)	(t = 0)	(t = 50)
3 x 1	1,41	2,76	2,25	3 x 1	1,59	3,46	2,84
2 x 1	1,12	2,17	1,78	2 x 1	1,27	2,51	2,18
1,5 x 1	**0,93**	1,35	1,24	1,5 x 1	1,01	2,29	2,15
1,25 x 1	**0,81**	1,10	**0,97**	1,25 x 1	**0,80**	1,65	1,53

H = 9 m   H = 12 m

- In Set – 2 bridges, analyses with uncracked section, ϕM_n / M_u values generally increased with increase in column heights from 9 m to 12 m. For all other cases, the response in change of ϕM_n / M_u was opposite to the above observation.

- In Set – 2 bridges, for cracked section analyses, ϕM_n / M_u values increased when column height increased from 3 m to 6 m and 6 m to 9 m. On the other hand, when column height changed from 9 m to 12 m, there was no specific relation between column height and column moment capacity over demand ratio.

- Investigation of results of all 48 bridge models has revealed that results of 14 models about 29,2 % of bridge population in Set – 2 exceeded the column moment capacity. When models had cracked column sections, the same ratio was computed to be 6,25 % and for models with 50 years of deterioration, the same ratio was found to be 18,75 %.

- Mostly, columns of Set - 1 bridges had higher ϕM_n / M_u values than Set - 2.

- In Set – 3 bridges, each pier had a different column height. This condition lead to variation in pier stiffness's at adjacent piers. Therefore, each pier had a different moment and shear values. Piers had almost shared the total load of the system inversely proportional to their column heights.

- In Set- 3, about 28,13% of investigated columns exceeded the column moment capacity. When the models had cracked column sections, the same ratio was computed to be 6,25% and for models with fifty years of deterioration, the same ratio was determined to be 12,5 %.

- Column moment capacity over maximum column moment ratio change in case of fixed column height and fix column section dimensions were graphed separately in Figure 4.3 and Figure 4.4. These graphs clearly showed that effective section analysis at t = 0, resulted in highest ϕM_n / M_u values.

Table 4.5: $\phi M_n / M_u$ values of Set - 2 Bridges

Column Section	$\phi M_n / M_u$			Column Section	$\phi M_n / M_u$		
	I_{GROSS}	I_{EFF}	I_{EFF}		I_{GROSS}	I_{EFF}	I_{EFF}
	(t = 0)	(t = 0)	(t = 50)		(t = 0)	(t = 0)	(t = 50)
3 x 1	1,66	1,92	1,42	3 x 1	1,27	1,93	1,48
2 x 1	1,09	1,29	1,04	2 x 1	**0,91**	1,39	1,13
1,5 x 1	**0,80**	1,04	**0,90**	1,5 x 1	**0,72**	1,27	1,16
1,25 x 1	**0,64**	**0,84**	**0,75**	1,25 x 1	**0,62**	1,06	**0,98**

a) H = 3 m   b) H = 6 m

Column Section	$\phi M_n / M_u$			Column Section	$\phi M_n / M_u$		
	I_{GROSS}	I_{EFF}	I_{EFF}		I_{GROSS}	I_{EFF}	I_{EFF}
	(t = 0)	(t = 0)	(t = 50)		(t = 0)	(t = 0)	(t = 50)
3 x 1	1,25	2,27	1,86	3 x 1	1,34	2,78	2,32
2 x 1	**0,96**	1,75	1,44	2 x 1	1,04	2,00	1,74
1,5 x 1	**0,78**	1,66	1,55	1,5 x 1	**0,83**	1,89	1,72
1,25 x 1	**0,67**	1,35	1,22	1,25 x 1	**0,64**	1,32	1,24

c) H = 9 m   d) H = 12 m

Table 4.6: $\phi M_n / M_u$ values of Set - 3 Bridges

Column Section	P1 = 3 m			P1 = 9 m		
	$\phi M_n / M_u$			$\phi M_n / M_u$		
	I_{GROSS}	I_{EFF}	I_{EFF}	I_{GROSS}	I_{EFF}	I_{EFF}
	(t = 0)	(t = 0)	(t = 50)	(t = 0)	(t = 0)	(t = 50)
3 x 1	1,42	1,61	1,20	1,5	2,84	2,32
2 x 1	**0,92**	1,09	**0,88**	1,18	2,20	1,79
1,5 x 1	**0,67**	**0,89**	**0,77**	**0,98**	2,03	1,87
1,25 x 1	**0,54**	**0,72**	**0,65**	**0,84**	1,62	1,46

a) Column Heights, 3 – 9 m

Column Section	P1 = 6 m			P1 = 9 m		
	$\phi M_n / M_u$			$\phi M_n / M_u$		
	I_{GROSS}	I_{EFF}	I_{EFF}	I_{GROSS}	I_{EFF}	I_{EFF}
	(t = 0)	(t = 0)	(t = 50)	(t = 0)	(t = 0)	(t = 50)
3 x 1	1,17	1,78	1,37	1,36	2,46	2,01
2 x 1	**0,84**	1,30	1,05	1,05	1,89	1,54
1,5 x 1	**0,67**	1,21	1,10	**0,85**	1,75	1,63
1,25 x 1	**0,57**	1,01	**0,94**	**0,72**	1,41	1,28

b) Column Heights, 6 – 9 m

Table 4.7: $\phi M_n / M_u$ values of Set - 3 Bridges

Column Section	P1 = 9 m			P1 = 9 m		
	$\phi M_n / M_u$			$\phi M_n / M_u$		
	I_{GROSS}	I_{EFF}	I_{EFF}	I_{GROSS}	I_{EFF}	I_{EFF}
	(t = 0)	(t = 0)	(t = 50)	(t = 0)	(t = 0)	(t = 50)
3 x 1	1,25	2,27	1,86	1,25	2,27	1,86
2 x 1	**0,96**	1,75	1,44	**0,96**	1,75	1,44
1,5 x 1	**0,78**	1,66	1,55	**0,78**	1,66	1,55
1,25 x 1	**0,67**	1,35	1,22	**0,67**	1,35	1,22

a) Column Heights, 9 – 9 m

Column Section	P1 = 12 m			P1 = 9 m		
	$\phi M_n / M_u$			$\phi M_n / M_u$		
	I_{GROSS}	I_{EFF}	I_{EFF}	I_{GROSS}	I_{EFF}	I_{EFF}
	(t = 0)	(t = 0)	(t = 50)	(t = 0)	(t = 0)	(t = 50)
3 x 1	1,54	2,90	2,41	1,09	2,17	1,79
2 x 1	1,10	2,07	1,79	**0,90**	1,70	1,39
1,5 x 1	**0,85**	1,87	1,72	**0,74**	1,63	1,52
1,25 x 1	**0,66**	1,39	1,26	**0,64**	1,32	1,20

b) Column Heights, 12 – 9 m

a) H = 3 m

b) H = 6 m

c) H = 9 m

d) H = 12 m
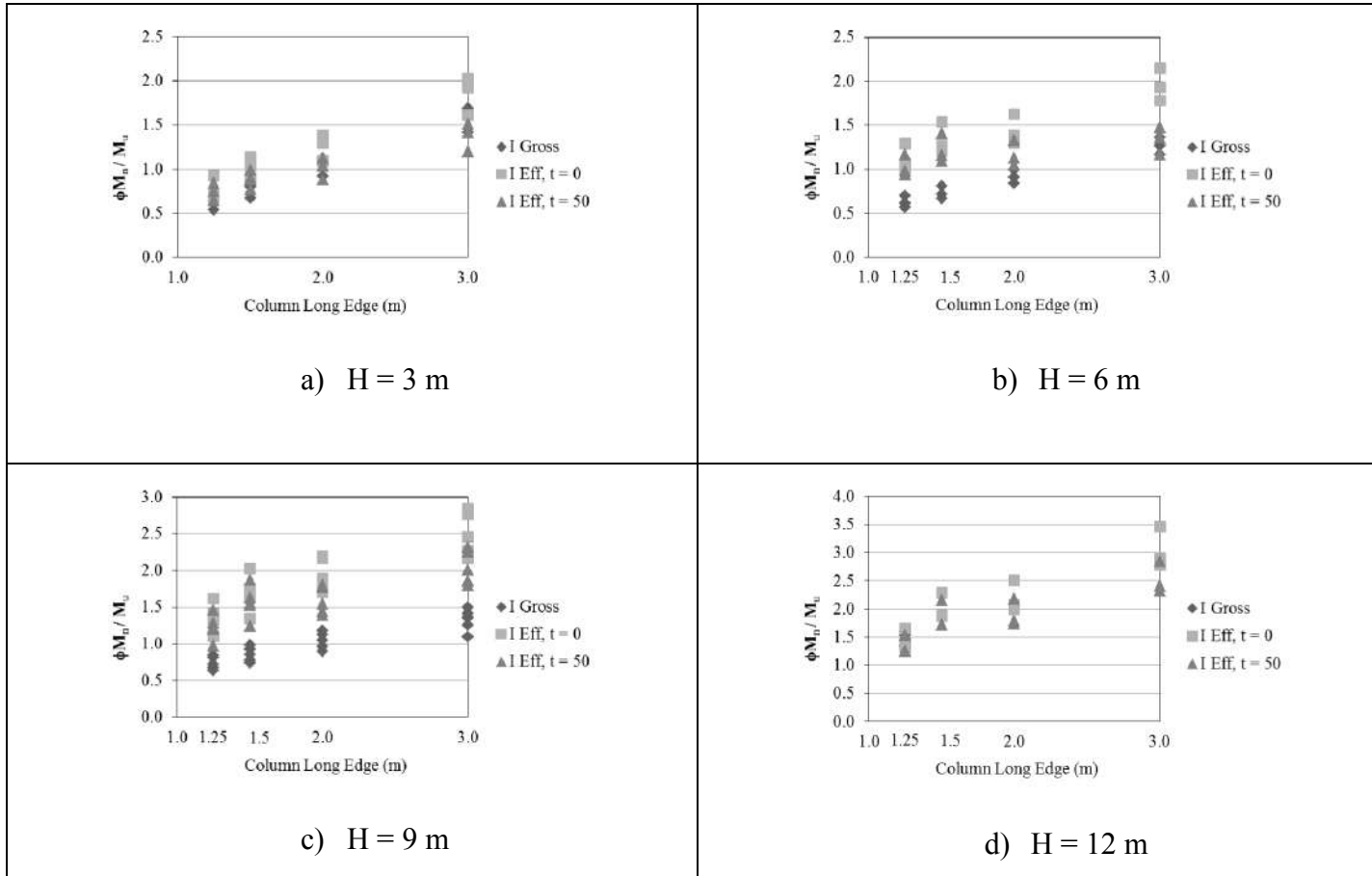
Figure 4.3: Column Long Edge versus $\phi M_n / M_u$

a) Column Section: 3 x 1

b) Column Section: 2 x 1

c) Column Section: 1,5 x 1

d) Column Section: 1,25 x 1
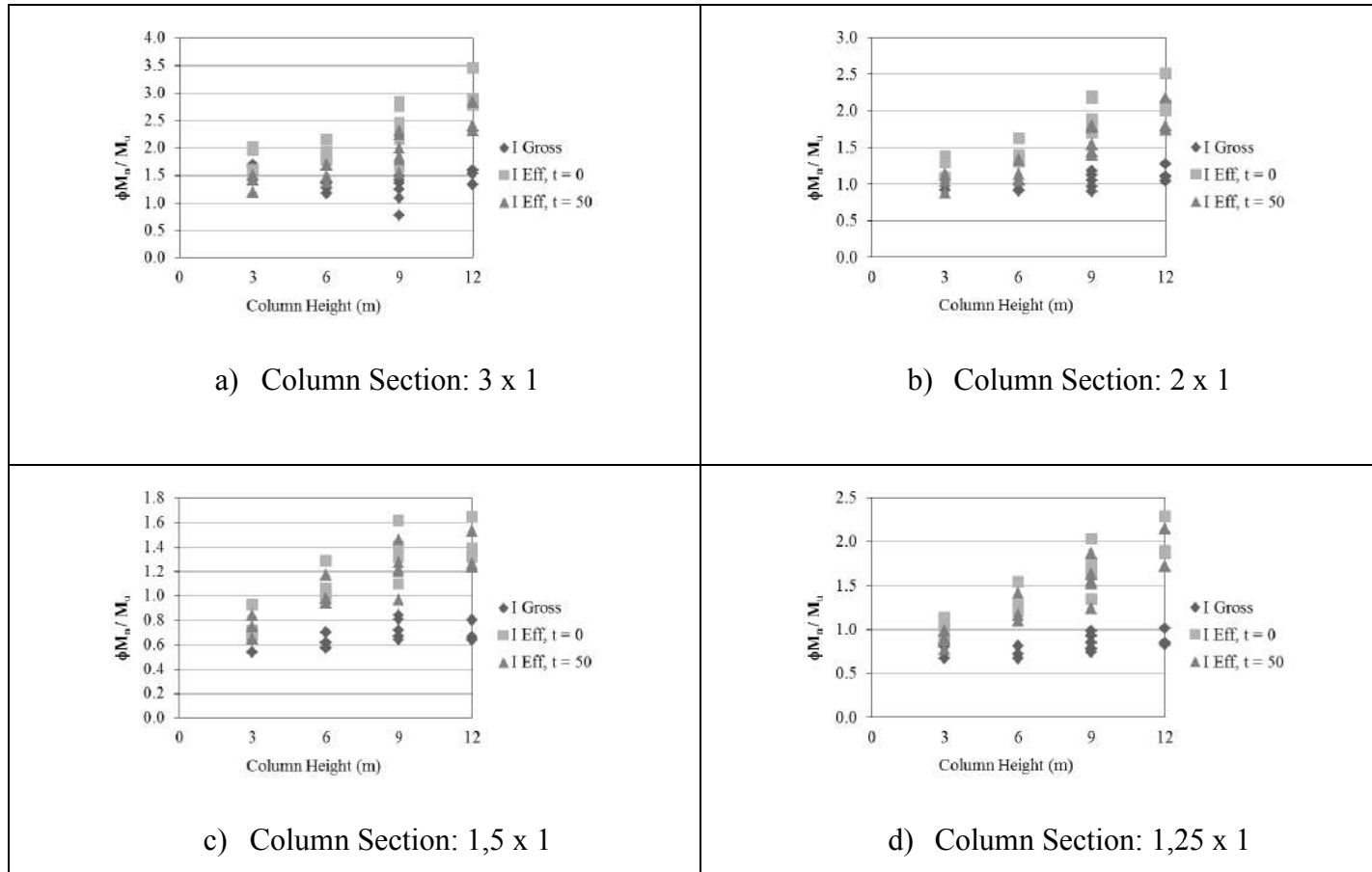
Figure 4.4: Column Height versus ϕMn / Mu

4. 3   Displacement Capacity Over Displacement Demand Ratios

Displacement capacities of columns were obtained from push-over analysis and maximum displacement of column tips were determined from models. These two parameters and their ratio were tabulated in Table 4.8 - Table 4.14.

- In Set- 1 bridges, it was determined that for the same column section, as column height increased, displacement capacity and tip displacement increased. Additionally displacement capacity over demand ratio increased.

- When $t = 0$ and $t = 50$ were compared, it was observed that as bridge operating time increased, column displacement capacity generally decreased whereas column tip displacement always increased.

- The lowest Δ_c / Δ_d value was found as 2,88 for 3 m height having 1,25 x 1 column section when $t = 50$.

- In Set- 2 bridges, it was determined that for the same column section, as column height increased displacement capacity and tip displacement increased. Additionally displacement capacity over demand ratio increased with only one exception.

- The lowest Δ_c / Δ_d value was found as 2,60 for 3 m height having 1,25 x 1 column section when $t = 50$.

- Higher Δ_c / Δ_d values were observed in models with one pier rather than two piers. As number of piers increased, column tip displacement increased.

- In Set- 3 bridges, in same model, higher columns had higher Δ_c, Δ_d and Δ_c / Δ_d values.

- In case of fixed second pier height, as height of first column increased, Δ_c / Δ_d values generally increased.

- When Set – 2 and Set – 3 were compared, it was clearly understood that difference in column stiffness's caused different column tip displacements. As stiffness ratio increased Δ_c / Δ_d values increased.

Table 4.8: Δ_c / Δ_d for Set-1 Bridges, H = 3 m and H = 6 m

Column Section	3 x 1		2 x 1		1,5 x 1		1,25 x 1	
Ageing (year)	t = 0	t = 50	t = 0	t = 50	t = 0	t = 50	t = 0	t = 50
Δ_c (cm)	10,96	11,84	11,41	11,20	9,37	9,25	8,46	8,08
Δ_d (cm)	1,44	1,66	1,80	1,97	2,43	2,63	2,64	2,81
Δ_c / Δ_d	7,61	7,13	6,34	5,69	3,86	3,52	3,20	2,88

a) H = 3 m

Column Section	3 x 1		2 x 1		1,5 x 1		1,25 x 1	
Ageing (year)	t = 0	t = 50	t = 0	t = 50	t = 0	t = 50	t = 0	t = 50
Δ_c (cm)	34,11	36,52	35,74	34,91	29,82	29,38	27,00	25,63
Δ_d (cm)	4,68	5,06	5,35	5,47	6,15	6,35	6,35	6,45
Δ_c / Δ_d	7,29	7,22	6,68	6,38	4,85	4,63	4,25	3,97

b) H = 6 m

Table 4.9: Δ_c / Δ_d for Set-1 Bridges, H = 9 m and H = 12 m

Column Section	3 x 1		2 x 1		1,5 x 1		1,25 x 1	
Ageing (year)	t = 0	t = 50	t = 0	t = 50	t = 0	t = 50	t = 0	t = 50
Δ_c (cm)	68,74	73,31	72,45	70,56	60,90	59,99	55,25	52,41
Δ_d (cm)	7,44	7,74	7,90	7,98	8,42	8,43	8,43	8,59
Δ_c / Δ_d	9,24	9,47	9,17	8,84	7,23	7,02	6,55	6,10

a) H = 9 m

Column Section	3 x 1		2 x 1		1,5 x 1		1,25 x 1	
Ageing (year)	t = 0	t = 50	t = 0	t = 50	t = 0	t = 50	t = 0	t = 50
Δc (cm)	114,60	121,60	120,69	117,81	101,98	100,17	92,67	88,32
Δd (cm)	9,25	9,48	9,48	9,54	9,76	9,86	9,81	9,87
$\Delta c / \Delta d$	12,39	12,83	12,73	12,35	10,45	10,16	9,45	8,95

b) H = 12 m

Table 4.10: Δ_c / Δ_d for Set-2 Bridges, H = 3 m and H = 6 m

Column Section	3 x 1		2 x 1		1,5 x 1		1,25 x 1	
Ageing (year)	t = 0	t = 50	t = 0	t = 50	t = 0	t = 50	t = 0	t = 50
Δ_c (cm)	10,99	11,87	11,43	11,23	9,40	9,29	8,48	8,10
Δ_d (cm)	1,51	1,76	1,92	2,12	2,67	2,91	2,92	3,12
Δ_c / Δ_d	7,28	6,74	5,95	5,30	3,52	3,19	2,90	2,60

a) H = 3 m

Column Section	3 x 1		2 x 1		1,5 x 1		1,25 x 1	
Ageing (year)	t = 0	t = 50	t = 0	t = 50	t = 0	t = 50	t = 0	t = 50
Δ_c (cm)	34,31	36,60	35,42	34,48	29,89	29,50	27,04	25,83
Δ_d (cm)	5,44	5,84	6,25	6,42	7,47	7,79	7,79	8,04
Δ_c / Δ_d	6,31	6,27	5,67	5,37	4,00	3,79	3,47	3,21

b) H = 6 m

Table 4.11: Δ_c / Δ_d for Set-2 Bridges, H = 9 m and H = 12 m

Column Section	3 x 1		2 x 1		1,5 x 1		1,25 x 1	
Ageing (year)	t = 0	t = 50	t = 0	t = 50	t = 0	t = 50	t = 0	t = 50
Δ_c (cm)	68,90	73,55	72,61	70,80	61,06	60,15	55,41	52,57
Δ_d (cm)	9,11	9,59	9,87	10,01	10,74	10,96	10,93	11,04
Δ_c / Δ_d	7,56	7,67	7,36	7,07	5,69	5,49	5,07	4,76

a) H = 9 m

Column Section	3 x 1		2 x 1		1,5 x 1		1,25 x 1	
Ageing (year)	t = 0	t = 50	t = 0	t = 50	t = 0	t = 50	t = 0	t = 50
Δ_c (cm)	114,87	121,86	120,96	118,07	102,25	100,43	92,93	88,45
Δ_d (cm)	11,75	12,11	12,07	12,26	12,68	12,79	12,73	12,83
Δ_c / Δ_d	9,78	10,06	10,02	9,63	8,06	7,85	7,30	6,89

b) H = 12 m

Table 4.12: Δ_c / Δ_d for Set - 3 Bridges, H = 3 – 9 m

Column Section	3 x 1		2 x 1		1,5 x 1		1,25 x 1	
Ageing (year)	t = 0	t = 50	t = 0	t = 50	t = 0	t = 50	t = 0	t = 50
Δ_c (cm)	10,99	11,87	11,43	11,23	9,31	9,32	8,48	8,10
Δ_d (cm)	1,80	2,09	2,28	2,49	3,12	3,40	3,41	3,63
Δ_c / Δ_d	6,11	5,68	5,95	4,51	2,98	2,74	2,49	2,23

a) H = 3 m

Column Section	3 x 1		2 x 1		1,5 x 1		1,25 x 1	
Ageing (year)	t = 0	t = 50	t = 0	t = 50	t = 0	t = 50	t = 0	t = 50
Δ_c (cm)	69,90	73,55	72,69	70,88	61,06	60,15	55,41	52,57
Δ_d (cm)	7,21	7,60	7,82	8,01	8,72	9,01	8,99	9,18
Δ_c / Δ_d	9,56	9,68	9,30	8,85	7,00	6,68	6,16	5,73

b) H = 9 m

Table 4.13: Δ_c / Δ_d for Set - 3 Bridges, H = 6 – 9 m

Column Section	3 x 1		2 x 1		1,5 x 1		1,25 x 1	
Ageing (year)	t = 0	t = 50	t = 0	t = 50	t = 0	t = 50	t = 0	t = 50
Δ_c (cm)	34,31	36,60	35,81	34,99	29,89	29,62	61,06	60,15
Δ_d (cm)	5,89	6,32	6,72	6,90	7,88	8,19	10,15	10,42
Δ_c / Δ_d	5,83	5,79	5,33	5,07	3,79	3,62	6,02	5,77

a) H = 6 m

Column Section	3 x 1		2 x 1		1,5 x 1		1,25 x 1	
Ageing (year)	t = 0	t = 50	t = 0	t = 50	t = 0	t = 50	t = 0	t = 50
Δ_c (cm)	69,90	73,55	72,61	70,80	61,06	60,15	55,41	52,57
Δ_d (cm)	8,37	8,83	9,16	9,31	10,15	10,42	10,40	10,55
Δ_c / Δ_d	8,23	8,33	7,93	7,60	6,02	5,77	5,33	4,98

b) H = 9 m

85

Table 4.14: Δ_c / Δ_d for Set - 3 Bridges, H = 12 – 9 m

Column Section	3 x 1		2 x 1		1,5 x 1		1,25 x 1	
Ageing (year)	t = 0	t = 50	t = 0	t = 50	t = 0	t = 50	t = 0	t = 50
Δ_c (cm)	114,84	121,86	120,96	118,07	102,25	101,39	92,93	88,00
Δ_d (cm)	11,24	11,64	11,90	11,87	12,36	12,52	12,51	12,59
Δ_c / Δ_d	10,22	10,47	10,16	9,95	8,27	8,10	7,43	6,99

a) H = 12 m

Column Section	3 x 1		2 x 1		1,5 x 1		1,25 x 1	
Ageing (year)	t = 0	t = 50	t = 0	t = 50	t = 0	t = 50	t = 0	t = 50
Δ_c (cm)	68,90	73,55	72,61	70,80	61,06	60,15	55,41	52,57
Δ_d (cm)	9,52	9,98	10,19	10,34	10,99	11,58	11,16	11,25
Δ_c / Δ_d	7,24	7,37	7,13	6,85	5,56	5,19	4,97	4,67

b) H = 9 m

According to Türkiye Köprü Mühendisliğinde Tasarım ve Yapıma İlişkin Teknolojilerin Geliştirilmesi Teknik Kılavuzu (2016), 2,5 is the limit value for minimum damage level for displacement capacity over demand ratio. Hereunder, if Δ_c / Δ_d was greater than 2,5, minimum damage was occurred and no retrofitting was required. It was expected to have Δ_c / Δ_d values smaller than 2,5 when $\phi M_n / M_u$ was smaller than 1,0. But results showed that although in 27 columns moment – axial load pairs were outside the moment – interaction diagrams, in only two of them Δ_c / Δ_d smaller than 2,5. The lowest displacement capacity over demand ratio was recorded as 2,23. In this model column moment capacity over demand ratio was found as 0,65.

CHAPTER 5

DISCUSSION OF RESULTS AND CONCLUSIONS

5.1 Discussion of Results

Results of obtained ϕM_n / M_u values and Δ_c / Δ_d values were provided in this subchapter. The relationship of ϕM_n / M_u and Δ_c / Δ_d was investigated. The effects of deterioration were also mentioned. Finally using cracked and uncracked column sections were also compared.

5. 1. 1 Discussion on ϕM_n / M_u Values

Ratios of column nominal moment capacity, ϕM_n, to column maximum demand moment, M_u, were provided in Table 4.4 - Table 4.7 for Set – 1, Set – 2 and Set- 3 bridge models respectively.

For column section with small cross-sectional area, the nominal capacity of columns (ϕM_n) and ϕM_n / M_u ratio were usually decreased compared to the other cases as expected.

Generally, increase in column height resulted in increase in ϕM_n / M_u for cross-section with fixed amount of reinforcement. The underlying reason for this outcome could be explained as the shorter columns had higher stiffness that attracted much higher shear force during a seismic event. Even if the taller columns had higher moment arm between superstructure and base, the moment induced by the shear force can not exceed the ones with shorter columns.

ϕM_n / M_u values computed for bridges of Set -1 (with two abutments and one pier) were typically higher than the ones determined for Set – 2 bridges (with two abutments and two piers). In Set-1 bridges, the weight carried by the abutments was

89

higher compared to the Set - 2 bridges and the piers of Set-2 bridges were most likely to carry more than Set - 1 bridges. It has also been observed that the periods of Set - 2 bridges were slightly softer than Set-1 bridges an indication of higher mass contribution on piers. The higher mass participation on piers can result in higher shear seismic forces as well as moments, M_u. ϕM_n being the same for cross-section, $\phi M_n / M_u$ ratio decreased

When adjacent piers had substantially different column heights, the bridge may not have a balanced stiffness distribution among the piers. The stiffer pier would be subjected to higher seismic effects resulting in uneven distribution of damage. In Set – 3, the column height of second pier was fixed to 9 m and column height of first pier was varied from 3m to 12m. The maximum $\phi M_n / M_u$ was observed in second pier when the column heights of first pier was 3m as expected. When stiffness ratios of adjacent piers were closer to each other, they shared the moments and axial loads more homogenously and they had similar $\phi M_n / M_u$ values. In Caltrans Seismic Design Criteria Version 1.7 (2013), recommendations were made for balanced stiffness system in such a way that the effective stiffness variation shall not exceed 25% of the reference pier stiffness. In this research, the 25% variation in stiffness only yielded to about 4% difference in pier seismic forces. If a 10% difference was targeted for even distribution of pier seismic forces, the variation in adjacent effective stiffness of piers could be around 50% of the reference pier.

In Figure 5.1, results of three different models of Set-3 had been displayed. The stiffness variation of adjacent piers in exceedance of 50% significantly changed the seismic forces in more than 10%. The investigated models were named "a", "b" and "c". The model "a" had 3 x 1 m column cross-section for a bridge with 50 years of deterioration. The model "b" had the same cross-section as model "a" but investigated at new condition. The model "c" had the fifty years of deterioration and had a column cross-section of 2 x 1 m. The results of bridge at new condition had less variation in forces compared to the aged models with unbalanced stiffness.
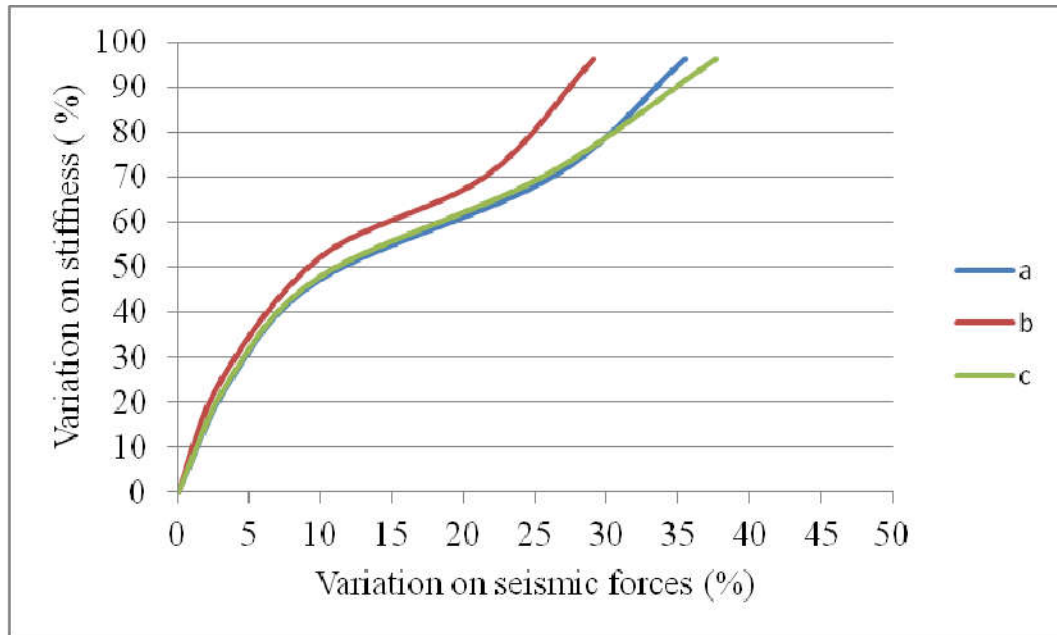
Figure 5.1: Variation on Stiffness versus Variation on Seismic Forces

Cracked section analyses gave higher $\phi M_n / M_u$ values rather than uncracked section analyses in all of the models for same selected years of deterioration. The use of effective sections caused more flexible columns and more flexible the columns get, less seismic moments and higher $\phi M_n / M_u$ values they experienced. Column nominal moment capacity over column maximum demand ratio could increase up to 127% in case of using effective sections instead of gross sections.

Fifty years of deterioration caused strength loss. According to results, $\phi M_n / M_u$ values decreased within a range of 5,9% and 25,9%.

5. 1. 2 Discussion on $\Delta c / \Delta d$ Values

Displacement capacity over demand ratio was one of the major response measures of displacement based design. Ratios of displacement capacity, Δ_c, to displacement demand, Δ_d, were provided in Table 4.8 - Table 4.14 for Set – 1, Set – 2 and Set- 3 bridge models respectively.

It can be concluded that increase in column height resulted in increase in Δ_c / Δ_d for cross-section with fixed amount of reinforcement. The reason was that as the column height increased, columns got more slender and flexible which lead to increase in displacement capacity. The capacity equations (3.21, 3.22, 3.23, 3.24) were presented in Chapter 3, were function of column height. The increase in displacement demand was not as significant as presented in Figure 5.2 - Figure 5.4.
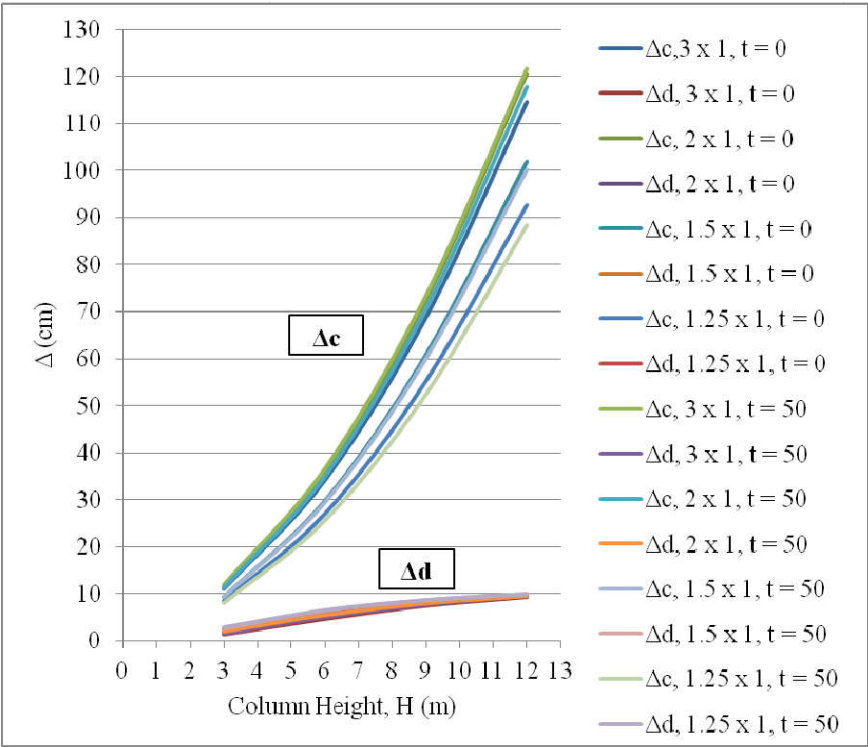

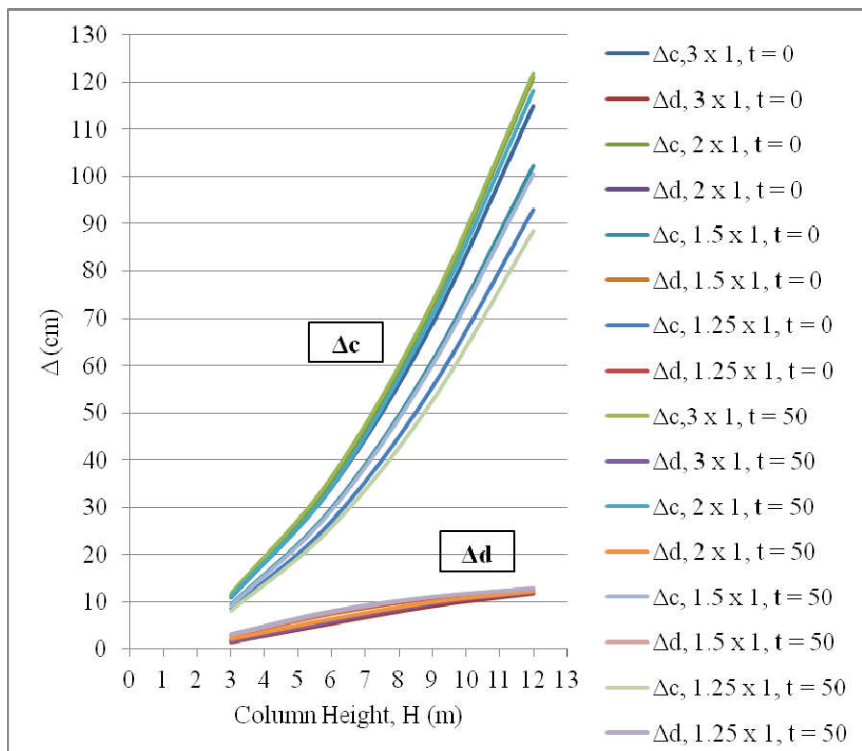Figure 5.2: Δ_c & Δ_d versus Column Height (Set – 1 bridges)

92

Figure 5.3: Δ_c & Δ_d versus Column Height (Set – 2 bridges)
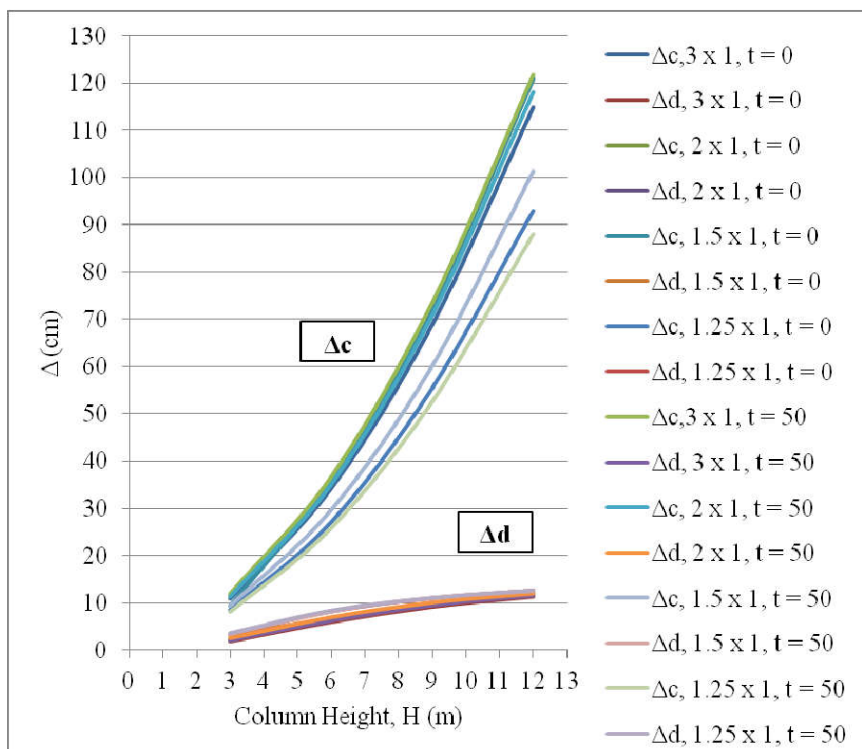
Figure 5.4: Δ_c & Δ_d versus Column Height (Set – 3 bridges)

93

In the case of fixed column height, as column section got smaller in size, obtained tip displacements of columns increased because of decrease in rigidity. Increase in displacement demand caused smaller Δ_c / Δ_d.

Deterioration caused lower effective inertias and higher displacement values in seismic analyses. Δ_c / Δ_d values decreased up to 10% because of fifty years of deterioration. In general, the displacement capacities or demands were not much affected as member forces.

Lower Δ_c / Δ_d values were observed in Set - 2 bridges rather than Set – 1 bridges such as observed for $\phi M_n / M_u$ values.

In Set – 3 bridges, piers having shorter columns had lower Δ_c / Δ_d. In case of keeping the height of column as 9 m in second pier, the maximum difference between Δ_c / Δ_d values of piers were observed when the first pier column height was 3m since the difference in rigidity between piers got the highest value between columns with 3m and 9m heights.

Figure 5.5: Variation on stiffness versus variation on Δ_c / Δ_d values

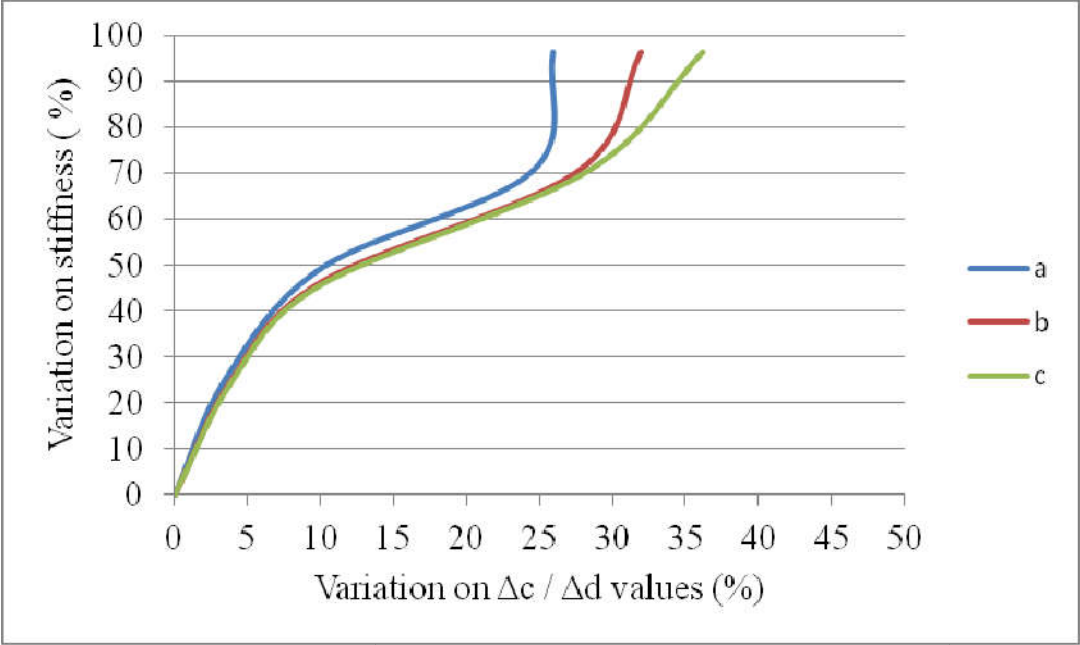In Figure 5.5, results of three different models of Set-3 had been displayed. The stiffness variation of adjacent piers in exceedance of 50% significantly changed the Δ_c / Δ_d values between 10% and 15%. The 25% variation in stiffness only yielded to about 4% difference in Δ_c / Δ_d values. Variation on stiffness caused similar % of variation in both seismic forces and Δ_c / Δ_d values. The investigated models were named "a", "b" and "c" were the same models in Figure 5.1.

The lowest displacement capacity over demand ratio was recorded as 2,23, smaller than 2,5 which was the limit for minimum damage level suggested by Yılmaz and Caner (2012).

5. 1. 3 Relation between $\phi Mn / Mu$ and $\Delta c / \Delta d$

Obtained $\phi M_n / M_u$ and Δ_c / Δ_d values were compared in Chapter 4. The trend of $\phi M_n / M_u$ and Δ_c / Δ_d values showed similarities. When the column nominal capacity over column maximum moment ratio got its maximum value, corresponding displacement capacity over demand ratio was one of the maximum values among Δ_c / Δ_d. Similarly, the lowest Δ_c / Δ_d and $\phi M_n / M_u$ values were obtained from same model. This bridge model had a pier having 3 m column height and 1.25 x 1m column cross section. Δ_c / Δ_d and $\phi M_n / M_u$ values of this column was found as 2,23 and 0,65 respectively which was the smallest values determined from the analyses results with cracked section.

It was expected that when $\phi M_n / M_u$ values become less than one, corresponding Δ_c / Δ_d values would be smaller than 2,5. However, results showed that in cracked section analyses, $\phi M_n / M_u$ values of 13 columns were less than one; only two of these, did not satisfy minimum damage level. It means that 85% of these 13 columns experienced Δ_c / Δ_d values greater than 2,5.

The graphs in Figure 5.6 and Figure 5.7 gave the linear relation between $\phi M_n / M_u$ and Δ_c / Δ_d. When the minimum damage level was considered as 2,5, the required $\phi M_n / M_u$ values to satisfy to "Displacement Based Design Method" requirements were provided in Table 5.1.

Table 5.1: Required ϕMn / Mu Values

Bridge Models	Required $\phi M_n / M_u$ Value
Set - 1	0,75
Set -2	0,80
Set -3	0,79
All bridge models	0,80
Bridge models at t = 0	0,82
Bridge models at t = 50	0,79

It can be concluded that the values outside the interaction diagram could be tolerated up to a level of 20%.
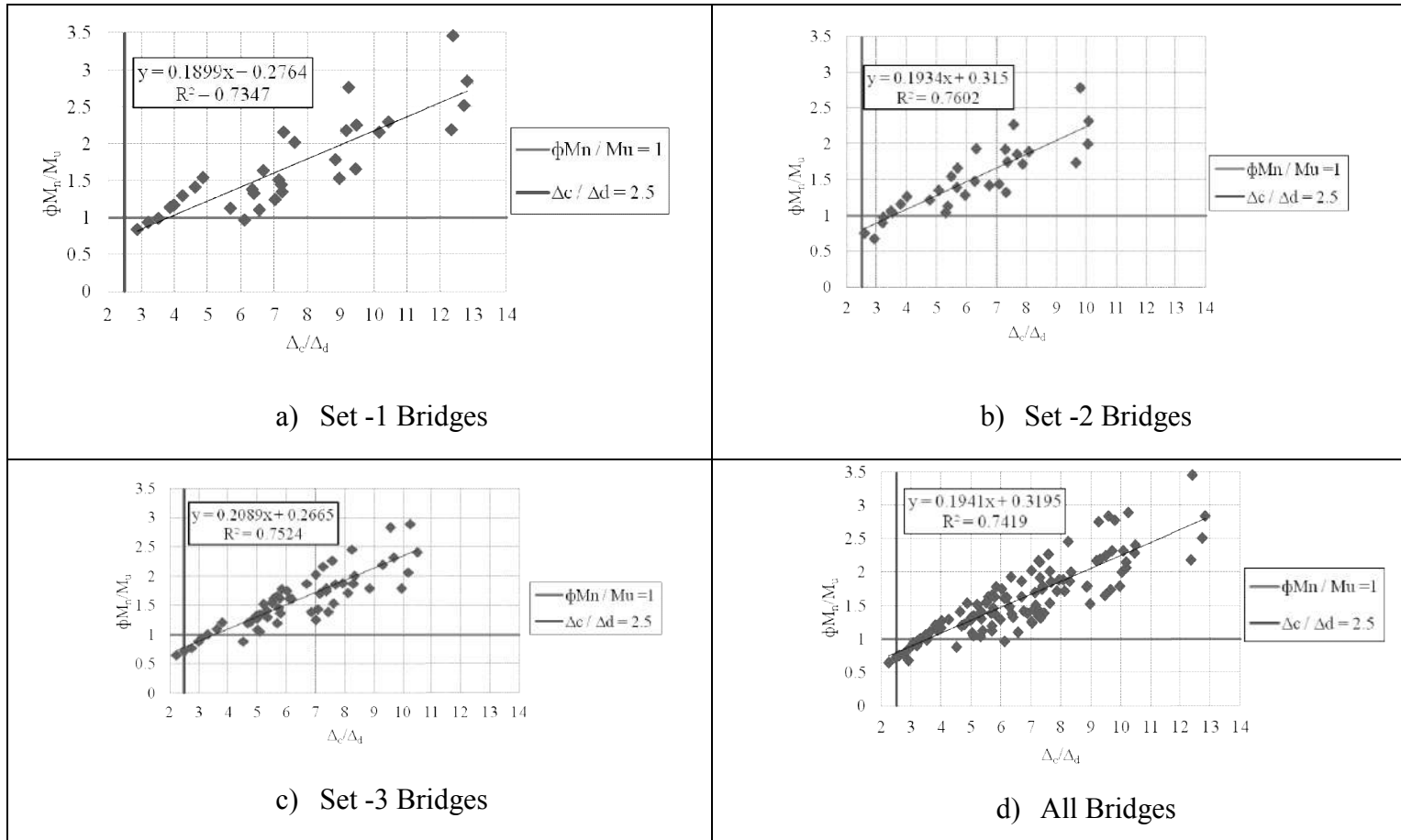
Figure 5.6: $\phi M_n / M_u$ and Δ_c / Δ_d Relationship
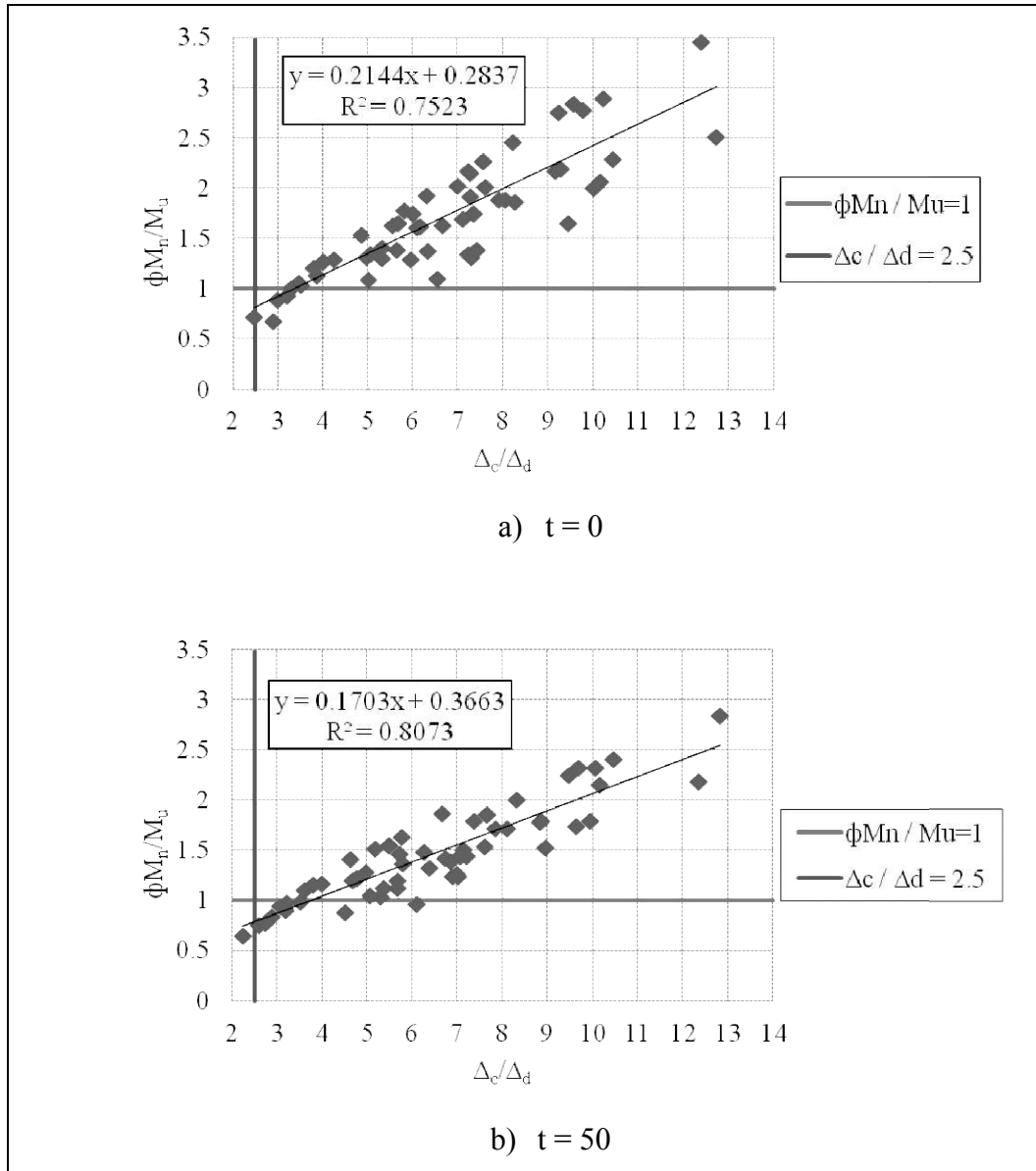
Figure 5.7: $\phi M_n / M_u$ and Δ_c / Δ_d Relationship

5. 1. 4 Discussion on corrosion effect

A deterioration model was applied to all bridge models to find out the effects of corrosion on strength of columns. Bridge models were subjected to fifty years of deterioration. After fifty years, decrease in $\phi M_n / M_u$ values was observed in the range of 5,9% to 25,9%. The average value of decrease was determined as 13,8 % with the coefficient of variation of 5,67%. Accordingly, 20% of strength loss which

corresponded a reduction factor of 0,8 was suggested for fifty years of deterioration in the column design.

On the other hand, AASHTO Guide Manual for Condition Evaluation and Load Resistance Factor Rating (LRFR) of Highway Bridges (2003) suggests a condition factor that provided a reduction to account for the increased uncertainty in the resistance of deteriorated members and the likely increased future deterioration of these members during the period between inspection cycles. The condition factors are based on the specific condition of members as provided in Table 5.2.

Table 5.2: LRFR Condition Factor, ϕ_c

Structural Condition of Member	ϕ_c
Good or Satisfactory	1,00
Fair	0,95
Poor	0,85

Proposed reduction factor is 0,8 for structures under moderate level of corrosion. It was evaluated that structural condition of the members should be poor after at least fifty years of service life. LRFR (2003) suggests a reduction factor of 0.85 for members in poor condition which is nearly same as our proposed value.

Proposed deterioration model was applied considering meteorological and seismic properties of Çanakkale in order to compare the results with another study conducted by Caner et al. (2008) in the same region.

Besides using a deterioration model to determine the loss of strength, reliability analyses which were depended on regular periodic inspection records could be conducted. Caner et al. (2008) studied deterioration of bridge rates for 21 highway bridges on a part of Route D200 connecting Bursa to Çanakkale. According to this study the deterioration rate of main body components were determined to be 0.0403 per year. If the condition rating of the bridge component at new condition was assumed 7,0, after fifty years of deterioration it decreased to 4,985. It means that

after fifty years of deterioration bridge members lost 29% of their functions. This study which based on bridge inspection gave more conservative results when compared to AASHTO-LRFR (2003) and proposed deterioration model (Table 5.3).

AASHTO-LRFR (2003) and Caner et al. (2008) depend on only visual inspection and they can vary from person to person. Proposed deterioration model, based on structural analysis is expected to give more realistic results than other two studies.

Table 5.3: Comparison of Studies

	Loss of Function (%)
AASHTO-LRFR (2003)	15
Proposed Model	**20**
Caner et al. (2008)	29

From displacement point of view, fifty years of deterioration caused the decrease in Δ_c / Δ_d values up to 10%.

5. 1. 5 Discussion on condition of piers

Bridge models were analyzed by considering cracked and uncracked condition of piers obtained using moment-curvature relationship to effective stiffness evaluation. Results showed that for the same column height and column cross section, the ratio of column strength could increase up to a range of 1,13 to 2,26 times in case of using effective section rather than gross section. Moreover, investigation of results of all 64 columns have revealed that nominal moment capacity over maximum demand of 57 columns about 89 % of total population in all sets were higher after fifty years of deterioration than at new condition, analyzed with gross column section properties. These results showed how the Turkish bridges were overdesigned and explained the success of the Turkish bridges after earthquake.

5.2   Summary and Conclusion

One hundred forty four different computer models were investigated in this study to find the reason of success of Turkish bridges during earthquakes. Studied bridge models were selected considering the most common types found in Turkish bridge engineering practice. Seismic evaluation of bridges included deterioration and ageing in addition to condition of pier; uncracked and cracked section properties.

Seismic performances of bridges were investigated based on engineering design methods. In the literature, there were studies that utilized probabilistic methods (Choe et al. (2010), Talley et al. (2014). However, these studies did not offer probability distributions of seismic effects. According to National Cooperative Highway Research Program (NCHRP) Report 489 (2003), the coefficient variation of seismic effects is not a constant value, varies from city to city. Since there exist limited data for probabilistic approach, deterministic methods were used in this study.

A deterioration model was proposed to calculate the corrosion rate and with the corrosion rate proposed, diameter and yield strength of reinforcement steel after fifty years of deterioration were computed.

The following conclusions can be drawn for this study:

- Bridge models having cracked section pier properties gave more than two times of column strength than bridge models having uncracked section pier properties. The reason of that Turkish bridges performed well during earthquake was evaluated as using gross section properties instead of effective section properties.

- For fifty years of deterioration, a reduction factor of 0,8 for column strength was suggested under moderate level of corrosion.

- Generally increase in column nominal moment capacity over column maximum demand ratio and displacement capacity over demand ratio were observed as the column height increased and column section gets bigger in size.

101

- Column nominal moment capacity over column maximum demand ratios observed in three spanned bridges were higher than two spanned bridges.

- The ratio of displacement capacity over demand was higher in two spanned bridges than three spanned bridges.

- In the systems which consisted of adjacent piers having different column stiffness, variation of effective stiffness of columns was increased up to 50% which corresponded 10% of change in seismic forces.

- In the systems which consisted of adjacent piers having different column stiffness, shorter columns had lower displacement capacity over demand ratios.

- In "Force Based Design Method" column nominal moment capacity over column maximum demand ratio should be higher than one. On the other hand in "Displacement Based Design Method", displacement capacity over demand ratio should be higher than 2,5 to satisfy minimum damage level. Studies showed that when the ratio of column nominal moment capacity over column maximum demand was equal to one, the ratio of displacement capacity over demand was observed as more than 2.5. Likewise when the ratio of displacement capacity over demand was equal to 2,5, the ratio of column nominal moment capacity over column maximum demand for the related section was determined as less than one. In the lights of these studies, it was recommended that when column nominal moment capacity over column maximum demand ratio was between 0,8 and 1,0; displacement capacity over demand ratio should be controlled and if it is more than 2,5, the design could be proceeded.

5.3   Recommendation for Further Studies

Corrosion model can be verified by experimental studies. Case studies can be expanded by using different column sections and column heights, different span lengths and increasing number of spans. Different soil conditions and seismic properties can be applied.

REFERENCES

ABC News, C., Andrade, C., Rodriguez, J., & Diez, J. M. (1998). Factors controlling cracking of concrete affected by reinforcement corrosion. *Materials and Structures*, *31*(7), 435–441. http://doi.org/10.1007/BF02480466

Ahmad, S., and Bhattacharjee, B. (2000). Empirical modeling of indicators of chloride-induced rebar corrosion. *J. Struct. Eng., 27(3),* 195-207.

Alonso, C., Andrade, C., Rodriguez, J., & Diez, J. M. (1998). Factors controlling cracking of concrete affected by reinforcement corrosion. *Materials and Structures*, *31*(7), 435–441. http://doi.org/10.1007/BF02480466

American Association of State Highway and Transportation Officials (AASHTO). (2002). Standard *Specifications for Highway Bridges*, Washington D.C.

American Association of State Highway and Transportation Officials (AASHTO). (2003). *Guide Manuel for Condition Evaluation and Load Resistance Factor Rating (LRFR) of Highway Bridges.*

American Society of Civil Engineers (ASCE). (2010). Infrastructure Report Card.

Andrade, C., Alonso, C., & Molina, F. J. (1993). Cover cracking as a function of bar corrosion: Part I-Experimental test. *Materials and Structures*, *26*(8), 453–464. http://doi.org/10.1007/BF02472805

Applied Technology Council, ATC (1996). Improved Seismic Design Criteria For California Bridges: Resource Document, *California Department of Transportation*, Redwood, California.

Balafas, I., & Burgoyne, C. J. (2010). Environmental effects on cover cracking due to corrosion. *Cement and Concrete Research*, *40*(9), 1429–1440. http://doi.org/10.1016/j.cemconres.2010.05.003

Bertolini, L., Bernhard, E., Pietro, P., & Rob, P. (2004). Corrosion of Steel in Concrete. *WILEY-VCH KGaA, Weinheim, Germany*

Biondini, F., Camnasio, E., & Palermo, A. (2012). Life-Cycle Performance of Concrete Bridges Exposed to Corrosion and Seismic Hazard. *Structıres Congress 2012.*

General Directorate of Highways (2015). Bridge Inventory Data.

Burton, C. (2016, June 7). Partial Bridge Collapse in Texas Kills 12-Year-Old Girl. *ABC News*. Retrieved from http://abcnews.go.com/US/partial-bridge-collapse-texas-kills-12-year-girl/story?id=40409733. (last accessed September 2016)

Caltrans Seismic Design Criteria Version 1.7 (2013).

Caner, A., Melih Yanmaz, ; A, Yakut, A., Avsar, O., & Yilmaz, T. (2008.). Service Life Assessment of Existing Highway Bridges with No Planned Regular Inspections.

Caner, A. & Yılmaz. T. (2012). Target Damage Level Assessment for Seismic Performance Evaluation of Two-Column Reinforced Concrete Bridge Bents. *Bridge Structures – Assessment, Design & Construction 8,* 135-146.

Chiu, C.-K. (2014). Reliability-based service life assessment for deteriorating reinforced concrete buildings considering the effect of cumulative damage. *Structure and Infrastructure Engineering*, *10*(9), 1101–1118. http://doi.org/10.1080/15732479.2013.793722

Choe, D., Asce, M., Gardoni, P., Rosowsky, D., & Asce, F. (2010). Fragility Increment Functions for Deteriorating Reinforced Concrete Bridge Columns. *Journal of Engineering Mechanics*, (August), 969–978. http://doi.org/10.1061/(ASCE)EM.1943-7889.0000147

Cook, W. (2014). Bridge Failure Rates, Consequences, and Predictive Trends, 116. Retrieved from http://digitalcommons.usu.edu/etd/2163. (last accessed September 2016)

Domanic, K. A. (2008). Effects of Vertical Excitation on Seismic Performance of Highway Bridges and Hold-Down Device Requirements. *Ph.D. thesis,* Middle East Technical University , Ankara.

Due, Y., Clark, L. A., & Chan, A. H. C. (2005). Residual Capacity of Corroded Reinforcing Bars. *Magazine of Concrete Research*, *57*(3), 227–238.

DuraCrete. (200). Brite EuRam: DuraCete –Final Technical Report. DuraCrete-Probabilistic Performance Based Durability Design of Concret Structures. *Contract BRPR-CT95-0132, Project BE95-1347, Document BE95-1347/R17.* Brussels, Belgium.

Erdik, M. (2001). *Report on 1999 Kocaeli and Düzce (Turkey) Earthquakes*. *Structural Control for Civil and Infrastructure Engineering - Proceedings of the 3rd International Workshop on Structural Control*. http://doi.org/10.1142/9789812811707_0018

General Directorate of Mineral Research and Exploration. (2012). Active Fault Map of Turkey. (http://www.mta.gov.tr/v2.0/eng/daire-baskanliklari/jed/index.php?id=products-active-fault, last accessed September 2016)

Guo, T., Sause, R., Frangopol, D. M., & Li, A. (2010). Time-Dependent Reliability of PSC Box-Girder Bridge Considering Creep, Shrinkage and Corrosion. *Journal of Bridge Engineering*, *16*(1), 29–43. http://doi.org/10.1061/(ASCE)BE.1943-5592.0000135

Guo, Y., Trejo, D., & Solomon, Y. (2014). New Model for Estimating the Time-Variant Seismic Performance of Corroding RC Bridge Columns. *Journal of Structural Engineering*, *141*(6), 1-12. http://doi.org/10.1061/(ASCE)ST.1943-541.0001145

Gonzalez, J. A., Andrade, C., Alonso, C., & Feliu, S. (1995). Comparison of rates of general corrosion and maximum pitting penetration on concrete embedded steel reinforcement. *Cement and Concrete Research*, *25*(2), 257–264. *http://doi.org/10.1016/0008-8846(95)00006-2*

Kandilli Observatory and Earthquake Research Institute . (http://www.koeri.boun.edu.tr/sismo/2/deprem-verileri/depremsellik-haritalari/ last accessed September , 2016)

Kobayashi, K., & Shuttoh, K. (1991). Oxygen diffusivity of various cementitious materials. *Cement and Concrete Research*, *21*(2), 273–284. http://doi.org/10.1016/0008-8846(91)90009-7

Kwon, S. J., Na, U. J., Park, S. S., & Jung, S. H. (2009). Service life prediction of concrete wharves with early-aged crack: Probabilistic approach for chloride diffusion. *Structural Safety*, *31*(1), 75–83. http://doi.org/10.1016/j.strusafe.2008.03.004

Li, C. Q. (2004). Reliability Based Service Life Prediction of Corrosion Affected Concrete Structures, (October), 1570–1578. http://doi.org/10.1061/(ASCE)0733-9445(2004)130

Liu, T., & Weyers, R. . (1998). Modeling the Dynamic Corrosion Process in Chloride Contaminated Concrete Structures. *Cement and Concrete Research*, *28*(3), 365–379. http://doi.org/10.1016/S0008-8846(98)00259-2

Martinez, I., & Andrade, C. (2009). Examples of reinforcement corrosion monitoring by embedded sensors in concrete structures. *Cement and Concrete Composites*, *31*(8), 545–554. http://doi.org/10.1016/j.cemconcomp.2009.05.007

National Cooperative Highway Research Program (NCHRP) Report 489. (2003).

New York State Department Of Transportation (NYDOT). (2004). *Bride Safety Assurance: Hydraulic Vulnarability Manuel.*

Orta Doğu Teknik Üniversitesi Deprem Mühendisliği Araştırma Merkezi. (2011). *23 Ekim 2011 Mw= 7.2 Van Depremi Sismik ve Yapısal Hasara İlişkin Saha Gözlemleri,* Ankara.

Otieno, M. B., Beushausen, H. D., & Alexander, M. G. (2011). Modelling corrosion propagation in reinforced concrete structures - A critical review. *Cement and Concrete Composites*, *33*(2), 240–245. http://doi.org/10.1016/j.cemconcomp.2010.11.002

Özdemir, S., & Topkara, N. (2015). Remaining Service Life Assessment of River Bridges with Cracked Members. *IABMAS2016*.

Phurkhao, P., & Kassir, M. K. (2005). Note on Chloride-Induced Corrosion of Reinforced Concrete Bridge Decks. *Journal of Engineering Mechanics*, *131*(1), 97–100. http://doi.org/10.1061/(ASCE)0733-9399(2005)131:1(97)

Saad, T., & Fu, C. C. (2015). Determining Remaining Strength Capacity of Deteriorating RC Bridge Substructures, *29*(5), 1–12. http://doi.org/10.1061/(ASCE)CF.1943-5509.0000467.

Sap2000, Advanced 14.2.4, Structural Analysis Program (1995), Berkeley, CA.

Seismic Retrofitting Manual for Highway Structures: Part-1 Bridges (2013)

Shafei, B., & Alipour, A. (2013). Assessment of Extent of Capacity Loss in Deteriorated Highway Bridges. *Structures Congress 2013*, 622–631. http://doi.org/10.1061/9780784412848.055

Specifications for Buildings to be Built in Seismic Zones (2007). Ministry of Public Works and Settlement, Republic of Turkey, Ankara.

Stewart, M. G., & Rosowsky, D. V. (1998). Structural Safety and Serviceability of Concrete Bridges Subject to Corrosion. *Journal of Infrastructure Systems*, *4*(4), 146–155. http://doi.org/10.1061/(ASCE)1076-0342(1998)4:4(146)

Talley, K. G., Arrellaga, J., & Breen, J. E. (2014). Computational Modeling of Existing Damage in Concrete Bridge Columns. *Tunnelling and Underground Space Technology*, *40*(12), 127–140. http://doi.org/10.1061/(ASCE)ST.1943-541X.0001115.

Tapan, M., & Aboutaha, R. S. (2008). Strength Evaluation of Deteriorated RC Bridge Columns. *Journal of Bridge Engineering*, *13*(3), 226–236. http://doi.org/10.1061/(ASCE)1084-0702(2008)13:3(226)

The Associated Press (2007, August 1). Bridge Collapses in Minnesota. *The Denver Post*. Retrieved from http://www.denverpost.com/2007/08/01/bridge-collapses-in-minnesota/ (last accessed September 2016)

Thomas, M. D. A., & Bentz, E. C. (2002). Computer Program for Predicting the Service Life and Life-Cycle Costs of Reinforced Concrete Exposed to Chlorides. *Life365 Manuel*.

Tutti, K. (1982). Corrosion Steel in Concrete. *Rep. No.4*, Swedish Cement and Concrete Institute, Stockholm, Swedan.

Türkiye Köprü Mühendisliğinde Tasarım ve Yapıma İlişkin Teknolojilerin Geliştirilmesi Teknik Kılavuzu. (2016).

U.S. Departmant of Transportation. (2006). *Seismic Retrofitting Manuel for Highway Structures: Part -1 Bridges*.

Val, D. V., & Pavel, T. A. (2008). Probabilistic evaluation of initiation time of chloride-induced corrosion. *Reliability Engineering and System Safety*, *93*(3), 364–372. http://doi.org/10.1016/j.ress.2006.12.010

Virginia.gov. (2014). Infrastructure Condition. Retrieved from http://doi.org/10.1016/j.ress.2006.12.010 (last accessed September 2016)

Vu, K. A. T., & Stewart, M. G. (2000). Structural reliability of concrete bridges including improved chloride-induced corrosion models. *Structural Safety*, *22*(4), 313–333. http://doi.org/10.1016/S0167-4730(00)00018-7

Vu, K. A. T., Stewart, M. G., & Mullard, J. (2005). Corrosion-Induced Cracking: Experimental Data and Predictive Models. *ACI Structural Journal*, *102*(5), 719-726.

Williamson, G. S. (2007). Service Life Modeling of Virginia Bridge Decks. *Ph.D. thesis,* Virginia Polytechnic Institute and State University, Blacksburg.

Yalçın, H., & Ergun, M. (1996). The prediction of corrosion rates of reinforcing steels in concrete. *Cement and Concrete Research*, *26*(10), 1593–1599. http://doi.org/10.1016/0008-8846(96)00139-1

Yılmaz, Ç., & Turer, A. (2002). 2300 Metre Uzunluğundaki Bolu Viyadüğünün Dizayn Felsefesi ve Deprem Davranışı, (1), 50–65.

Zhu, W., & Franc, R. (2015). Structural performance of RC beams in relation with the corroded period in chloride environment, 1757–1769. http://doi.org/10.1617/s11527-014-0270-2

APPENDIX A

VERIFICATION OF ANALYSES TOOLS

A.1 Moment – Curvature Diagram

In this study, a moment – curvature software program developed by Tamer Fenercioğlu (2008) was used. This software was generated in Microsoft Excel. The results obtained using this program were verified using a software namely "KSU RC" which was created by Asad Esmaeily from Kansas State University, Civil Engineering Department.

Moment – curvature diagrams were obtained using both of the programs for circular and rectangular sections by taking the section and material properties same.

Compressive strength of concrete, yielding strength and modulus elasticity of reinforcement steel were chosen as 30 MPa, 420 MPa and 200000 MPa respectively with a clear cover of 5 cm.

A. 1. 1   Rectangular Section

Geometric properties and reinforcement details of rectangular section were provided in Figure A.1. Rectangular section was subjected to an axial load of 4400 kN.
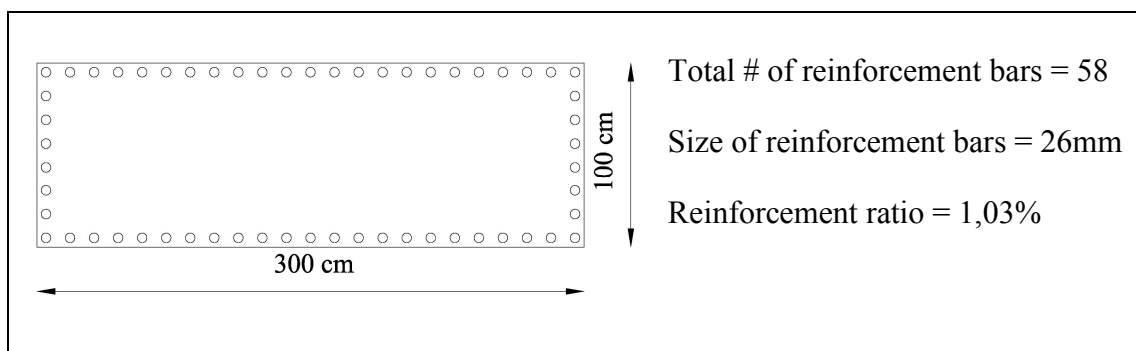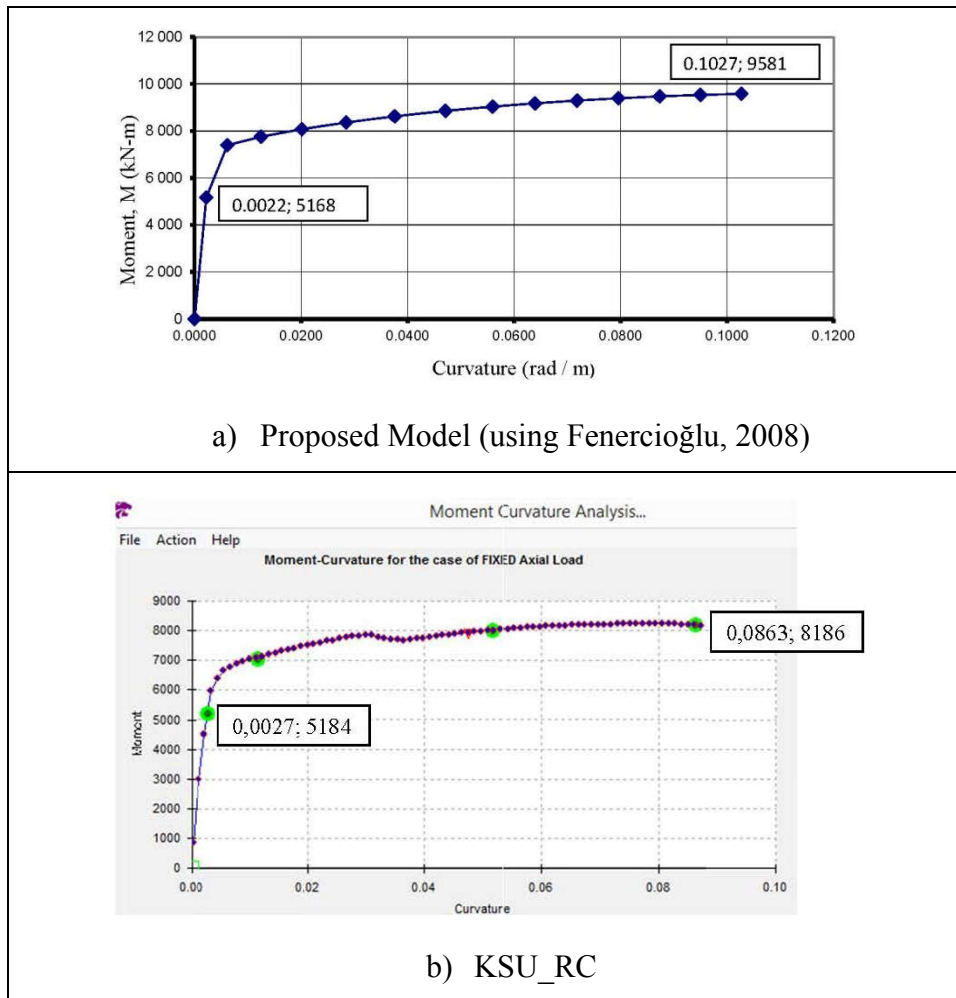

Figure A. 1: Rectangular section

a) Proposed Model (using Fenercioğlu, 2008)

b) KSU_RC

Figure A.2: Moment – Curvature Diagrams

Table A.1: Comparison of Moment – Curvature Programs

Parameters	M_1 / ϕ_1 (kN-m^2)(10^6)	ϕ_1 (rad/m)	ϕ_2 (rad/m)
Proposed Model	2,35	0,0022	0,1027
KSU_RC	1,92	0,0027	0,0863
Difference Ratio (%)	18	23	16

Moment – curvature diagrams generated from two different programs for the rectangular section were provided in Figure A.2. The initial slope of the diagram was

110

utilized in order to find effective inertia of the columns. The curvatures of the first yielding point and ultimate point were used to determine the displacement capacity of the columns. So, comparison of these three parameters was provided in Table A.1. Accordingly maximum difference between these two programs was found as 23% .

A. 1. 2   Circular Section

Geometric properties and reinforcement details of rectangular section were provided in Figure A.3.

Total # of reinforcement bars = 58

Size of reinforcement bars = 26mm
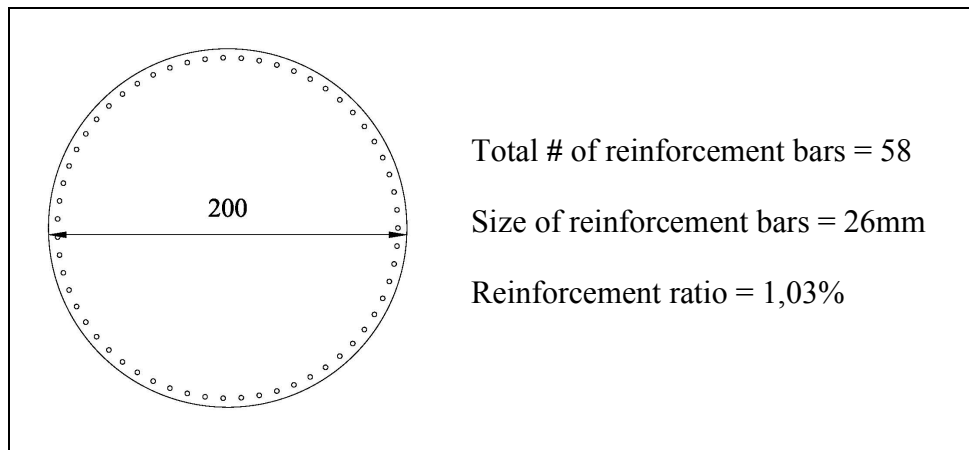
Reinforcement ratio = 1,03%

Figure A.3: Circular Section

Moment – curvature diagrams generated from two different programs for the circular section were provided in Figure A.4. The initial slope of the diagram was utilized in order to find effective inertia of the columns and the curvatures of the first yielding point and ultimate point were used to determine the displacement capacity of the columns. So, comparison of these three parameters was presented in Table A.2. Accordingly maximum difference between these two programs was found as 7% for circular section.
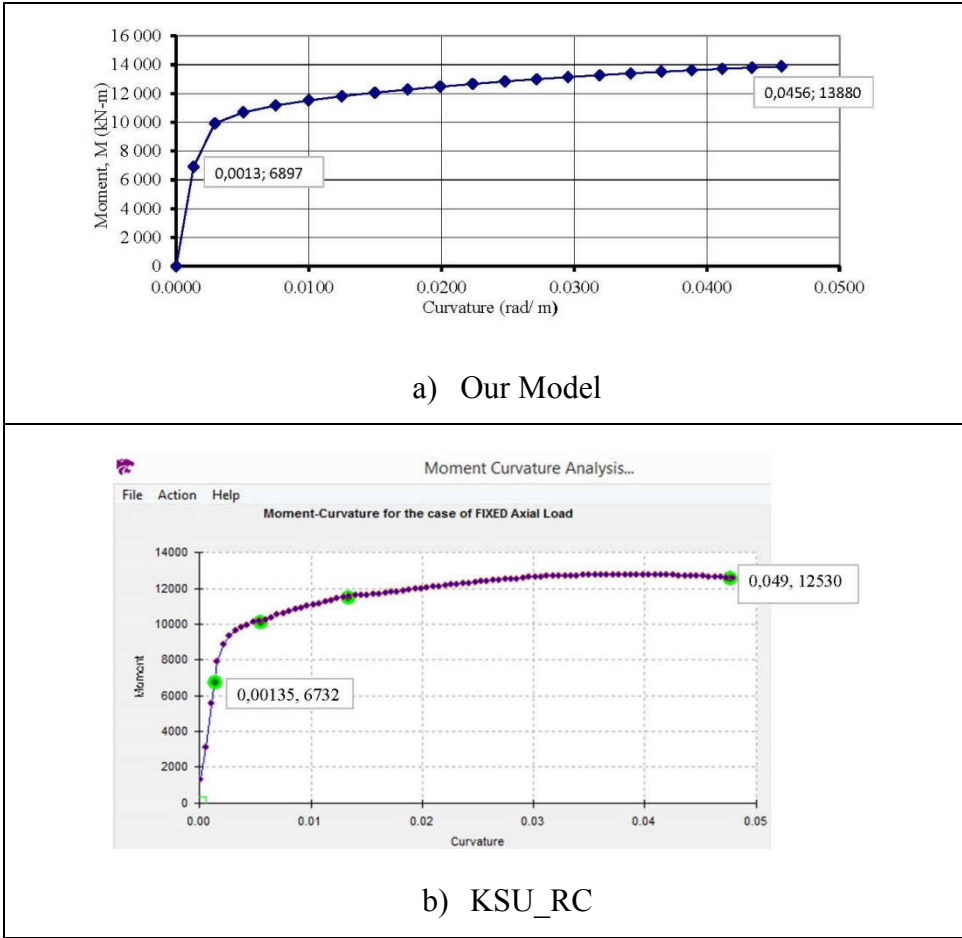
a) Our Model

b) KSU_RC

Figure A.4: Moment – Curvature Diagrams

Table A.2: Comparison of moment – curvature programs

Parameters	M_1 / ϕ_1 (kN-m^2)(10^6)	ϕ_1 (rad/m)	ϕ_2 (rad/m)
Our Model	5,31	0,00130	0,0456
KSU_RC	4,99	0,00135	0,0049
Difference (%)	6	4	7

A.2 Moment – Axial Load Interaction Diagram

Moment – axial load interaction diagram used in this research was compared with a software program developed by Güney Özcebe and Uğur Ersoy (2006). Results of both programs were presented in Figure A.5

a) Proposed Model

b) Özcebe and Ersoy (2006)

Figure A.5: Moment – Axial Load Interaction Diagrams
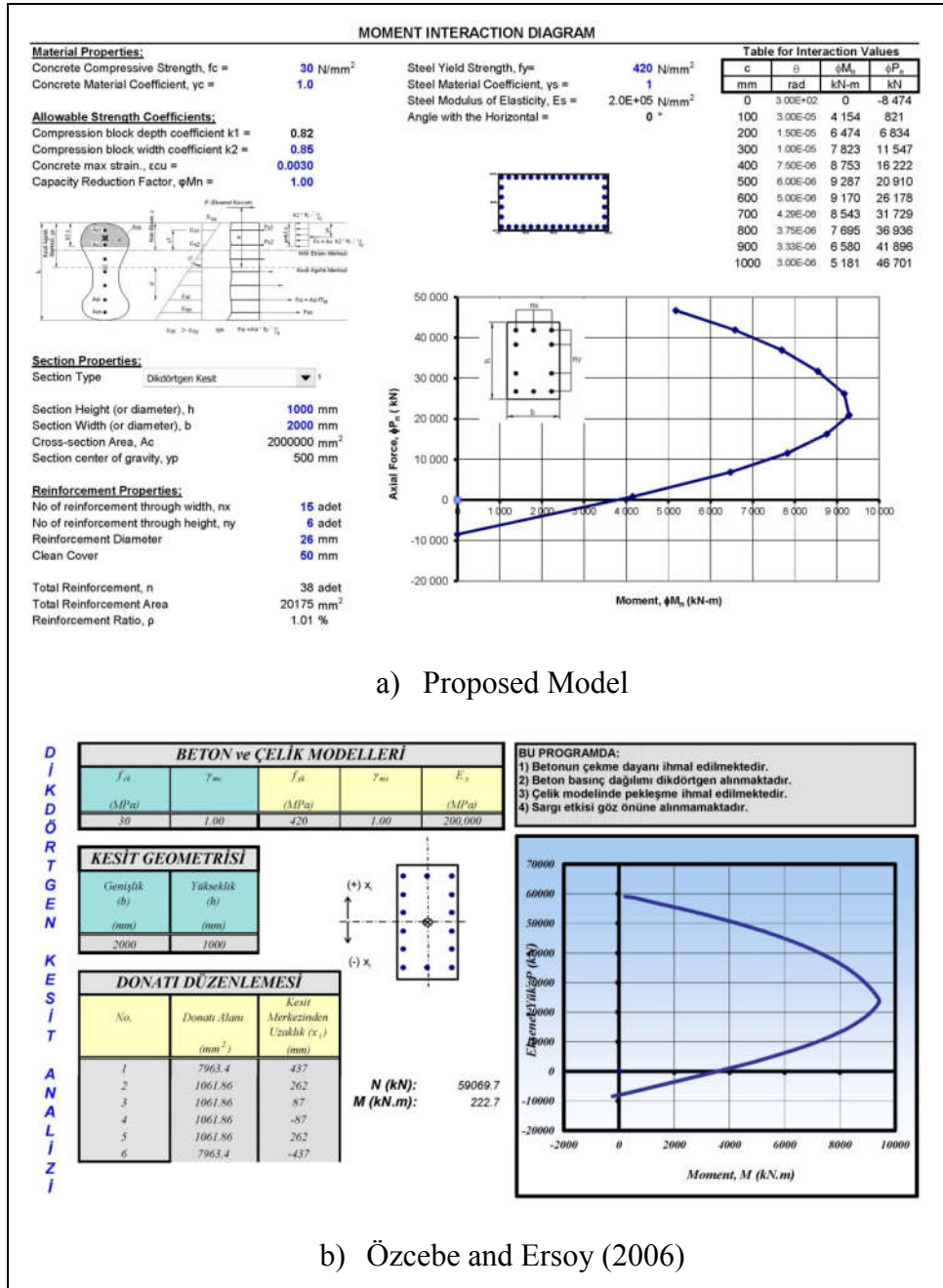
In both programs, a rectangular section having 2.0 x 1.0m dimensions was analyzed. Maximum section moments together with x and y intercepts of the graphs were tabulated in Table A.3. Accordingly maximum difference between these two programs was found as 5,68% .

Table A.3: Comparison of moment – axial load interaction programs

Parameters	Maximum	Axial Load	Moment
Our Model	9287	-8474	3787
Özcebe and Ersoy	9433	-7992	3568
Difference (%)	1,57	5,68	5,80

A.3 Proposed Corrosion Rate Model

The corrosion rate models proposed in the literature were used considering the same environmental conditions and concrete properties for fifty years of deterioration. The corrosion rate values were obtained within a range of 0,5 to 2,6 which satisfied the value of 1,03 obtained by using proposed model as provided in Table A.4.

Table A.4: Comparison of corrosion rates

Corrosion Rate Model	i_{corr} ($\mu A / cm^2$)
Stewart and Rosowsky (1998)	1,50
Yalçın and Ergun (1996)	0,50
Vu and Stewart (2000)	2,36
Li (2004)	2,57
Guo etc al. (2014)	0,70
Proposed Corrosion Model	**1,03**

APPENDIX B

MODAL PARTICIPATING MASS RATIOS OF A MODEL

Table B.1: Modal Participating Mass Ratios of a Model

Mode Number	Period (sec)	UX	UY	UX	SUMX	SUMY	SUMZ
1	0.85	0.97	0.00	0.00	0.97	0.00	0.00
2	0.75	0.00	0.48	0.00	0.97	0.48	0.00
3	0.71	0.00	0.30	0.00	0.97	0.79	0.00
4	0.71	0.00	0.16	0.00	0.97	0.95	0.00
5	0.14	0.02	0.00	0.00	0.99	0.95	0.00
6	0.09	0.00	0.00	0.00	0.99	0.95	0.00
7	0.08	0.00	0.00	0.51	0.99	0.95	0.51
8	0.06	0.00	0.05	0.00	0.99	0.99	0.51
9	0.05	0.00	0.00	0.11	0.99	0.99	0.62
10	0.05	0.00	0.00	0.35	0.99	0.99	0.97
11	0.04	0.00	0.00	0.00	0.99	0.99	0.97
12	0.03	0.00	0.00	0.00	0.99	0.99	0.97
13	0.03	0.01	0.00	0.00	1.00	0.99	0.97
14	0.02	0.00	0.00	0.00	1.00	0.99	0.97
15	0.02	0.00	0.00	0.00	1.00	0.99	0.97
16	0.02	0.00	0.00	0.00	1.00	0.99	0.97

Table B.1: Cont'd

Mode Number	Period (sec)	UX	UY	UX	SUMX	SUMY	SUMZ
17	0.01	0.00	0.00	0.00	1.00	0.99	0.97
18	0.01	0.00	0.00	0.00	1.00	0.99	0.97
19	0.01	0.00	0.00	0.01	1.00	0.99	0.98
20	0.01	0.00	0.00	0.00	1.00	0.99	0.98
21	0.01	0.00	0.01	0.00	1.00	1.00	0.98
22	0.01	0.00	0.00	0.00	1.00	1.00	0.99
23	0.01	0.00	0.00	0.00	1.00	1.00	0.99
24	0.01	0.00	0.00	0.00	1.00	1.00	0.99
25	0.01	0.00	0.00	0.00	1.00	1.00	0.99
26	0.01	0.00	0.00	0.00	1.00	1.00	0.99
27	0.01	0.00	0.00	0.01	1.00	1.00	1.00
28	0.01	0.00	0.00	0.00	1.00	1.00	1.00
29	0.01	0.00	0.00	0.00	1.00	1.00	1.00
30	0.00	0.00	0.00	0.00	1.00	1.00	1.00
31	0.00	0.00	0.00	0.00	1.00	1.00	1.00
32	0.00	0.00	0.00	0.00	1.00	1.00	1.00
33	0.00	0.00	0.00	0.00	1.00	1.00	1.00
34	0.00	0.00	0.00	0.00	1.00	1.00	1.00
35	0.00	0.00	0.00	0.00	1.00	1.00	1.00
36	0.00	0.00	0.00	0.00	1.00	1.00	1.00

Table B.1: Cont'd

Mode Number	Period (sec)	UX	UY	UX	SUMX	SUMY	SUMZ
37	0.00	0.00	0.00	0.00	1.00	1.00	1.00
38	0.00	0.00	0.00	0.00	1.00	1.00	1.00
39	0.00	0.00	0.00	0.00	1.00	1.00	1.00
40	0.00	0.00	0.00	0.00	1.00	1.00	1.00
41	0.00	0.00	0.00	0.00	1.00	1.00	1.00
42	0.00	0.00	0.00	0.00	1.00	1.00	1.00
43	0.00	0.00	0.00	0.00	1.00	1.00	1.00
44	0.00	0.00	0.00	0.00	1.00	1.00	1.00
45	0.00	0.00	0.00	0.00	1.00	1.00	1.00
46	0.00	0.00	0.00	0.00	1.00	1.00	1.00
47	0.00	0.00	0.00	0.00	1.00	1.00	1.00
48	0.00	0.00	0.00	0.00	1.00	1.00	1.00
49	0.00	0.00	0.00	0.00	1.00	1.00	1.00
50	0.00	0.00	0.00	0.00	1.00	1.00	1.00
51	0.00	0.00	0.00	0.00	1.00	1.00	1.00
52	0.00	0.00	0.00	0.00	1.00	1.00	1.00
53	0.00	0.00	0.00	0.00	1.00	1.00	1.00
54	0.00	0.00	0.00	0.00	1.00	1.00	1.00
55	0.00	0.00	0.00	0.00	1.00	1.00	1.00
56	0.00	0.00	0.00	0.00	1.00	1.00	1.00

Table B.1: Cont'd

Mode Number	Period (sec)	UX	UY	UX	SUMX	SUMY	SUMZ
57	0.00	0.00	0.00	0.00	1.00	1.00	1.00
58	0.00	0.00	0.00	0.00	1.00	1.00	1.00
59	0.00	0.00	0.00	0.00	1.00	1.00	1.00
60	0.00	0.00	0.00	0.00	1.00	1.00	1.00